

Multiscale simulation of heterophase polymerization
Application to the synthesis of multicomponent colloidal polymer particles

Dissertation

zur Erlangung des akademischen Grades
"doctor rerum naturalium"
(Dr. rer. nat.)
in der Wissenschaftsdisziplin "Kolloidchemie"

eingereicht an der
Mathematisch-Naturwissenschaftlichen Fakultät
der Universität Potsdam

von

Hugo Fernando Hernández García
geboren am 24. Dezember 1978 in Tunja, Kolumbien

Potsdam, Oktober 2008

Online published at the
Institutional Repository of the Potsdam University:
<http://opus.kobv.de/ubp/volltexte/2008/2503/>
<urn:nbn:de:kobv:517-opus-25036>
[<http://nbn-resolving.de/urn:nbn:de:kobv:517-opus-25036>]

Dedicado a mis Padres, Elsa Isabel y José Miguel

Dedicado a Silvia, mi Princesita Preciosa

Dedicado a Dios, el más Grande de todos los Maestros

Molecules do not know about Thermodynamics...

Abstract

Heterophase polymerization is a technique widely used for the synthesis of high performance polymeric materials with applications including paints, coatings, inks, adhesives, synthetic rubber, biomedical applications and many others. Due to the heterogeneous nature of the process, many different relevant length and time scales can be identified. Each of these scales has a direct influence on the kinetics of polymerization and on the physicochemical and performance properties of the final product. Therefore, from the point of view of product and process design and optimization, the understanding of each of these relevant scales and their integration into one single model is a very promising route for reducing the time-to-market in the development of new products, for increasing the productivity and profitability of existing processes, and for designing products with improved performance or cost/performance ratio.

In the present work, a particular case of multiscale integration in heterophase polymerization is addressed. The process considered is the synthesis of structured or composite polymer particles by multi-stage seeded emulsion polymerization. This type of process is used for the preparation of high performance materials where a synergistic behavior of two or more different types of polymers is obtained. Some examples include the synthesis of core-shell or multilayered particles for improved impact strength materials and for high resistance coatings and adhesives. The kinetics of the most relevant events taking place in an emulsion polymerization process has been investigated using suitable numerical simulation techniques at their corresponding time and length scales. These methods, which include Molecular Dynamics (MD) simulation, Brownian Dynamics (BD) simulation and kinetic Monte Carlo (kMC) simulation, have been found to be very powerful and highly useful for gaining a deeper insight and achieving a better understanding and a more accurate description of all phenomena involved in emulsion polymerization processes, and can be potentially extended to investigate any type of heterogeneous process. The novel approach of using these kinetic-based numerical simulation methods can be regarded as a complement to the traditional thermodynamic-based macroscopic description of emulsion polymerization. The particular events investigated include molecular diffusion, diffusion-controlled polymerization reactions, particle formation, absorption/desorption of radicals and monomer, and the colloidal aggregation of polymer particles.

Molecular diffusion, which is caused by the permanent random collisions between the different molecules in the system, is characterized by the diffusion coefficient. The characteristic diffusion coefficient of a particular system can be very precisely determined using MD simulation based on a suitable intermolecular interaction potential function (e.g. Lennard-Jones, Buckingham, Morse, etc.). Once the diffusion coefficient has been determined, molecular diffusion can be simulated at a larger length and time scale using BD simulation. Using BD simulation it was possible to precisely determine the kinetics of absorption/desorption of molecular species by polymer particles, and to simulate the colloidal aggregation of polymer particles. For diluted systems, a very good agreement between BD simulation and the classical theory developed by Smoluchowski was obtained. However, for

concentrated systems, significant deviations from the ideal behavior predicted by Smoluchowski were evidenced. BD simulation was found to be a very valuable tool for the investigation of emulsion polymerization processes especially when the spatial and geometrical complexity of the system cannot be neglected, as is the case of concentrated dispersions, non-spherical particles, structured polymer particles, particles with non-uniform monomer concentration, and so on. In addition, BD simulation was used to describe non-equilibrium monomer swelling kinetics, which is not possible using the traditional thermodynamic approach because it is only valid for systems at equilibrium.

The description of diffusion-controlled polymerization reactions was successfully achieved using a new stochastic algorithm for the kMC simulation of imperfectly mixed systems (SSA-IM). In contrast to the traditional stochastic simulation algorithm (SSA) and the deterministic rate of reaction equations, instead of assuming perfect mixing in the whole reactor, the new SSA-IM determines the volume perfectly mixed between two consecutive reactions as a function of the diffusion coefficient of the reacting species. Using this approach it was possible to describe, using a single set of kinetic parameters, typical mass transfer limitations effects during a free radical batch polymerization such as the cage effect, the gel effect and the glass effect.

Particle formation, which is one of the most complex and most difficult to investigate events in emulsion polymerization, was described using a new model which considers the desorption of radicals from segregated phases, the spontaneous emulsification of monomer and the release of heat during propagation. According to this model, the radicals present in the continuous phase can be absorbed and desorbed by polymer particles or by small monomer droplets formed by spontaneous emulsification. The transfer of a radical from one phase to another takes place when the kinetic energy of the radical overcomes the energy barrier for the corresponding phase transfer. Since during radical growth, the most important source of energy is the heat released at each propagation reaction, unless the energy barrier for desorption of a given radical becomes much larger than the energy released, the radical will very probably return to the continuous phase upon propagation. Since the energy barrier for desorption increases with increasing chain length, the critical energy barrier is reached at a certain critical chain length. If a radical reaches the critical chain length inside a monomer droplet, then a new polymer particle is formed.

Using multiscale integration it was possible to investigate the formation of secondary particles during the seeded emulsion polymerization of vinyl acetate over a polystyrene seed. Three different cases of radical generation were considered: generation of radicals by thermal decomposition of water-soluble initiating compounds, generation of radicals by a redox reaction at the surface of the particles, and generation of radicals by thermal decomposition of surface-active initiators "inisurfs" attached to the surface of the particles. The simulation results demonstrated the satisfactory reduction in secondary particles formation achieved when the locus of radical generation is controlled close to the particles surface.

Allgemeinverständliche Zusammenfassung

Eine der industriell am meisten verwendeten Methoden zur Herstellung von Hochleistungspolymeren ist die Heterophasenpolymerisation. Industriell von besonderer Bedeutung ist die sogenannte Saatemulsionspolymerisation bei der kleine Saateilchen durch die sequentielle Zugabe von weiteren Monomeren gezielt modifiziert werden, um Kompositpolymerteilchen mit den gewünschten mechanischen und chemischen Gebrauchseigenschaften herzustellen. Ein häufig auftretendes Problem während dieser Art der Heterophasenpolymerisation ist die Bildung von neuen, kleinen Teilchen im Polymerisationsverlauf. Diese sogenannte sekundäre Teilchenbildung muss vermieden werden, da sie die Herstellung der gewünschten Teilchen mit den angestrebten Eigenschaften verhindert.

Ein spezieller Fall der Saatemulsionspolymerisation ist die Kombination von Vinylacetat als Monomer, das auf Saateilchen aus Polystyrol polymerisieren soll. Die Unterdrückung der Teilchenneubildung ist in diesem Beispiel besonders schwierig, da Vinylacetat eine sehr hohe Wasserlöslichkeit besitzt.

In der vorliegenden Arbeit wurden zur Lösung der Aufgabenstellung verschiedene numerische Simulationsalgorithmen verwendet, die entsprechend den charakteristischen Längen- und Zeitskalen der im Verlauf der Polymerisation ablaufenden Prozesse ausgewählt wurden, um die passenden Bedingungen für die Unterdrückung der sekundären Teilchenbildung zu finden. Die verwendeten numerischen Methoden umfassen Molekulare Dynamik Simulationen, die benutzt werden, um molekulare Bewegungen zu berechnen; Brownsche Dynamik Simulationen, die benutzt werden, um die zufälligen Bewegungen der kolloidalen Teilchen und der molekularen Spezies zu beschreiben, und kinetische Monte Carlo Simulationen, die das zufällige Auftreten von individuellen physikalischen oder chemischen Ereignissen modellieren.

Durch die Kombination dieser Methoden ist es möglich, alle für die Beschreibung der Polymerisation relevanten Phänomene zu berücksichtigen. Damit können nicht nur die Reaktionsgeschwindigkeit und die Produktivität des Prozesses simuliert werden sondern auch Aussagen bezüglich der physikalischen und chemischen Eigenschaften des Produktes sowie den Applikationseigenschaften getroffen werden. In dieser Arbeit wurden zum ersten Mal Modelle für die unterschiedlichen Längen- und Zeitskalen bei Heterophasenpolymerisationen entwickelt und erfolgreich zur Modellierung des Prozesses angewendet. Die Ergebnisse führten zu bedeutenden Verbesserungen der Theorie von Emulsionspolymerisationen insbesondere für die Beschreibung des Massenaustausches zwischen den Phasen (bspw. Radikaleintritt in und Radikalausritt aus die Polymerteilchen), der Bildung von neuen Teilchen, und der Polymerisationskinetik unter den heterogenen Reaktionsbedingungen mit uneinheitlicher Durchmischung.

Table of Contents

	Page
1. Introduction	1
2. Theoretical Background.....	4
2.1. Principles of polymerization.....	4
2.2. Free-Radical Emulsion Polymerization	6
2.3. Structured polymer particles.....	10
3. Methods	15
3.1. Numerical Simulation Methods.....	15
3.1.1. Molecular Dynamics Simulation	15
3.1.2. Brownian Dynamics Simulation	20
3.1.3. Kinetic Monte Carlo (Stochastic) Simulation.....	29
3.2. Experimental Methods	34
3.2.1. Optical Microscopy (OM).....	34
3.2.2. Electron Microscopy (EM)	36
3.2.3. Dynamic Light Scattering (DLS).....	39
4. Kinetics of Emulsion Polymerization.....	43
4.1. Molecular diffusion	46
4.2. Diffusion-controlled polymerization kinetics	51
4.3. Particle formation.....	53
4.4. Radical capture	60
4.5. Radical desorption.....	70
4.6. Monomer swelling	77
4.7. Colloidal aggregation	87
4.8. Particle morphology development.....	92
5. Multiscale Stochastic Simulation.....	94
5.1. Multiscale Integration in Heterophase Polymerization	94
5.2. Multiscale Stochastic Simulation of Seeded Emulsion Polymerization	95
6. Conclusions.....	101
Appendix A. Experimental Examples.....	104
A.1 Chemicals and Equipment.....	104
A.2 Polystyrene/Poly(n-butyl Methacrylate) core-shell particles	106
A.3 Polystyrene/Poly(Vinyl Acetate) structured particles prepared by multi-stage emulsion polymerization.....	107
A.4 Micron-sized Polystyrene/Poly(Vinyl Acetate) composite particles	110

A.5 Multi-stage Polystyrene/Poly(Methyl Methacrylate) emulsion polymerization	112
Appendix B. Sample simulation codes (Matlab)	114
B.1 Molecular Dynamics Simulation	114
B.2 Brownian Dynamics Simulation.....	117
B.3 Kinetic Monte Carlo Simulation – Perfect mixing.....	119
B.4 Kinetic Monte Carlo Simulation – Imperfect mixing.....	121
B.5 Multiscale Simulation.....	124
References	131
Acknowledgments	137
Publications and Presentations.....	139

Chapter 1

Introduction

Heterophase polymerization is a highly complex dynamic process in which several simultaneous and usually competitive chemical (radical generation, propagation, termination, chain transfer) and physical events (absorption, desorption, nucleation, coagulation) occur at very different time scales and dimensions. These events take place in a typical free-radical emulsion polymerization at rates ranging from about 10^0 to 10^9 s^{-1} and involving entities of very different length scales, such as ions and molecules (< 1 nm), macromolecules (1 – 10 nm), polymer particles (10 nm – 1 μ m) and monomer droplets (>1 μ m). The multi-scale nature of emulsion polymerization can be appreciated in Figure 1.1, where at least seven relevant different length scales can be identified.

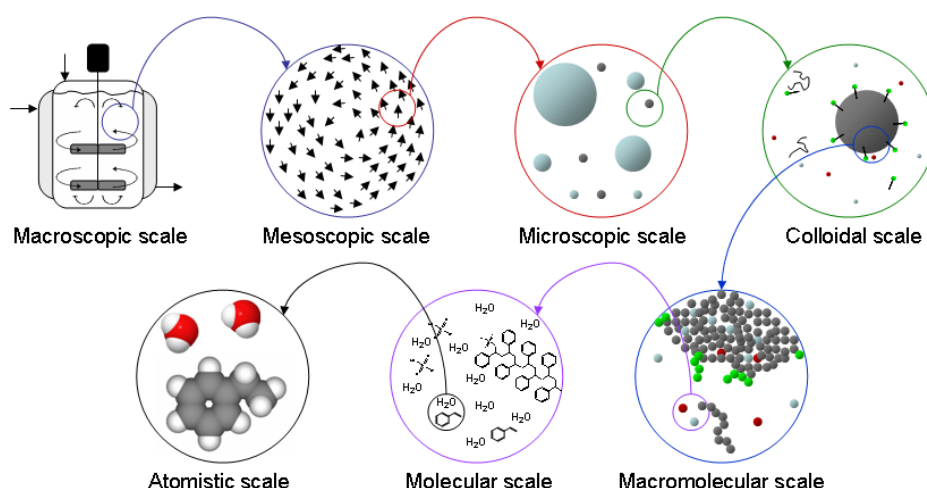


Figure 1.1 Emulsion polymerization as a multi-scale process

Nowadays, millions of tons of synthetic polymer dispersions are prepared by heterophase polymerization techniques to be used in a wide variety of applications including adhesives, paints and coatings, inks, synthetic rubber, binders for non-woven fabrics, additives in paper and textile manufacturing, additives for leather treatment, additives for construction materials, impact modifiers for plastics, rheological modifiers, latex foam, carpet backing, flocculants for water treatment, chromatographic separations systems, and more recently for the synthesis of diagnostic tests and drug delivery systems for biomedical and pharmaceutical applications.^[1-3]

An increasingly important technique used in industrial heterophase polymerization is the *multi-stage* polymerization method, also known as *seeded* or *sequential* polymerization. Using multi-stage polymerization it is possible to synthesize structured multicomponent colloidal polymer particles, which

are particles consisting of two or more different polymer phases. Structured polymer particles are industrially important because of their improved (synergistic) physicochemical performance in applications such as film forming materials, impact modifiers, medical diagnosis systems and high performance composite materials in general.^[4-9]

The basic principle of multi-stage polymerization is the polymerization of a single monomer or monomer mixture in the presence of previously prepared polymer dispersions. The particles of the original dispersion, which are called "seed" particles, act as loci of the next stage polymerization. However, they are not the only possible polymerization loci in the system because polymerization can also proceed in the continuous phase. The polymer chains formed in the continuous phase will eventually lead to the formation of secondary polymer particles unless they are captured by the seed particles. There is a permanent competition between the formation of structured polymer particles and secondary particle nucleation. On the other hand, the final morphology of the structured polymer particles produced depends on many kinetic and thermodynamic factors including the temperature of the system, the type and amount of surfactant used, the type of initiator used, the order of addition of the monomers, the internal viscosity of the particles, and many others.

The successful synthesis of structured polymer particles is only possible if the appropriate conditions are used for suppressing or minimizing the production of secondary particles in the system and for obtaining the desired particle morphology.

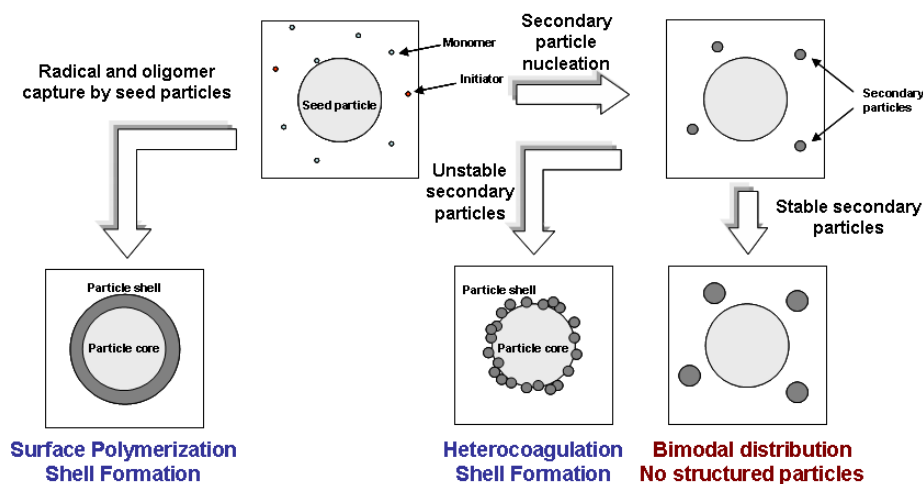


Figure 1.2 Possible outcomes in seeded emulsion polymerization

The first condition for synthesizing structured polymer particles can be achieved by suppressing secondary nucleation (increasing the ratio of the capture rate of radicals and oligomers to the rate of secondary nucleation) or promoting secondary particles coagulation on the surface of seed particles (increasing the ratio of secondary particle coagulation rate to secondary particle growth rate). In this case, the competition between the capture of radicals, oligomers and oligomeric aggregates by seed particles, and secondary particle nucleation is the determining factor, as depicted in Figure 1.2.

The second requirement can be fulfilled by selecting the correct order of addition and addition policies of the components. If the desired morphology is the equilibrium morphology, monomer pre-swelling and batch polymerization processes are recommended; if not, semi-batch monomer-starved feed conditions and the use of crosslinkers may be required. The optimal process conditions for obtaining the desired particle morphology have been extensively investigated in the last decades.^[8-15]

The aim of this work is the investigation, using multiscale stochastic simulation methods, of the most important mechanisms involved in the formation of secondary particles, some of which still remain controversial:^[16-19]

- Particle formation (nucleation).
- Capture of primary radicals and oligomers by seed particles.
- Radical desorption.
- Colloid particles aggregation.
- Monomer swelling.

The novel multiscale stochastic approach presented in this work is necessary because of the spatial and timely multiscale nature of the process. The fundamental principles of heterophase polymerization are qualitatively presented in Chapter 2. The simulation and experimental methods used to investigate the synthesis of structured polymer particles are described in Chapter 3. In Chapter 4, the different physical and chemical mechanisms involved in the synthesis of multicomponent polymer particles by heterophase polymerization are investigated individually using adequate simulation methods at the corresponding scales. One of the most important features of the models presented along this chapter is the extensive use of kinetic and not thermodynamic principles to describe the dynamics of emulsion polymerization. In Chapter 5, the different mechanisms are integrated into a single multi-scale simulation of the process, which is employed to determine the adequate conditions for suppressing secondary particle formation in seeded emulsion polymerization.

Chapter 2

Theoretical Background

2.1. Principles of polymerization

A *polymerization process* is a process leading to the synthesis of large molecules (*macromolecules*) as a result of the chemical (covalent) binding of molecular building blocks called *monomers*. The term "monomer" is derived from the Greek words *mono* (one) and *meros* (part). Similarly, the macromolecules are designated as *polymers* (many parts), while short polymers are usually denoted as *oligomers* (some parts).

Polymerization processes can be classified into two main groups: *addition polymerization* and *condensation polymerization*. The basic difference between these two groups is that the mass of a macromolecule formed by addition polymerization is exactly the sum of the molecular masses of all the monomers used in its synthesis. On the contrary, the molecular mass of a macromolecule formed by condensation is less than the sum of its components because during the incorporation of a monomer into the chain a small by-product molecule is formed.

According to the chemical mechanism of monomer incorporation, most addition polymerization processes can be classified into *free-radical polymerization*, *ionic polymerization* and *coordination polymerization*. In free-radical polymerization, the growing chain contains at least one unpaired electron which reacts readily with a molecule with at least one unsaturated bond, leading to chain growth. In free-radical polymerization, the radicals can be generated in very different ways. The simplest case is the thermal degradation of monomer molecules leading to the formation of radical species. It is also possible to generate radicals from the decomposition of sensitive molecules called *initiators*. Some initiators decompose with temperature (*thermal initiators*), some others under the effect of light (*photoinitiators*), and others generate radicals after an electron transfer reaction (*redox initiators*).

In ionic polymerization, the growing chain contains a strong nucleophilic or electrophilic ionic end group which is also capable of reacting with an unsaturated bond or with a ring compound. However, ionic polymerization is very sensitive to the presence of other ions or strongly polar molecules (such as water), and therefore, it is not well suited for aqueous polymerization processes. Coordination polymerization is a special type of ionic polymerization characterized by the use of a transition metal

compound (*coordination initiator*) which strongly interacts with the double bond of a monomer. This interaction is stereo-selective and is referred to as *coordination*. Due to the high electronic density of the transition metal, the molecular orbitals of the monomer are strongly perturbed and the double bond can be easily broken.

From a physical point of view, the polymerization processes can be classified into *homogeneous* and *heterogeneous* depending on the state of the reaction mixture. If the monomer molecules as well as the polymer obtained are soluble in the medium, the process is said to be homogeneous. Typical examples of homogeneous polymerization processes are *bulk* (when the monomer is the medium and the polymer formed is soluble in it) and *solution* polymerization (when an inert solvent is used). Otherwise, the process is designated as heterogeneous or *heterophase polymerization* because more than one phase may be present at some moment during the polymerization (i.e. one or more phases dispersed in a continuous phase).

When the final polymeric material is distributed in a fluid medium forming stable individual particles it is called a *polymer dispersion*. Although any liquid can be used as dispersion medium as long as it is not a solvent for the dispersed polymer, for safety and environmental reasons water is the most commonly used continuous phase. The aqueous polymer dispersions are also known as *polymer latexes*. In recent years, aqueous heterophase polymerization processes have become increasingly important technologically and commercially, not only because of the production of high performance polymeric materials, but also for being environmentally-friendlier. ^[2-3,20-21]

Considering that the size of the dispersed phase is important for the kinetics of polymerization and the performance of the polymer dispersion in its final application, it is necessary to prevent coagulation and flocculation of the segregated phase. The stability of the dispersed phase is achieved by using *amphiphilic molecules*, which are composed of one moiety soluble in the continuous phase and the other soluble in the dispersed phase (or at least insoluble in the continuous phase). These amphiphilic molecules are also called *stabilizers* or *surface active agents (surfactants)*. The stabilizers can be *ionic* (anionic, cationic or zwitterionic) or *non-ionic* (block copolymers, graft copolymers). There are different possible mechanisms of stabilization using amphiphiles including *electrostatic*, *steric*, *electrosteric* and *depletion stabilization*. The final (stable) size of the dispersed phase strongly depends on the amount and nature of the stabilizer used. The stable surface area of the dispersed phase increases with an increase in the amount of stabilizer, and thus, smaller particles can be obtained.

Depending on the size and composition of the different phases formed during the polymerization, heterophase polymerization processes in dispersed emulsion phases can be classified into: *Precipitation*, *suspension*, *microsuspension*, *dispersion*, *emulsion (macroemulsion)*, *miniemulsion* and *microemulsion polymerization*. It is important to notice that these names are not systematic and can be misleading. Sometimes they designate the initial condition of the system (e.g. emulsion polymerization), whereas in others they indicate the final state of the system (e.g. precipitation

polymerization). The most relevant characteristics of the different types of homogeneous and heterogeneous polymerization processes are compared in Table 2.1.

Although the physical appearance of the reaction mixture, as well as the physical and chemical properties of the final product obtained are different for each type of polymerization process, the physical and chemical mechanisms involved in all cases are in principle the same. In the following section, a detailed picture of emulsion polymerization is presented, which is the most general, most representative and perhaps most complex type of free-radical polymerization.

Table 2.1 Types of polymerization processes^[3,21]

Type of polymerization	Continuous phase	Initiator	Stabilizer	Monomer solubility	Particle size	Special features
Bulk	monomer	lyophilic	none	soluble	-	
Solution	any	lyophilic	none	soluble	-	
Precipitation	any	any	none	soluble	>1 mm	
Suspension	any	lyophobic	polymeric or colloid	low	10-500 μm	
Microsuspension	any	lyophobic	polymeric + surfactant	low	1-10 μm	
Dispersion	any	lyophilic	polymeric	low-soluble	1-20 μm	a
Emulsion	water	any	any type (low amounts)	low	5 nm – 10 μm	b, c
Miniemulsion	water	any	any (high amounts)	insoluble	50-500 nm	b, c, d
Microemulsion	water	any	any (very high amounts)	low*	30-100 nm	b, e

Notes:

* The monomer solubility is originally low. After addition of the stabilizer, solubilization of the monomer as nanodroplets in the continuous phase is achieved.

a No gel effect

b High polymerization rate

c High molecular weight

d High energy input required for emulsification

e No energy required for emulsification

2.2. Free-Radical Emulsion Polymerization

Emulsion polymerization is considered frequently as polymerization of slightly water-soluble monomers in an aqueous continuous phase, and in the presence of a suitable stabilizing (amphiphile) or stability-promoter compound (including hydrophilic monomers, hydrophilic initiators or any other molecule). The term *emulsion polymerization* is sometimes misleading because an *emulsion* is a liquid in liquid dispersion whereas the final product is a solid polymer in liquid dispersion. There are two main technologies of emulsion polymerization: *ab initio* (no polymer particles present at the beginning of the process) and seeded emulsion polymerization (previously prepared polymer particles are used). Emulsion polymerization can be carried out in batch, semi-batch or continuous operation.

In particular, the modeling of batch *ab initio* emulsion polymerization processes is more complicated and more challenging than that of seeded semi-batch or continuous processes. At the beginning of

the batch *ab initio* process, monomer, water and the stabilizer are added to the reactor. After mixing, a liquid/liquid dispersion will be formed. If the dispersed phase is in the colloidal range (around 1 nm – 1 μ m), the dispersion is called an *emulsion*. Depending basically on the relative amount of each component and on the relative affinity of the stabilizer to each phase, a dispersion of monomer in water (O/W) or a dispersion of water in monomer (W/O) can be obtained. The relative affinity of the stabilizer to both phases is usually quantified using the HLB (*Hydrophilic-Lipophilic Balance*) parameter. The formation of O/W dispersions is favored by high-HLB (>8) surfactants which are more easily dissolved in the aqueous phase, while W/O dispersions formation is preferred by low-HLB (<8) surfactants which dissolve more easily in the monomer phase.

Under the usual conditions used at the beginning of emulsion polymerization an O/W dispersion of monomer droplets in water is obtained. The size of the droplets will depend basically on the type and amount of amphiphile used, and on the mechanical energy applied to disperse the monomer (stirring rate, ultrasound power, etc.). If the energy applied is very high, “critically” stabilized emulsions (*miniemulsions*) can be formed. They are considered to be critically stabilized because the surfactant coverage is at its critical value; below this value, the emulsion reaches the instability region. If large amounts of amphiphile are used, thermodynamically stable emulsions (*microemulsions*) can be obtained.

After the preparation of the initial emulsion, the polymerization is started by adding an initiating compound to the system. The initiator molecules are decomposed by a suitable mechanism (thermal motion, photolysis, electron transfer) generating *primary free radicals* in the continuous phase. A free radical is simply a molecule with an unpaired electron. This condition makes radicals extremely reactive. Free radicals can react in many different ways in a typical polymerization process (Figure 2.1). Some of the most relevant reactions involving radicals include:

- Addition to carbon-carbon double bonds: Given the high electron density and relative weakness of a carbon-carbon double (or triple) bond in an unsaturated molecule, the unpaired electron of the radical easily breaks one of the bonds and adds covalently to one of the carbon atoms. After this addition, the atom at the opposite side of the double bond ends with an unpaired electron due to the bond breakage. By means of this mechanism, both the free radical and the unsaturated molecule become covalently bonded, and the new molecule is also a free radical but now the unpaired electron belongs to a different atom. In polymerization, if the original radical is a primary radical this reaction is known as *initiation*; otherwise, it is known as *propagation*.
- Termination: Termination is the reaction between a pair of radicals. As a result of this reaction, both radicals are consumed. There are two different types of termination reactions depending on the products obtained: *recombination* and *disproportionation*. In termination by recombination, a new covalent bond is formed between both unpaired electrons. The final product is therefore a single molecule. On the other hand, in termination by

disproportionation a hydrogen molecule is transferred from one of the free radicals to the other causing formation of a double bond in the hydrogen-donor molecule while the other molecule remains saturated. By means of disproportionation, both radicals disappear, but one of the reacting molecules (the former hydrogen-donor) can react again with a free radical via a propagation reaction.

- **Chain transfer:** Chain transfer is basically a hydrogen-transfer reaction. If the free radical is in the vicinity of a molecule with a weakly-bonded hydrogen atom, the hydrogen atom is easily abstracted by the radical and forms a bond with the unpaired electron, whereas the broken bond results in an unpaired electron transferring the radical to the second molecule. When the new radical formed is stable (i.e. no or low reactivity), this process is known as *inhibition* or *retardation*. There are different types of chain transfer reaction depending on the nature of the hydrogen donor which can be: a solvent molecule (e.g. water in emulsion polymerization), a monomer molecule, a polymer molecule (leading to branching or grafting), another part of the chain itself (back-biting), a surfactant molecule, an initiator molecule (*iniferter*), an inhibitor or any molecule deliberately incorporated to promote chain transfer reactions (e.g. mercaptans), allowing a certain control over the molecular weight of the chains. The molecules added for this purpose are denoted as *chain transfer agents*.

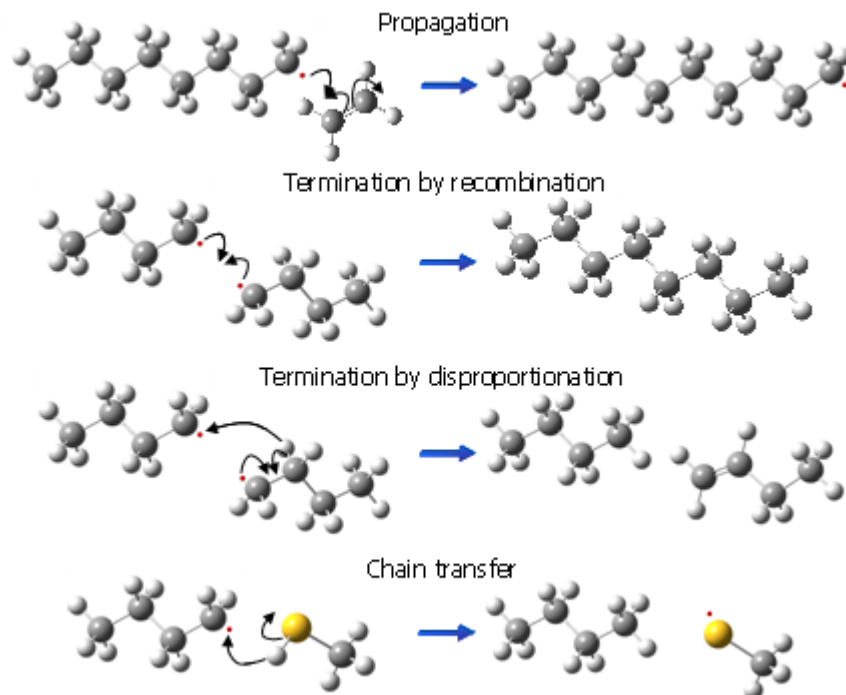


Figure 2.1 Typical reactions of free radicals in a polymerization process. White: Hydrogen atoms, Gray: Carbon atoms, Yellow: Sulfur atoms, Red: Unpaired electrons

These typical free radical reactions, which can take place in any phase of the reacting system, produce macromolecular chains with different sizes, giving rise to a molecular weight distribution of the macromolecules. If the interaction between a macromolecule and the solvent molecules is stronger than the interaction between macromolecules or the intramolecular interaction of the

macromolecule, it can remain solubilized in the continuous phase. Otherwise, a single macromolecule will form aggregates with other chains or with other species in the system forming a separate new phase. This phase change corresponds to a *nucleation*-type first-order transition known as *particle formation*. Polymer particles can be formed in the absence as well as in the presence of surfactant. In the latter case the situation is more complex, especially at high surfactant concentration. Surfactants facilitate the emulsification of the hydrophobic monomers in the form of small emulsion drops and swollen micelles, and hence, the effective monomer concentration in water is enhanced. Consequently, the rate of polymerization is initially increased and more and smaller particles can be stabilized. Under these conditions, the segregation effect (isolated radicals in individual particles) can become dominant, increasing the rate of polymerization and the molecular weight of the chains.

Surfactants are also important for controlling the number of particles produced and their final particle size as a result of the balance between aggregation and stabilization of polymer particles. Surfactants should be carefully chosen according to their effects on the product characteristics and on the final application properties. Some of these properties include the wettability of the latex and adhesion of the polymer to certain surfaces for coating and adhesive applications, the rheological behavior of the dispersion, or the compatibility with other materials (fillers, pigments, etc.).^[22] Most commercial recipes contain mixed surfactants and additional ingredients depending on the specific requirements of the final application or the specific conditions needed during polymerization.^[3]

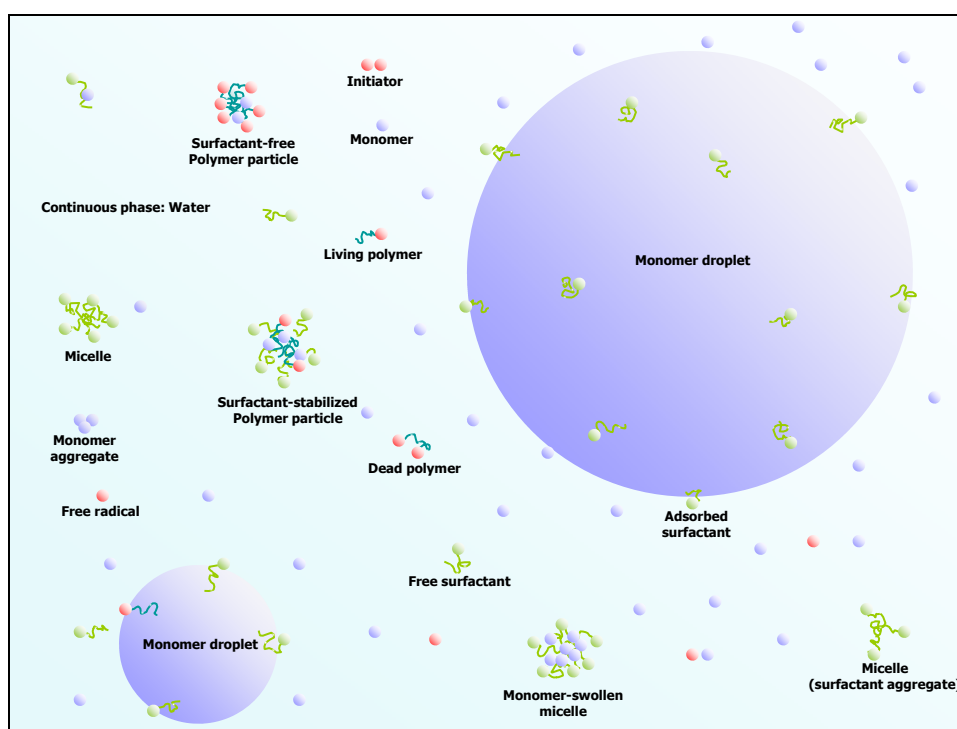


Figure 2.2 Graphical representation of emulsion polymerization

A typical picture of an emulsion polymerization system is presented in Figure 2.2. It includes the monomer droplets with sizes ranging from the micrometer to the millimeter range, monomer aggregates or nanodroplets ($< 1 \mu\text{m}$), molecularly dissolved monomer, initiator molecules, primary

free radicals, macromolecular free radicals (living polymers), dead polymers, monomer-polymer aggregates (surfactant-free polymer particles), surfactant molecules (free or adsorbed), surfactant aggregates (micelles), monomer-surfactant aggregates (monomer-swollen micelles) and monomer-polymer-surfactant aggregates (surfactant-stabilized polymer particles), all immersed in a continuous phase of water molecules.

Thus, the size of the entities involved in a typical emulsion polymerization process ranges from molecular species of less than 1 nm in size to almost millimeter-sized monomer droplets. For a certain amount of a given component, the number concentration of the corresponding entities is strongly dependent on its size distribution. The size and concentration of the different entities involved in an emulsion system can be determined using a combination of different experimental techniques including electron microscopy, light scattering, ultracentrifugation, spectroscopy, chromatography and many others. ^[23-24]

The industrial development of emulsion polymerization has been motivated by many different factors, including: ^[21,25-26]

- The possibility of simultaneously obtaining polymers of very high molecular weight at high polymerization rates, which are required for certain high performance applications (segregation effect).
- The technology of feed procedures that allows carrying out on the one hand polymerization at the maximum rate and on the other hand to produce particles with the desired morphology and composition on nanometer-size scales.
- The easy processability of the high molecular weight material, due to the low viscosity of the dispersion.
- The increased safety and productivity of the reaction, as water works also as a sink for the energy liberated during the polymerization reaction, allowing a better temperature control and a reduced risk of thermal runaway at high polymerization rates.
- The necessity of substituting solvent-based products by environmentally-friendly water-borne systems as a result of the increasingly demanding environmental regulations.
- The wide range of products with different physical, chemical and performance properties that can be obtained by emulsion polymerization.

2.3. Structured polymer particles

Today, aqueous polymer dispersions with a heterogeneous particle structure (*structured polymer particles*) are extensively used for high performance applications in different industrial fields including coatings, adhesives, impact modifiers, medical diagnostics and many others. These dispersions are mainly prepared by *multi-stage* or *seeded* heterophase polymerization techniques. Suppression of secondary particle nucleation and control of particle morphology are essential for the successful synthesis of latex particles with the required structure. ^[9,11,27]

The multi-stage (seeded) polymerization technique consists on the sequential polymerization of monomers or monomer mixtures, which are added to previously prepared dispersions of polymer particles. The first step of a multi-stage polymerization process is the *ab initio* polymerization of a first monomer to produce a dispersion of "seed" particles. In the following stages, the polymer dispersion obtained in the previous step is used as a seed for the polymerization of the next monomer or monomer mixture. This procedure is repeated several times until all the components have been polymerized onto the particles. Multi-stage polymerization is commonly used to produce composite particles where different types of polymers are present in the particles as different phases. If all the components were added from the beginning of the process, single-phase copolymer particles with completely different properties would be formed.

There are three basic types of monomer addition methods: pre-swelling, batch, and semi-batch or semi-continuous.^[6,28-30] The pre-swelling method consists on the addition of the monomer to the seed particle dispersion, allowing the monomer to diffuse into the particles for a certain time before starting polymerization. In the batch method, the polymerization is started immediately after the addition of the monomer. In this case, the rate of particle growth is thermodynamically controlled by monomer diffusion from the monomer droplets to the polymer particles. In semi-continuous processes, the monomer is continuously added during the whole polymerization. In this case, the rate of particle growth can be controlled by the rate of monomer addition.

During the seeded polymerization steps, depending on the polymerization conditions and the nature of the monomer used, secondary particle formation may occur and a bimodal (or multimodal) dispersion of polymer particles may be produced.^[31] If the primary radicals or the oligomers produced in the continuous phase are captured by the seed particles before secondary nucleation takes place, the synthesis of structured polymer particles will be successful.^[32] If not, the formation of structured particles is still possible as long as the second generation of particles is unstable and *heterocoagulation* (the coagulation of the new particles on the surface of the seed particles) takes place. Okubo et al.,^[33] for example, described a method for the preparation of core/shell composite particles by stepwise heterocoagulation of small cationic hard particles onto large anionic soft particles. Unfortunately, at some point of the reaction in this case the seed particles will have a very low or zero net surface charge and the latex may become unstable.^[34]

On the other hand, successive stages can have quite different hydrophobicities, glass transition temperatures and morphologies. Because of this, the colloidal stability of latex particles can vary significantly from stage to stage, usually leading to poor mechanical stability, coagulation and gel formation. For this reason, extra emulsifier will have to be added at each successive stage to protect the particles.^[35] One of the critical parameters for latex stability is surfactant coverage.^[36] Too little emulsifier leads to emulsion instability and coagulation, while too much emulsifier favors secondary particle formation. Sajjadi^[37] reported that particle coagulation occurs if the particle coverage drops

below 25%, while new particles can be stabilized above a surface coverage of 55%. This value strongly depends on the type of surfactant used to stabilize the polymer particles.

Apparently, the surface area of the seeds must exceed a critical value to suppress the nucleation of new particles. If the seed particle concentration does not allow exceeding this critical value, small particles may be formed in a later stage of reaction, producing polymodal size distributions.^[38] For this reason, as seed particle size is increased, higher solids contents are needed to suppress secondary nucleation. At some point, the required solids contents are beyond physical limits, and secondary nucleation can no longer be avoided. Schmutzler^[39] suggested that the occurrence of new particle generation during seeded emulsion polymerizations of vinyl acetate drops to zero if the number of seed particles exceeds 10^{16} L^{-1} . Considering the homogeneous nucleation model, Thickett and Gilbert^[40] found this limit to be only of 10^{14} L^{-1} for styrene. Butucea et al.^[41] determined from experimental data on seeded emulsion polymerization of vinyl chloride that:

- There is a minimum surface area of polymer seed particles necessary to capture all ion-oligoradicals generated in aqueous phase at a given initiator concentration. Beyond this value, no more particles are generated.
- There is a maximum critical concentration of initiator per unit surface of polymer particle under which the formation of new polymer particles is avoided.

Sudol et al.^[42] reported that the preparation of monodisperse latexes by successive seeding from a small particle size to sizes greater than $1 \mu\text{m}$ is difficult using aqueous phase initiators because of the formation of new stable particles during polymerization. Cook et al.^[43] stated that latex particles of up to $2 \mu\text{m}$ can be made by standard emulsion polymerization methods, but attempts at larger sizes usually results in a crop of smaller particles or coagulation of the latex.

A monomer with slower aqueous-phase propagation frequency would allow more time for entry or termination events to occur before the radical propagates sufficiently to become a new particle.^[44] Therefore, long reaction times allow for the collection of the particles by the latex, while starved feed conditions ensure that there is no ready supply of monomer to promote growth of newly nucleated particles.^[43]

Another strategy for avoiding secondary nucleation is the use of an organic-phase initiator.^[5] When an oil-soluble initiator is used, the particles that form in water have limited colloidal stability because they do not have ionic stabilization and thus are more likely to be captured by latex particles.^[43]

Once the polymer formed is successfully incorporated into the seed particles, the internal morphology of the particles will be determined by many factors. These factors fall into two broad categories: *Thermodynamic* and *kinetic*. Thermodynamic factors determine the equilibrium morphology of the final composite particle, while kinetic factors determine the ease with which the thermodynamically favored morphology can be achieved. The most important factors determining particle morphology are

summarized in Table 2.2. Some of the most commonly obtained polymer particle morphologies are presented in Figure 2.3.

Table 2.2 Thermodynamic and kinetic factors determining particle morphology^[11,45]

Thermodynamic Factors	Kinetic Factors
Sequence and amount of monomer fed into the system	Method of addition of monomer
Hydrophilicity of monomers (and polymers)	Molecular weight of polymers
Surface and interfacial tensions	Viscosity of polymers
Compatibility between polymers	Crosslinking
Polymerization temperature	

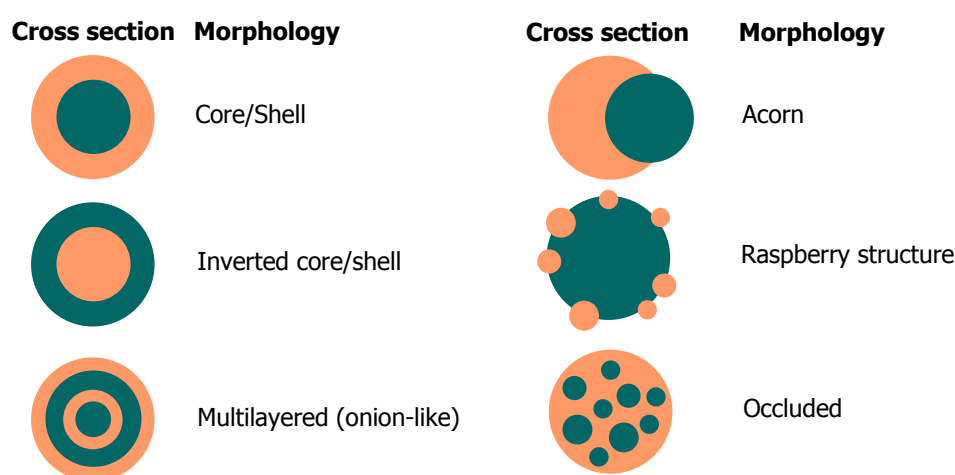


Figure 2.3 Common examples of composite polymer particle morphologies

Thermodynamic control of particle morphology is driven by the Gibbs free energy of the system, and in particular, by the interfacial Gibbs free energy contribution. Thus, the thermodynamically preferred morphology will be the one that exhibits the minimum interfacial free energy. On the other hand, kinetic control of morphology is largely due to the slow diffusion rates of the reacting polymer radicals within the latex particles during the polymerization of the successive stages. By reducing the chain mobility, the particle morphology will be determined by the order of addition of the components. By allowing chain mobility, the particle morphology with the lowest free energy change will prevail.^[10,29,46] The interfacial tension between the various polymer phases in the composite latex particles plays a very important role in determining their final morphology. Sundberg and coworkers^[12,15] found that by simply varying the type of surfactant used in the emulsion, the particle morphology can change in agreement with thermodynamic predictions.

Lee and Rudin^[13] found that in two-stage latexes where the first polymer is more hydrophilic than the second and there is enough mobility in the system, inversion of the core and shell can occur. The degree of phase mobility is influenced by several factors such as the inherent glass transition temperature of the polymers, the amount of low molecular weight species present (which may act as plasticizer agents), and the degree of crosslinking in the polymers.^[47] The particle structure is

particularly sensitive to the level of crosslinking. At a certain degree of crosslinking the elastic forces of the gel counteract the interfacial forces; above this point, the morphology of the particles cannot be thermodynamically controlled.^[14,45] For this reason, crosslinking is used to increase the kinetic barrier to phase inversion and create more stable non-equilibrium morphologies. If crosslinking is not possible (e.g. for some applications where the molecular weight of the polymer particles must be controlled), starve feeding of monomers is used to obtain non-equilibrium particle morphologies. In this method, each stage monomer is added at a rate which is less than the corresponding polymerization rate.^[14] The polymer layers accumulate in the order of their formation and result in multilayered composite polymer particles even if the morphology is thermodynamically unstable.^[48]

Some representative examples of structured polymer particles are the following:

- "Core-shell" poly(butyl acrylate) core/polystyrene shell polymer particles for improved impact strength.^[8,43]
- "Core-shell" composite particles^[47,49] and "Onion-like" particles of alternate layers^[45,48,50] of poly(methyl methacrylate) and polystyrene.
- Multilayered particles of poly(vinylidene chloride) and an ester of an ethenoid acid for paper coatings resistant to the passage of water and other vapors, gases, greases and oils.^[51]
- Incorporation of hard, relatively high- T_g polymer such as polystyrene or poly(methyl methacrylate) into poly(vinyl acetate) polymer as an approach to improve heat and creep resistance of adhesives while retaining their film-forming properties.^[7,34]

In Appendix A, various seeded emulsion polymerization experimental procedures are presented leading to the formation of different types of structured polymer particles.

Chapter 3

Methods

3.1. Numerical Simulation Methods

Methods of numerical simulation have found a wide application in the investigation of equilibrium and kinetic properties in molecular systems. Recently, they have also been applied to colloids to overcome the known difficulties associated with the necessity of taking into account the interactions between many particles.^[52] Some of the most important simulation methods relevant to heterophase polymerization include: Molecular Dynamics Simulation (MD), Brownian Dynamics Simulation (BD), Dissipative Particle Dynamics (DPD), kinetic Monte Carlo Simulation (kMC), Quantum Mechanics (QM), Monte Carlo (MC) Simulation, Lattice-Boltzmann (LB), Coarse-grained (CG) Simulation and Finite Element Methods (FEM). Properly executed computer simulations can provide the solution to any well-defined problem, thus, they can be used to test the validity and accuracy of analytic theories. Of course, the correctness of the simulation results depends on the use of the correct values of the simulation parameters, which can only be established by comparison with real experiments. In the present Section, the most important numerical simulation methods used to investigate the synthesis of structured polymer particles in heterophase polymerization are presented.

3.1.1. Molecular Dynamics Simulation

Molecular Dynamics (MD) Simulation is a method used to follow the trajectories and velocities of an ensemble of atoms or molecules subject to interatomic or intermolecular forces for a certain period of time. Although the atoms and molecules are composed of quantum particles, their motion can be satisfactorily described by the classical *Newton's equations of motion*.^[53,54]

$$\frac{dv_i}{dt} = \frac{1}{m_i} \sum_{j \neq i} F_{ij} \quad (3.1)$$

$$\frac{dx_i}{dt} = v_i \quad (3.2)$$

where v_i is the velocity, m_i is the mass and x_i is the position of the i -th molecule, F_{ij} is the interaction force between the i -th and j -th molecules, and t is the time. Additional external or internal (mean field) forces can also be considered.

By means of MD simulation, different equilibrium and non-equilibrium properties of a system can be determined. Some relevant examples include: the conformation of a molecule in a certain medium, the calculation of transport properties of the system (viscosity, thermal conductivity and diffusion) and the estimation of the total energy of the system (potential energy + kinetic energy).

The MD algorithm consists on three different stages: *Initialization*, *equilibration* and *production*. During initialization, the following simulation conditions must be defined: Size and geometry of the simulation cell, type of boundary conditions, type of simulation ensemble, number of molecules in the simulation cell, initial positions and velocities of the molecules, number of equilibration and production steps, and the type, parameters and range of the intermolecular interaction forces. The usual geometry used in MD simulation is the cubic cell, and normally the boundary conditions are assumed to be periodic. In a system under periodic boundary conditions, a molecule abandoning the simulation cell through one face of the simulation cell will immediately re-appear at the opposite side. In a similar way, the molecules close to the boundary are influenced by the interaction forces of the molecules at the opposite side of the simulation cell. If strong spatial gradients are present in the system, they must be considered in the determination of the new position and velocity of the molecule after crossing the boundary. The use of periodic boundary conditions allows the use of relatively small simulation cells without imposing artificial boundaries to the system. The size of the simulation cell (and therefore, the number of molecules simulated) is usually determined as a compromise between the computational power capability and the desired accuracy and reproducibility of the results, both increasing with the number of molecules simulated.

Different types of ensembles can be simulated in MD. Perhaps the most commonly used ensembles are the canonical or NVT ensemble (constant number of molecules N , volume V and temperature T) and the microcanonical or NVE (constant number of molecules N , volume V and energy E). However, it is also possible to simulate Grand-canonical or μ VT (constant chemical potential μ , volume and temperature), isothermal-isobaric or NpT (constant number of molecules, pressure p and temperature), and isoenthalpic-isobaric or NpH ensembles (constant number of molecules, pressure and enthalpy H), by using adequate algorithms for solving the equations of motion. The initial positions of the molecules can be set randomly or they can be placed in a lattice in the simulation cell. The last method has the advantage that molecular overlapping can be easily avoided, but in this case, larger equilibration times may be required. The initial velocities can be determined from a Maxwell-Boltzmann distribution function or a Gaussian distribution function. After a certain simulation time, however, a Maxwell-Boltzmann velocity distribution is obtained independently of the initial distribution.

There are different types of intermolecular forces. According to their nature, intermolecular forces can be classified into three categories:^[55-57]

- *Electrostatic or Coulomb forces* between charged particles (ions) and between permanent dipoles, quadrupoles, and higher multipoles. They arise from the interaction between the

static charge distributions of the two molecules. They are strictly pairwise additive and may be either attractive or repulsive.

- *Induction forces* between a permanent dipole (or multipole) and an induced dipole, that is, a dipole induced in a molecule with polarizable electrons. The dipole moments are induced in atoms and molecules by the electric fields of nearby charges and permanent dipoles. Induction effects arise from the distortion of a particular molecule by the electric field of all its neighbors, and are always attractive and non-additive. The polarizability represents how easily the molecule's electrons can be displaced by an electric field.
- *Quantum mechanical forces*, which give rise to *specific or chemical forces* (covalent or chemical bonding, hydrogen bonds and charge-transfer complexation), *dispersion forces* and to the *repulsive steric or exchange interactions* (due to *Pauli's exclusion principle*) that balance the attractive forces at very short distances. Dispersion forces are always attractive and arise because the charge distributions of the molecules fluctuate as electrons move.

The interaction potential (ψ) between two molecules (or particles in general), also known as *pair potential*, is related to the force between the two molecules (F) by:

$$\vec{F}(r_{ij}) = -\frac{d\psi(r_{ij})}{dr_{ij}} \hat{r}_{ij} \quad (3.3)$$

where r_{ij} is the intermolecular separation. The work that must be done to separate two molecules from the intermolecular distance r_{ij} to infinite separation is $-\psi(r_{ij})$. By convention, attraction forces (and potentials) are negative and repulsion forces (and potentials), positive.

Purely electrostatic interaction potentials can be determined using *Coulomb's equation*:

$$\psi^C(r_{ij}) = \frac{q_i q_j}{4\pi\epsilon_0 r_{ij}} \quad (3.4)$$

where q_i and q_j are the net electric charges of molecules i and j respectively, and ϵ_0 is the dielectric permittivity of free space ($8.854 \times 10^{-12} \text{ C}^2/\text{Jm}$).

For non-ionic molecules, there are three main types of attractive interactions: *Keesom* (dipole-dipole) interactions (Eq. 3.5), *Debye* (dipole-non polar) interactions (Eq. 3.6) and *London dispersion* (non polar-non polar) interactions (Eq. 3.7). All these interactions are usually denoted as *van der Waals* interactions and have in common the same dependence with respect to the intermolecular separation (r_{ij}^{-6}):

$$\psi^K(r_{ij}) = -\frac{u_i^2 u_j^2}{3(4\pi\epsilon_0)^2 k_B T} \frac{1}{r_{ij}^6} \quad (3.5)$$

$$\psi^D(r_{ij}) = -\frac{u_i^2 \alpha_j}{(4\pi\epsilon_0)^2} \frac{1}{r_{ij}^6} \quad (3.6)$$

$$\psi^L(r_{ij}) = -\frac{3 h \nu_{ij} \alpha_i \alpha_j}{4 (4\pi\epsilon_0)^2} \frac{1}{r_{ij}^6} \quad (3.7)$$

where u is the electric dipole moment, k_B is Boltzmann's constant (1.381×10^{-23} J/K), α is the electric polarizability, and ν is the electronic ionization frequency. The van der Waals interaction is always attractive, and can in general be expressed as:

$$\psi^{vdW}(r_{ij}) = -\frac{C}{r_{ij}^6} \quad (3.8)$$

where C is the corresponding van der Waals interaction parameter. The repulsive interaction for non-ionic molecules is given by an exponential potential of the form:

$$\psi^R(r_{ij}) = A e^{-Br_{ij}} \quad (3.9)$$

where A and B are interaction parameters. The general expression for the interaction potential is then:

$$\psi^T(r_{ij}) = \psi^C(r_{ij}) + \psi^K(r_{ij}) + \psi^D(r_{ij}) + \psi^L(r_{ij}) + \psi^R(r_{ij}) \quad (3.10)$$

It is also possible to include additional potentials in equation 3.10, such as external potentials (e.g. gravity, electromagnetic fields, etc.), or specific or chemical interaction potentials.

For non-ionic molecules, a commonly used approximation is the *Lennard-Jones interaction potential* (equation 3.11), where the exponential repulsion interaction is approximated by a 12th-power of the intermolecular distance:

$$\psi^{LJ}(r_{ij}) = 4\epsilon \left[\left(\frac{\sigma}{r_{ij}} \right)^{12} - \left(\frac{\sigma}{r_{ij}} \right)^6 \right] \quad (3.11)$$

where σ is the equilibrium distance and ϵ is the energy well depth. The 6th power used for the attractive potential is very reasonable, based on the dependence of the van der Waals interactions. However, the use of a 12th power repulsive potential not always is a good approximation. Sometimes, it is better to use a *Buckingham* interaction potential, using an exponential repulsive interaction together with the van der Waals attractive interactions:

$$\psi^B(r_{ij}) = \epsilon \left[\frac{6}{\alpha - 6} e^{\alpha \left(1 - \frac{r_{ij}}{\sigma} \right)} - \frac{\alpha}{\alpha - 6} \left(\frac{\sigma}{r_{ij}} \right)^6 \right] \quad (3.12)$$

where α is an interaction parameter representing the steepness of the repulsive interaction.

During the equilibration and production stages of MD simulation, the net force acting on each molecule is calculated from the interaction pair potentials and then, the positions and velocities of the molecules are obtained from the equations of motion. The only difference between the equilibration and the production stages is that during the production, additional properties of the system (e.g. transport properties, thermodynamic properties, molecular conformations, etc.) are calculated. A representative flow diagram for a MD simulation algorithm is presented in Figure 3.1. The numerical solution of the equations of motion is usually made using an efficient method called *Verlet's algorithm*, obtained after some mathematical treatment of Newton's equations of motion:

$$r_i(t + \Delta t) = 2r_i(t) - r_i(t - \Delta t) + \frac{\Delta t^2}{m_i} \sum_{j \neq i} F_{ij} \quad (3.13)$$

$$v_i(t) = \frac{r_i(t + \Delta t) - r_i(t - \Delta t)}{2\Delta t} \quad (3.14)$$

For the canonical (NVT) ensemble, the average kinetic energy of the molecules should correspond to the temperature of the system. Therefore, the following condition should be met:

$$\frac{\sum_{i=1}^N m_i v_i^2}{2N} = \frac{3}{2} k_B T \quad (3.15)$$

In order to fulfill equation 3.15, different modified equations of motion can be used, usually called *thermostats*. The most commonly used thermostats are the *Anderson* and the *Nosé-Hoover* thermostats.^[54]

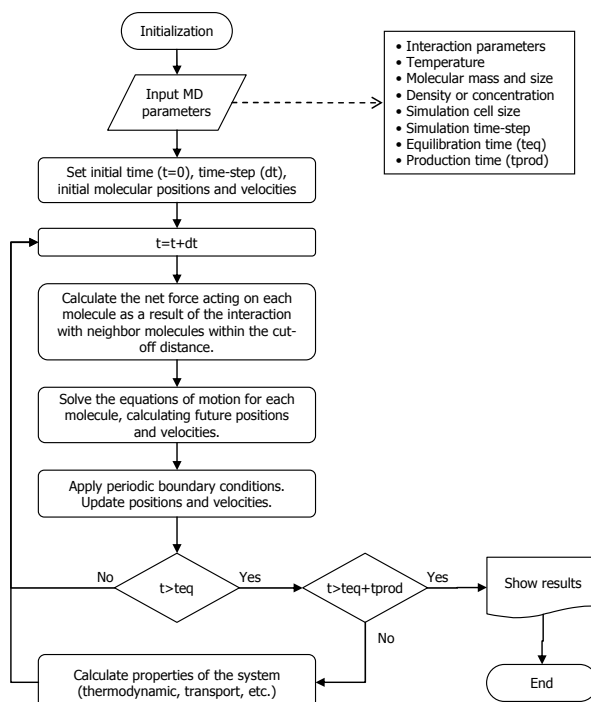


Figure 3.1 Molecular Dynamics Simulation algorithm for a canonical ensemble (NVT)

Given that the computational effort grows exponentially with the size of the system, for large systems an additional approximation is made in order to obtain more efficient simulations consisting in the incorporation of a cut-off in the range of the interaction forces:

$$F(r_{ij}) = \begin{cases} 0 & r_{ij} > r_c \\ F(r_{ij}) & r_{ij} < r_c \end{cases} \quad (3.16)$$

3.1.2. Brownian Dynamics Simulation

As a result of the multiple collisions between neighboring molecules, the force exerted on a single molecule will vary in direction and magnitude throughout time. It is possible to describe the force as the sum of two components, an average net force and a random force, as follows:

$$\sum_{j \neq i} \vec{F}_{ij}(t) = \langle \vec{F} \rangle + \vec{X}(t) \quad (3.17)$$

where the random force X has an average value of zero. The average net force is responsible for the ballistic, center of mass or *convective* motion of the molecules, while the random force causes a *random motion* giving rise to *diffusion*. If the magnitude of the average net force is much larger than the magnitude of the random force contribution, the diffusive behavior becomes unimportant.

The random motion is usually also denoted as *random walk* or *Brownian motion* because it was first evidenced and investigated by the botanist Robert Brown in 1827.^[58] After a series of experiments, he concluded that this random motion was not related to living motion since it could be observed also in suspensions of inorganic materials. An example of the trajectory described by a particle under Brownian motion in three dimensions is presented in Figure 3.2.

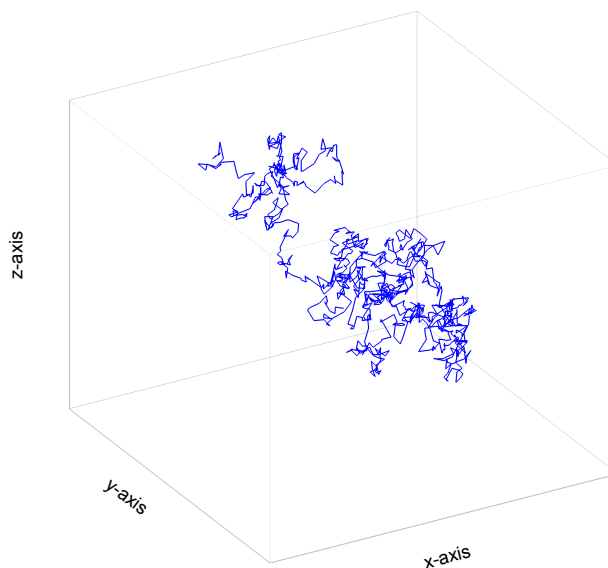


Figure 3.2 Trajectory obtained by 3-dimensional Brownian motion

Diffusion is the process by which matter is transported from one part of a system to another as a result of random molecular motions. As a consequence of random molecular motion, heat can also be transferred by a process called *conduction*, which is equivalent to the transfer of mass by diffusion. This equivalence was recognized by Fick in 1855^[59] who set the quantitative basis of diffusion by adopting the mathematical treatment of heat conduction previously derived by Fourier.^[60] For isotropic substances, that is, for substances where the structure and properties in the neighborhood of any point are the same, the motion of a single molecule has no preferential direction. If we consider a system with two zones of different concentration of a certain type of molecules, the total number of molecules diffusing from one zone to the other at a given instant will be proportional to the number of molecules present at each side of the interface. It is therefore evident that there will be a *net flux* of molecules from the zone of higher molecular concentration to the zone of lower concentration, and this flux will be proportional to the difference in concentration. It is important to notice that the driving force for diffusion is the random molecular motion and not the gradient in concentration, even though the latter determines the net flux of molecules in purely diffusive systems (or the gradient in chemical potential when external forces are present). For isotropic substances the net flux of molecules is proportional to the concentration gradient and the proportionality constant is the *diffusion coefficient* or *diffusivity* of the molecules in the system (Fick's first law of diffusion):

$$\vec{J} = -D \cdot \vec{\nabla} C \quad (3.18)$$

where J is the rate of transfer of molecules per unit area of a section (net flux), ∇C is the concentration gradient of diffusing substance and D is the diffusion coefficient. The negative sign arises because the net flux of molecules takes place from the higher to the lower concentration region. The magnitude of the diffusion coefficient will depend on the intermolecular forces present in the system.

For an anisotropic medium, the diffusion properties also depend on the direction in which they are measured, and the diffusion coefficient is actually a function of the local spatial composition around the diffusing molecule. Some common examples of anisotropic media are crystals, textile fibers, and polymer films in which the molecules have a preferential direction of orientation. In these cases, equation 3.18 remains valid but the diffusion coefficient is a tensor of rank 2 and not a scalar. It is possible to relate the rate of change in the concentration of the diffusing substance with the net diffusive flux J , simply from the continuity equation. By making use of the first law, Fick's second law of diffusion can be obtained:

$$\frac{\partial C}{\partial t} = -\vec{\nabla} \cdot \vec{J} = D \cdot \nabla^2 C \quad (3.19)$$

If the effect of composition on the diffusion coefficient can not be neglected, Fick's laws of diffusion become:

$$\bar{J} = -\bar{\nabla}[D(C) \cdot C] \quad (3.20)$$

$$\frac{\partial C}{\partial t} = \nabla^2[D(C) \cdot C] \quad (3.21)$$

For non-zero average net interaction forces, the net flux of molecules depends on the *chemical potential* rather than on the molecular concentration. The chemical potential or *cohesive energy* (μ) represents the total free energy of a molecule, and it includes the interaction potentials as well as the contribution associated with its thermal energy.

The development of a consistent theory of Brownian motion began with the early contributions of Albert Einstein^[61] and Marian von Smoluchowski.^[62] In their pioneering work they were able to relate the microscopic Brownian motion observed in colloidal particles with the macroscopic molecular Fickian diffusion coefficient.

There are some important considerations in Einstein's solution to the problem of Brownian motion:

- The motion is caused by the exceedingly frequent impacts on the particle of the incessantly moving molecules of fluid in which it is suspended.
- The motion of these molecules is so complicated that its effect on the particle can only be described probabilistically in terms of exceedingly frequent statistically independent impacts.
- Each individual particle executes a motion which is independent of the motions of all other particles.
- The movements of a given particle at different time intervals are independent processes.

Einstein's analysis led to the following conclusion:

$$\frac{\partial f(x,t)}{\partial t} = D \frac{\partial^2 f(x,t)}{\partial x^2} \quad (3.22)$$

where $f(x,t)$ is the probability function of finding a particle at position x in time t . This expression is equivalent to Fick's second law of diffusion in one dimension (Eq. 3.19), considering that the probability function is proportional to the concentration of the diffusing compound. This partial differential equation can be solved analytically for the case of diffusion from a single point (neglecting the interaction between the diffusing particles). The result is the Gaussian distribution function:

$$f(x,t) = \frac{n}{\sqrt{4\pi D}} \frac{\exp\left(-\frac{x^2}{4Dt}\right)}{\sqrt{t}} \quad (3.23)$$

such that:

$$\langle x^2 \rangle = 2Dt \quad (3.24)$$

Equation 3.24 is known as Einstein's diffusion equation, and is valid for the diffusion in one dimension. The generalization to three dimensions is simply:

$$\langle r^2 \rangle = 6Dt \quad (3.25)$$

where r is the distance to the initial position of the molecules.

The diffusion equations derived from Smoluchowski's treatment are mathematically identical to those obtained by Einstein. However, Smoluchowski considered a concentration-dependent diffusion coefficient, while Einstein's equation defines a constant diffusion coefficient.

Some time after Einstein's original derivation, Langevin presented an alternative method which was quite different from Einstein's and, according to him, "infinitely more simple". Langevin expressed the equation for Brownian motion as:^[63]

$$m \frac{d^2 x}{dt^2} = -6\pi\eta a \frac{dx}{dt} + X \quad (3.26)$$

where m is the mass of the Brownian entity (particle or molecule), a is its hydrodynamic radius, x is its position at a given time t , η is the viscosity of the continuous phase and X is a random fluctuating force which is the result of the collisions of the Brownian entity with the surrounding molecules of the continuous phase.

The basic assumptions in Langevin's approach are the following:

- There are two forces acting on the particle: a viscous drag and a fluctuating force X which represents the incessant impacts of the molecules of the liquid on the Brownian particle. The fluctuating forces should be positive and negative with equal probability.
- The mean kinetic energy of the Brownian particle in equilibrium should reach, in one dimension, a value of:

$$\left\langle \frac{1}{2} m v^2 \right\rangle = \frac{1}{2} k_B T \quad (3.27)$$

- The random force has an average mean value of zero and is independent of its previous values. That is, $\langle X \rangle = 0$ and $\langle X(t)X(t') \rangle = \Gamma \delta(t-t')$, where $\Gamma = 12\pi\eta a k_B T / \Delta t$ and δ is Dirac's delta function. This expression is usually known as the *Fluctuation-Dissipation Theorem*.

Langevin solved equation 3.26 and found that:

$$\frac{d(x^2)}{dt} = \frac{kT}{3\pi\eta a} + C \exp(-6\pi\eta a t / m) \quad (3.28)$$

where C is an arbitrary constant. Langevin estimated that the decaying exponential approaches zero with a time constant of the order of 10^{-8} s, which for any practical observation at that time, could be neglected. Integrating the last equation, it is found that

$$\langle x^2 \rangle = \frac{kT}{3\pi\eta a} t \quad (3.29)$$

which corresponds to the expression deduced by Einstein, provided that

$$D = \frac{kT}{6\pi\eta a} \quad (3.30)$$

This last expression is usually denoted as the Stokes-Einstein equation.

The numerical solution of Langevin's equation for Brownian motion (Eq. 3.26) is known as *Langevin Dynamics* simulation. If the system is assumed to relax completely, the solution of the equations of motion corresponds to the method of Brownian Dynamics (BD) simulation. There are several techniques for the numerical solution of Brownian motion.^[64] One of the most representative methods is the Monte Carlo random flight (MCRF) algorithm.^[65,66] The simulation is restricted to a small cell (usually cubic) containing a given number of Brownian entities. Periodic boundary conditions are applied to take into account the effect of large scale systems. In the MCRF method, the diffusive displacement on each direction for each molecule or particle at each time-step dt is obtained from a normal Gaussian distribution with mean zero and variance $\sqrt{2Ddt}$.

As a first step, the initial positions of the Brownian entities are randomly determined considering a uniform probability distribution in the simulation cell, always checking that particle superposition is not taking place. The Brownian motion of the Brownian entities is then simulated in time-steps given by

$$dt = \max\left(\alpha \frac{d_{min}^2}{D}, \frac{mD}{k_B T}\right) \quad (3.31)$$

where d_{min} is the minimum separation between the surface of two entities, D is the diffusion coefficient of the Brownian entities, α is a "damping" factor which is selected based on the probability of collision during the simulated time-step dt , m is the mass of the entities, T is the temperature of the system and k_B is the Boltzmann constant. The term $mD/k_B T$ expresses the relaxation time for the motion of the Brownian entities, which is the time resolution of the MCRF simulation method, and is obtained from equations 3.28 and 3.30. When the separation between particles is large, the computation efficiency can be improved by increasing the time step of the simulation proportionally to d_{min}^2/D .^[66] This means that the simulated time-step will be proportional to the squared distance between the two closest entities but the minimum time-step considered will be that of the corresponding relaxation time of the momentum of the Brownian entities. The probability of collision between the entities is related to the damping factor α , according to the expression $\alpha = (2Z^2)^{-1}$, where Z is the inverse of the normal cumulative probability of collision and corresponds to the closest distance between entities expressed in number of standard deviations. Thus, in order to obtain a collision probability of the order of 10^{-7} for time-steps larger than the relaxation time, a value of $\alpha = 0.01852$ is used.^[67] This value guarantees that practically every collision will occur with a resolution

corresponding to the momentum relaxation time. At each time-step, the movement of the entities in each direction (in rectangular coordinates) is calculated as:

$$dx = \xi_G \sqrt{2D_r dt} \quad (3.32)$$

where ξ_G is a random number obtained from a Gaussian distribution with mean 0 and variance 1.

The flowchart for the MCRF algorithm for BD simulation is presented in Figure 3.3.

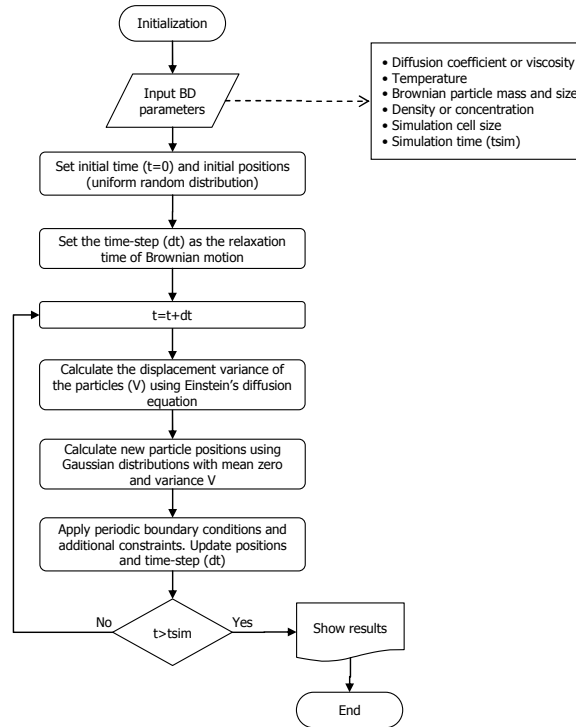


Figure 3.3 Monte Carlo Random Flight (MCRF) Algorithm

According to Langevin's equation (Eq. 3.26), external force fields and interaction potentials are neglected in the description of molecular Brownian motion, although the interaction potentials are implicitly considered in both the drag force and the random force through the viscosity term. It is possible to explicitly consider additional non-zero net forces in Eq. 3.26 and perform BD simulation assuming a net drift in the system as a result of these forces. This is the typical situation of the Brownian motion of a molecule or molecular cluster at the interface between two different phases. In the bulk of each phase, such molecule or cluster has a corresponding diffusion coefficient but at the interface the behavior may be completely different because the molecules at the interface are subject to different forces and thus, they have different mobility compared to the molecules in the bulk of each phase. As an approximation, only one interfacial molecular layer is considered. This situation is depicted in Figure 3.4. Assuming negligible differences in viscosity between both phases, the equation of motion in the direction normal to the interface (\vec{x}) can be expressed as:

$$m \frac{d^2 \vec{x}}{dt^2} = -6\pi\eta d_m \frac{d\vec{x}}{dt} + \vec{F} \quad (3.33)$$

where \vec{F} is the force acting on the molecule at the interface, and η is the bulk viscosity of the phase in the direction of the motion of the molecule.

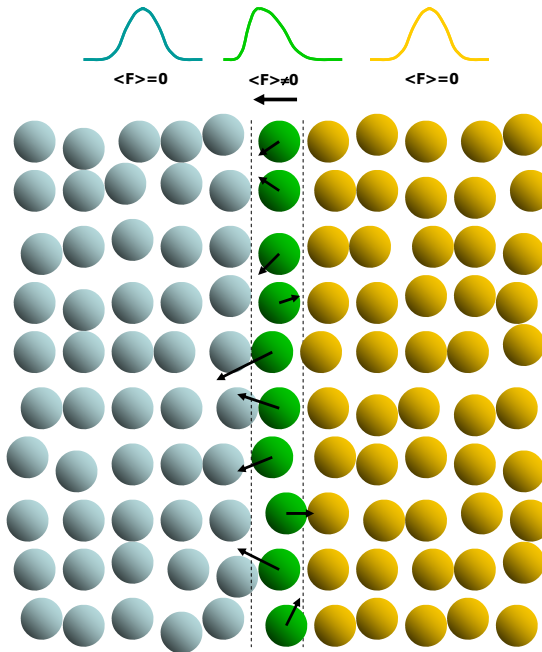


Figure 3.4 Diffusion of molecules at a flat interface

Averaging equation 3.33 and using equation 3.30:

$$m \frac{d^2 \langle \bar{x} \rangle}{dt^2} = -\frac{kT}{D} \frac{d \langle \bar{x} \rangle}{dt} + \langle \vec{F} \rangle \quad (3.34a)$$

$$\frac{d \langle \bar{v} \rangle}{dt^2} + \frac{kT}{mD} \langle \bar{v} \rangle = \frac{\langle \vec{F} \rangle}{m} \quad (3.34b)$$

where D is the diffusion coefficient of the molecule. Solving equation 3.34b, the following expression for the average velocity of the molecules at the interface is obtained:

$$\langle \bar{v} \rangle = \left(\frac{D}{kT} \right) \left(\langle \vec{F} \rangle - C m \exp \left(-\frac{kT}{mD} t \right) \right) \quad (3.35)$$

where C is an integration constant. Considering times longer than the relaxation time, the average drift experienced by the molecules is obtained:

$$\langle \bar{v} \rangle = \frac{d \langle \bar{x} \rangle}{dt} = \frac{D \langle \vec{F} \rangle}{kT} \quad (3.36)$$

The molecular velocity can be calculated as the sum of two contributions, the drift at the interface and Brownian motion:

$$\vec{v} = \langle \vec{v} \rangle + \vec{v}_{BM} \quad (3.37)$$

where \vec{v}_{BM} is described by a Gaussian distribution function with mean zero and standard deviation $\sqrt{2D/\Delta t}$.

Integrating equation 3.37 results:

$$\Delta \vec{x} = \frac{D \langle \vec{F} \rangle}{kT} \Delta t + \xi \sqrt{2D\Delta t} \hat{u}_x \quad (3.38)$$

where ξ is a random number obtained from a Gaussian distribution of mean zero and standard deviation 1, and \hat{u}_x is the unit vector in the positive direction. If the average net force acting on the molecules at the interface is zero, the behavior predicted by pure Brownian motion is obtained. In this case, the probability for a single molecule to move in the positive (\hat{u}_x) or negative ($-\hat{u}_x$) direction is 0.5. If the average net force is not zero, the molecules will have a higher probability of moving in the direction of the net force. Let us now consider a net average force acting on the molecules at the interface in the negative direction: $\langle \vec{F} \rangle = -F\hat{u}_x$, being $F > 0$. The probability of a molecule moving in the positive direction will be given by:

$$P(\Delta x > 0) = P\left(\xi > \frac{F}{2kT} \sqrt{2D\Delta t}\right) = 1 - P\left(\xi \leq \frac{F}{2kT} \sqrt{2D\Delta t}\right) \quad (3.39a)$$

$$P(\Delta x > 0) = \frac{1 - \text{erf}\left(\frac{F}{2kT} \sqrt{2D\Delta t}\right)}{2} \quad (3.39b)$$

The probability of a molecule moving in the positive direction subject to a net average force in the negative direction, relative to the probability under pure Brownian motion is:

$$f = \frac{P(\Delta x > 0)}{1/2} = 1 - \text{erf}\left(\frac{F}{2kT} \sqrt{2D\Delta t}\right) \quad (3.40a)$$

For relatively low drift values, the term $\sqrt{2D\Delta t}$ can be regarded as the net displacement of the molecule, and therefore:

$$F\sqrt{2D\Delta t} \approx F\Delta x = E_{transfer} \quad (3.41)$$

$E_{transfer}$ is the energy of phase transfer of the molecule, and corresponds to the work made by the system to displace the molecule a distance Δx by means of the force F . Therefore:

$$f \approx 1 - \operatorname{erf}\left(\frac{E_{\text{transfer}}}{2kT}\right) \quad (3.40b)$$

In addition, as can be seen in Figure 3.5, the efficiency function $f=1-\operatorname{erf}(y)$ can be approximated by an exponential function of the form (3.42), while the approximation $f=\exp(-y)$ is only valid for very low values of y .

$$f = 1 - \operatorname{erf}(y) \approx \frac{2}{\sqrt{\pi}} \exp(-2y) \quad (3.42)$$

From Eq. 3.41:

$$f \approx \frac{2}{\sqrt{\pi}} \exp\left(-\frac{E_{\text{transfer}}}{kT}\right) \quad (3.40c)$$

which is similar to the usual expression used to describe the efficiency of a process limited by an energy barrier. Equation 3.40c, valid for only one dimension, implies that the energy barrier against phase transfer can be supplied by the kinetic energy of the molecules. Since thermal motion takes place in three dimensions, the corrected expression for the efficiency factor is:

$$f_{3D} \approx \frac{2}{\sqrt{\pi}} \exp\left(-\frac{E_{\text{transfer}}}{3kT}\right) \quad (3.40d)$$

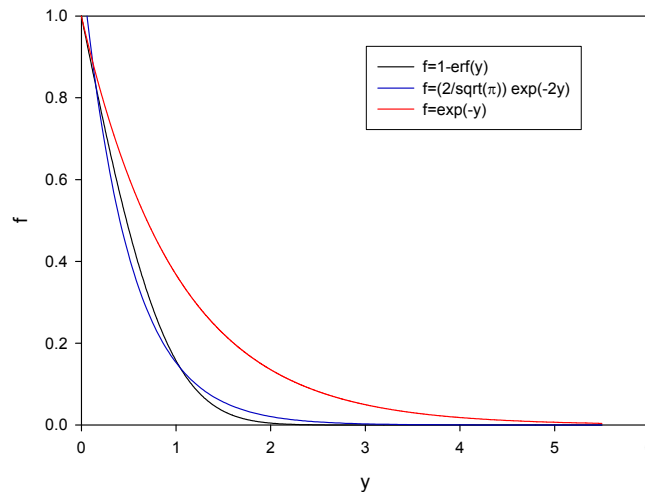


Figure 3.5 Approximation of the efficiency factor f by exponential functions

Equation 3.41 also indicates that the activation energy for the transfer of a molecule across an interface is proportional to the net average force opposing to the transfer acting at the interface. At a molecular scale, this force can be obtained from the interaction potentials between the molecules at the interface and their surrounding molecules. On the other hand, thermodynamics can also be used to calculate the energy as the function of the interfacial tension between the two phases. Finally, it is

important to notice that the mobility of the molecules is reduced at the interface as a result of the energy barrier for phase transfer.

Another important feature of BD simulation is the possibility of performing simulations on different length and time scales, depending on the definition of the Brownian entity. The exact functions used for the forces will depend also on the length and time scales selected. For example, if the molecular scale is considered, the conservative forces can be represented by the Lennard-Jones (Eq. 3.11) or the Buckingham interaction potential (Eq. 3.12). However, for larger clusters of molecules, a Hamaker-type approximation for the interaction potentials may be better suited. The Hamaker constant between two bodies is defined as:

$$A = \pi^2 \rho_1 \rho_2 C \quad (3.43)$$

where ρ_1 and ρ_2 are the densities of the two bodies, and C is the interaction parameter of the van der Waals potential (eq. 3.8).

The interaction potential of attraction between two bodies can be obtained as a function of the Hamaker constant, and the geometry of the system. Some examples of these expressions are presented in Table 3.1.

Table 3.1 Hamaker-type interaction potentials for different geometries^[68]

Geometry	Interaction potential
Two spheres of radii R_1, R_2 , at large surface separation d	$-\frac{A}{6} \left[\frac{2R_1R_2}{d^2 + 2d(R_1 + R_2)} + \frac{2R_1R_2}{d^2 + 2d(R_1 + R_2) + 4R_1R_2} + \ln \left(\frac{d^2 + 2d(R_1 + R_2)}{d^2 + 2d(R_1 + R_2) + 4R_1R_2} \right) \right]$
Two spheres at close distance ($R \gg d$)	$-\frac{A}{6} \frac{R_1R_2}{d(R_1 + R_2)}$
Two plates of equal thickness δ	$-\frac{A}{12\pi} \left[\frac{1}{d^2} + \frac{1}{(d + 2\delta)^2} - \frac{2}{(d + \delta)^2} \right]$
Two identical blocks ($\delta \rightarrow \infty$)	$-\frac{A}{12\pi d^2}$

Nowadays, several important applications of the interaction between Brownian entities (such as radicals, macromolecules or colloidal particles) can be found in the literature.^[65,69] BD simulation is perhaps the most suitable method for the simulation of systems at the colloidal scale, and it is also useful for the simulation of molecules in solution.

3.1.3. Kinetic Monte Carlo (Stochastic) Simulation

The kinetic Monte Carlo (kMC) method, also known as Stochastic Simulation Algorithm (SSA), was formally introduced by Gillespie^[70] as a method for obtaining singular realizations of processes described by the Chemical Master Equation (CME), as an alternative to the deterministic solutions obtained from the Rate of Reaction Equations (RRE). In the thermodynamic limit of a system, that is, for a system composed of an extremely large number of molecules, the results obtained using both kMC and RRE are identical.^[71] However, chemical reacting systems involving infrequent chemical

reactions or chemical species in limited amounts are better represented by stochastic than by deterministic methods. One main disadvantage of the original SSA formulation is that it is a very inefficient method for simulating stiff chemical reactions. Stiffness is observed when at least one reaction pathway is orders of magnitude more frequent than the others. Several approaches, including the hybrid stochastic method, have been proposed to overcome stiffness using stochastic algorithms.^[72,73]

In the original SSA formulation (also known as direct method), the time at which the next stochastic event occurs (τ) can be calculated using the following equation:

$$\tau = -\frac{\ln(\xi_U)}{\sum_i a_i} \quad (3.44)$$

where ξ_U is a uniformly distributed random number between 0 and 1, and a_i is the propensity function of the i -th stochastic event (in s^{-1}). In general, the propensity function can be expressed as:

$$a_i = c_i f(n_1, n_2, \dots) \quad (3.45)$$

where c_i is a reaction probability, and $f(n_1, n_2, \dots)$ is a function of the number of molecules in the system which depends on the order of the reaction. For the general case of a bimolecular reaction between the molecules A and B , $c_i = k_i / N_A V$, where k_i is the rate coefficient of the i -th reaction, and the propensity function is then given by:

$$a_i = \frac{k_i n_A n_B}{N_A V} \quad (3.46)$$

and can also be expressed as a function the molar concentrations (C):

$$a_i = k_i C_A C_B N_A V \quad (3.47)$$

Proceeding similarly with other types of reactions, it can be found that in general:

$$a_i = N_A V k_i f_i(C) \quad (3.48)$$

The type of event taking place at time τ is determined randomly, where the probability P of choosing an i -th event is:

$$P(i) = \frac{a_i}{\sum_j a_j} \quad (3.49)$$

A common feature of both stochastic and deterministic methods is the assumption of perfectly mixed reaction volumes. In this context, it is not sufficient that a system is homogeneous (that is, the local concentrations are the same for the whole volume), but also the probability of finding a given single

molecule at any position in the system must be uniform. This means that a single molecule has the same probability of reacting with every other molecule present in the system, which is not possible in real systems because of mass transfer limitations.

The SSA can be modified in order to consider also imperfectly mixed systems. In the stochastic simulation algorithm of imperfectly mixed systems (SSA-IM)^[74] the type of reaction must be determined before calculating the propensity functions. From equations 3.48 and 3.49, the probability of the i -th reaction being the next event is:

$$P(i) = \frac{k_i f_i(C)}{\sum_j k_j f_j(C)} \quad (3.50)$$

Notice that it is not necessary to know the volume of the system in order to determine the next event. Once the next reaction has been identified, we need to determine the time at which the next reaction takes place and the perfectly mixed volume for the particular reaction at the particular time.

Stickler^[75] proposed the use of Einstein's equation of Brownian motion (Eq. 3.25) for the determination of effective reaction volumes in diffusion-controlled reactions. Einstein's equation describes the diameter of a sphere inside which the probability of finding the diffusing molecule is 50%. Therefore, we can estimate the diffusion volume for the particular molecule as twice the volume of the sphere described by equation 3.25:

$$V_{dif} = \frac{8\pi}{3} (6D)^{3/2} \Delta t^{3/2} \quad (3.51)$$

An estimate of the perfectly mixed volume (V_{pm}) is then given by the diffusion volume of the fastest molecule involved in the next reaction, considering that $\Delta t = \tau$:

$$V_{pm} = \frac{8\pi}{3} [6\tau \max(D)]^{3/2} \quad (3.52)$$

Using equations 3.44 and 3.48, the next reaction time for the perfectly mixed volume is:

$$\tau = -\frac{1}{N_A V_{pm}} \frac{\ln(\xi_U)}{\sum_i k_i f_i(C)} \quad (3.53)$$

Combining equations 3.52 and 3.53, the next reaction time can be calculated as:

$$\tau = \left[-\frac{3}{8\pi N_{Av} (6 \max(D))^{3/2}} \frac{\ln(\xi_U)}{\sum_i k_i f_i(C)} \right]^{2/5} \quad (3.54)$$

and the perfectly mixed volume, after some algebra, is found to be:

$$V_{pm} = (1536\pi^2)^{1/5} \left[\frac{\max(D)}{N_A} \frac{\ln(\xi_U)}{\sum_i k_i f_i(C)} \right]^{3/5} \approx 6.857 \left[\frac{\max(D)}{N_A} \frac{\ln(\xi_U)}{\sum_i k_i f_i(C)} \right]^{3/5} \quad (3.55)$$

For this perfectly mixed volume, the number of molecules for each species is given by:

$$n_k = \text{int}(C_k V_{pm} N_A) \quad (3.56)$$

There are different ways to define the integer function (*int*) used in equation 3.56. Some common ways include rounding to the nearest integer, rounding to the next integer, or truncating the number. The method used to discretize the system may systematically overestimate or underestimate the actual number of molecules in the system. In order to reduce this effect, it is suggested to perform a Monte Carlo discretization, as follows:

$$n_k = \begin{cases} \text{ceil}(C_k V_{pm} N_A), & \xi_U < C_k V_{pm} N_A - \text{floor}(C_k V_{pm} N_A) \\ \text{floor}(C_k V_{pm} N_A), & \xi_U > C_k V_{pm} N_A - \text{floor}(C_k V_{pm} N_A) \end{cases} \quad (3.57)$$

where ξ_U is a uniform random number between 0 and 1, and *ceil* and *floor* are discretizing functions giving as a result the closest integer greater than or less than the number evaluated, respectively. An additional condition that must be checked after discretization is that the number of molecules of the fastest species for the selected next reaction should always be greater or equal than one, because this is the molecule around which the perfectly mixed volume is considered. Using the number of molecules actually present in the perfectly mixed volume, it is now possible to calculate the actual propensity function of the next reaction (equation 3.48). If the calculated propensity function is zero, the time is updated but no reaction takes place. If the actual propensity function is greater than zero, the event takes place and the concentrations of the species are updated:

$$C_{k,new} = C_{k,old} + \frac{v_{k,i}}{N_A V_{pm}} \quad (3.58)$$

where $v_{k,i}$ is the stoichiometric coefficient for the i -th reaction and k -th component. It should be noticed that the accuracy of this algorithm relies on the use of an adequate model for the estimation of diffusion coefficients in the reacting mixture. The flowcharts corresponding to the direct SSA and the SSA-IM are presented in Figures 3.6 and 3.7, respectively.

Examples of MATLAB® codes of the simulation methods described in this section, and used in Sections 4 and 5, are presented in Appendix B.

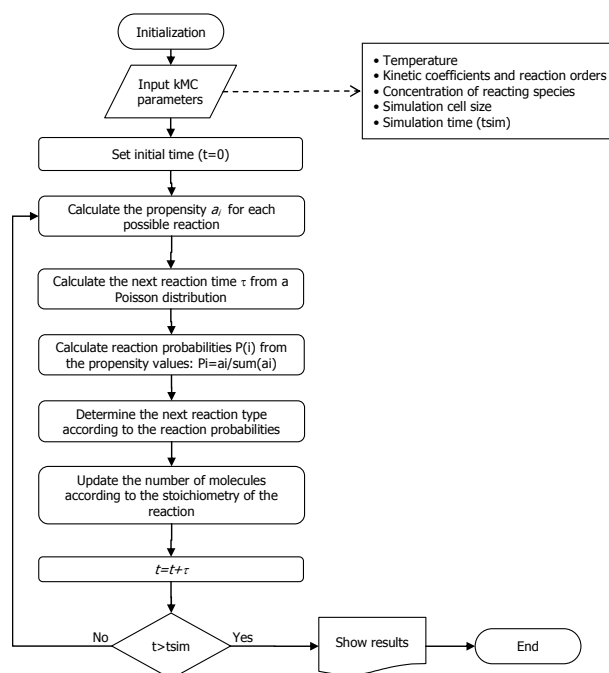


Figure 3.6 Direct Stochastic Simulation Algorithm (SSA) for kinetic Monte Carlo simulation of perfectly mixed reacting systems

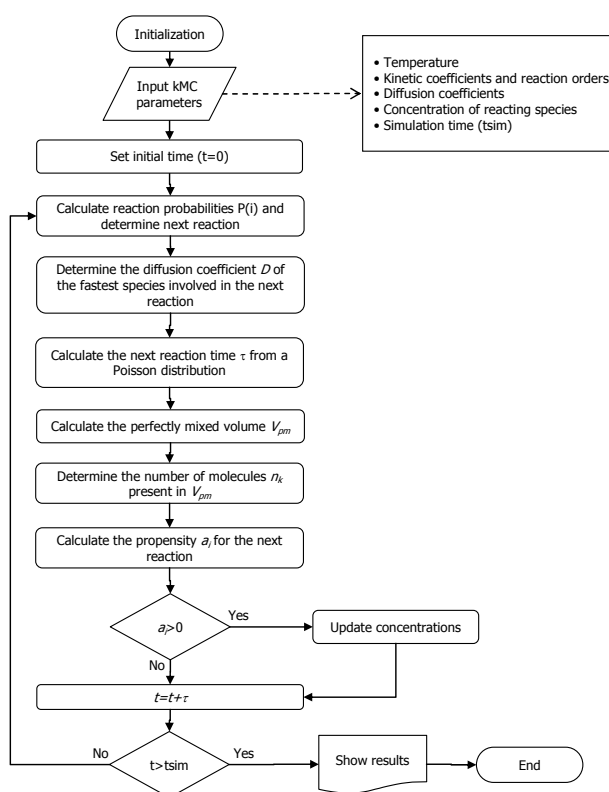


Figure 3.7 Stochastic Simulation Algorithm for kinetic Monte Carlo simulation of imperfectly mixed reacting systems (SSA-IM)

3.2. Experimental Methods

3.2.1. Optical Microscopy (OM)

A microscope is simply an optical system that transforms an object into an image, and microscopy is the study of the structure and morphology of objects with the use of a microscope. Simple microscopes have only one imaging lens and operate at low magnification to study large specimens. Compound microscopes have more than one imaging lens and operate at higher magnification and higher resolution, giving more detail of smaller specimens. The most common types of microscopes are optical or light microscopes (visible light-matter interaction, micrometer resolution) and electron microscopes (electrons-matter interaction, nanometer resolution).

Light interacts with matter in a variety of ways. Light incident on an object might be absorbed, transmitted, reflected or diffracted. Absorbed light may be re-emitted as visible light or it may be transformed into some other kind of energy such as thermal energy or chemical energy. Refraction consists in the deviation of a beam of light while passing through a transparent object such as a glass lens having a different refractive index. Diffraction takes place when the light is uniformly bent around the edges of large opaque objects or scattered by small particles and structures having dimensions similar to the wavelength of light itself. The diffraction of light by small structural elements in a specimen is the principal process governing image formation in the optical microscope (OM). There are two basic imaging modes. In bright field (BF) imaging, the direct unscattered beam is allowed to reach the image plane. Dark field (DF) is the opposite imaging mode, where only scattered radiation is allowed to form the image.

An example of optical microscope and its components is presented in Figure 3.8. The most important components for the image formation are: i) the *objective lens*, which collects light diffracted by the specimen and forms a magnified real image, and ii) the *condenser lens*, which focuses light from the illuminator onto a small area of the specimen. The objective lens is the most critical, and imperfections in it will affect the image quality directly.

The source of illumination is normally a small hot filament. The radiation emitted from the filament is efficiently collected by a condenser lens. Usually, a second condenser lens controls the transfer of the radiation to the specimen plane. There is an aperture associated with each condenser lens, and the apertures and lenses control the area illuminated and the angular divergence of the illumination. After the radiation has passed through the specimen, the scattered radiation is collected by the objective lens. For a given objective magnification, if the angular aperture of the microscope is increased the diffraction spots in the image grow smaller and the image is better resolved. In the light microscope, the angular aperture is described in terms of the *numerical aperture (NA)* as

$$NA = n \sin \theta \quad (3.59)$$

where θ is the half angle of the cone of specimen light accepted by the objective lens and n is the refractive index of the medium between the lens and the specimen. For dry lenses used in air, $n = 1$; for oil immersion objectives, $n = 1.515$. Because immersion oil has the same refractive index as the glass coverslip, refraction of specimen rays at the coverslip-air interface is eliminated, the effective half angle is increased, and resolution is improved.

The *resolving power* or *resolution* of the microscope is the minimum distance between two objects at which they can still be seen without interference. For dark-field microscopy the resolution is defined as

$$d = \frac{0.61\lambda}{NA} \quad (3.60a)$$

where d is the minimum resolved distance, λ is the wavelength of light, and NA is the numerical aperture of the objective lens. In the case of bright-field microscopy the resolution is given by

$$d = \frac{1.22\lambda}{\text{condenser } NA + \text{objective } NA} \quad (3.60b)$$

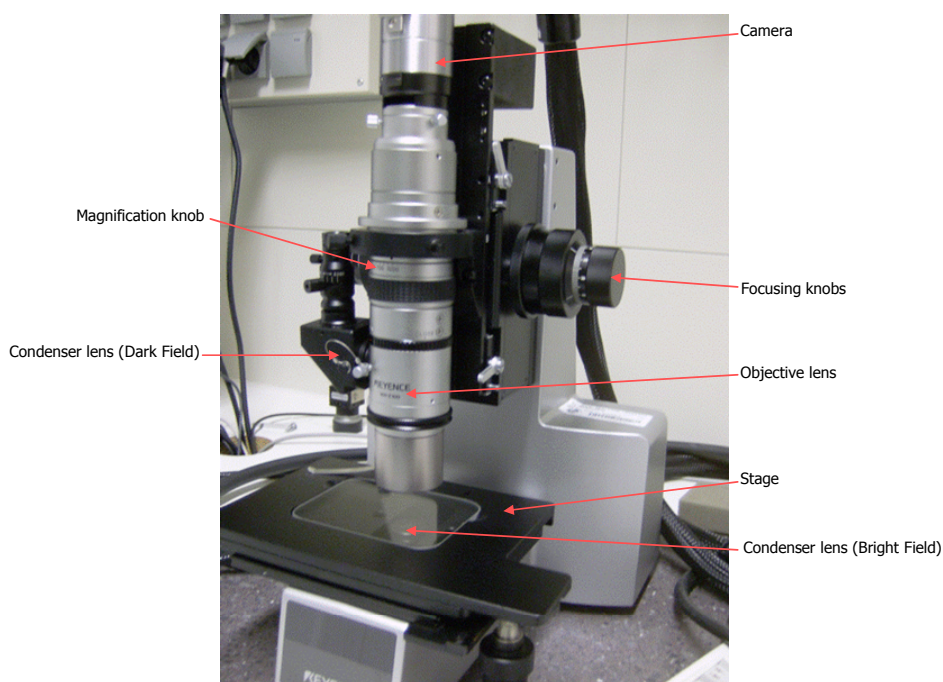


Figure 3.8 Optical microscope

The typical resolution of optical microscopes is on the order of $0.5 \mu\text{m}$, limited by the nature of the specimen, the objective lens and the wavelength of light. It is possible to obtain the best resolution by decreasing λ to 400 nm using green light or to about 200 nm using ultraviolet light, by setting the largest aperture possible and by using an oil immersion objective lens. The absolute resolution limit using green light is about 150 nm . Even sophisticated image processing techniques cannot improve on this fundamental limit. The optical limit of spatial resolution is important for interpreting microscope images. Irregularities in the shapes of particles greater than the limiting size just begin to be resolved; particles smaller than this limit appear as circular diffraction disks, and, regardless of their true sizes

and shapes, always have the same apparent diameter. The apparent variability in the sizes of particles below the resolution limit is due to variations in their intensities, and not to variability in the size of their diffraction spots.

In any microscope the image is only accurately in focus when the object lies in the appropriate plane. If part of the object being viewed lies above or below this plane, then the equivalent part of the image will be out of focus. The range of positions for which there is no change in the sharpness of the image is known as the depth of field. For diffraction-limited optics, the depth of field Z is given as

$$Z = \frac{n\lambda}{NA^2} \quad (3.61)$$

Thus, the larger the aperture angle, the shallower will be the depth of field. The depth of field along the z -axis is determined by several contributing factors, including principles of geometrical and physical optics, lens aberrations and overall magnification.

A wide aperture allows maximal spatial resolution, but decreases contrast (the fractional change in image brightness observed), while a smaller, constricted aperture improves visibility and contrast, but decreases spatial resolution. For all specimens, the ideal aperture location defines a balance between resolution and contrast.

3.2.2. Electron Microscopy (EM)

The use of electrons for microscopy brings a number of advantages, especially an improvement in resolution, magnification and depth of field because high energy electrons have a much smaller wavelength than light. However, electrons are more strongly scattered by gases than is light, and in order to use electrons in a microscope all the optical paths must be evacuated to a pressure lower than 10^{-10} Pa (vacuum). In addition, the samples must be conducting (in order to accelerate the electrons onto the sample) and, hence, non-conductive samples must have a metal (gold) layer deposited on its surface.

There are two types of electron microscopes: the scanning electron microscope (SEM) and the transmission electron microscope (TEM). In the TEM, the sample is a very thin specimen and contrast within the image is due to the spatial variations in intensity of the transmitted electron beam through the specimen. In the SEM, the image may be produced in a number of ways, from variations in the intensity of secondary electrons back-scattered from the specimen to X-ray emission produced by inelastic collisions of the primary beam with bound electrons in the specimen. The essential feature of a scanning microscope is that the image is formed point by point, by scanning a probe across the specimen.

With careful design of appropriate electric and magnetic fields within the instrument, an electron beam may be focused like an optical beam. The electrons are emitted by an incandescent cathode

source (electron gun), accelerated towards more positive grids through either electrostatic or magnetic field lens onto an object. In TEM, the specimen is supported on a very thin film to minimize the scattering of the electrons as they pass through the sample. Depending on the thickness and composition of the object, the electron beam experiences different attenuation as a function of position. A typical scheme of a transmission electron microscope is presented in Figure 3.9.

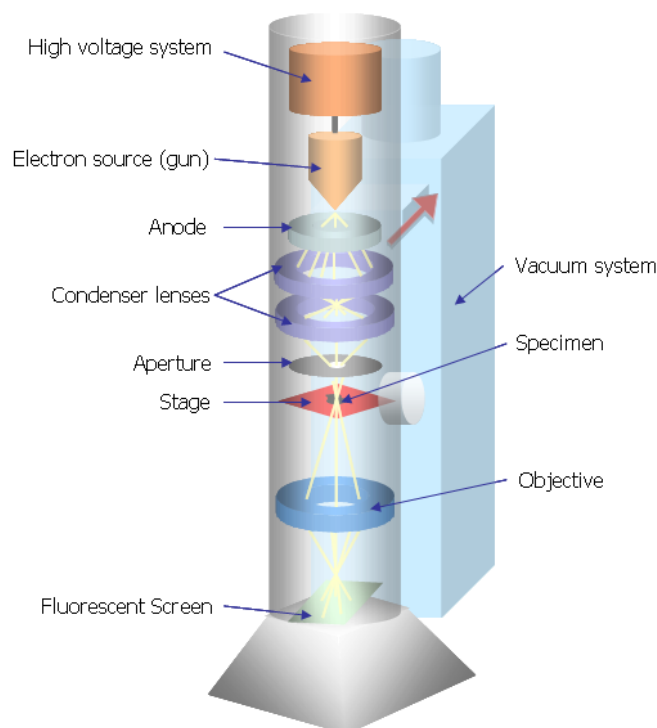


Figure 3.9 Transmission Electron Microscope

Typical acceleration voltages are $V \sim 120$ kV, which gives the electron an energy $E = 120$ keV ($1 \text{ eV} = 1.6 \times 10^{-19} \text{ J}$); the representative wavelength (λ) for these electrons is $3.35 \times 10^{-3} \text{ nm}$ computed from the De Broglie expression

$$\lambda = \frac{h}{\sqrt{2Em_e}} \quad (3.62)$$

where m_e is the electronic mass ($9.11 \times 10^{-31} \text{ kg}$) and h is Planck's constant ($6.626 \times 10^{-34} \text{ J}\cdot\text{s}$). Hence the electron microscope has potentially, one of the highest spatial resolutions of all of the microscope techniques. The typical resolution of an electron microscope is about 0.02 nm . This is much smaller than the size of a single atom. Unfortunately, this sort of resolution cannot be obtained because of the sensitivity to lens aberrations. In order to reduce the effect of aberrations, it is necessary to keep the angle θ small giving rise to large depths of field.

When the electrons hit the sample, several processes take place (scattering, absorption, etc.). These processes can be used to obtain information about the sample if they are collected by a suitable detector. Elastically scattered electrons are the main contributors to diffraction patterns. Inelastic scattering processes are responsible for the stopping of an electron by a solid. Almost all of the kinetic

energy which is carried by the primary electron ends up as heat in the specimen. A small proportion of the energy may escape as X-rays, light or secondary electrons. Secondary electrons are abundant and are used as imaging signal in SEM.

In TEM, absorption of electrons in the specimen is not usual and contrast is due basically to electron scattering. In the case of ordered or crystalline materials this gives diffraction contrast, which is strongly dependent on crystal orientation. In amorphous materials, mass thickness contrast results, where the image brightness depends on the local mass thickness. Contrast is greater at low accelerating voltages and at small objective aperture diameters. A high brightness in the image corresponds to the areas with a strong signal of electrons while a dark image is obtained in zones with weaker signal. In the case of polymers, since they have low atomic number, they scatter electrons weakly giving poor contrast in the TEM. They are also highly beam-sensitive; radiation damage causes destruction of crystalline order, chain scission or crosslinking, mass loss and dimensional changes. TEM micrographs of multiphase polymers often do not provide enough contrast to image the phases clearly. Methods which have proven useful in contrast enhancements include *shadowing* with a heavy metal in a vacuum evaporator and *staining*.

Staining, in the most general terms, involves the physical or chemical incorporation of heavy, electron dense atoms into the polymer, in order to increase the density and thus enhance contrast. Most of the stains applied to polymers are positive stains. In positive staining, the region of interest is stained dark by either a chemical interaction or by selective physical absorption. Chemical reactions are preferred because stains that are only physically absorbed may be removed in the vacuum of an electron microscope. In negative staining, the shape of small particles mounted on smooth substrates is obtained by staining the regions surrounding the particles rather than the particles themselves. Such staining methods are often applied to latex or emulsion materials.

Staining agents which exhibit high selectivity for certain polymers are required to characterize polymer particle morphology. For example, polymers with unsaturations (e.g. polystyrene, polybutadiene) or containing ether, alcohol, aromatic, amide or other oxidizable moieties in their structure, can be positively stained with ruthenium tetroxide (RuO_4).^[76] On the other hand, polymers with carbonyl groups (e.g. polyacrylates) can be treated with hydrazine and osmium tetroxide (OsO_4).^[9] RuO_4 is known to be a stronger oxidizing agent than OsO_4 and superior for staining rubber. RuO_4 can be prepared by oxidation of ruthenium trichloride with a solution of sodium hypochlorite according to equation 3.63. Care must be taken as ruthenium tetroxide is volatile and toxic.



Negative staining consists of placing a heavy metal outside the particles, such as uranyl acetate or phosphotungstic acid (PTA). Using negative staining, certain artifacts, such as imaginary shells and surface occlusions leading to incorrect conclusions, can be avoided. PTA is an anionic stain with a high

molecular weight which imparts high density to the stained material. PTA can react with surface functional groups such as hydroxyl, carboxyl and amines.

Thanks to the development of staining techniques, transmission electron microscopy (TEM) became the most important method for particle morphology characterization. Other techniques usually employed include small angle X-ray and neutron scattering (SAXS and SANS), atomic force microscopy (AFM) and nuclear magnetic resonance (NMR) spin-diffusion and spin-relaxation techniques. However these methods are not in widespread use and their ability to characterize the composition, size, shape and structure of the domains is somewhat limited.^[77]

3.2.3. Dynamic Light Scattering (DLS)

Light interacts with the charges constituting a given molecule resulting in a change in the spatial charge distribution. The charge distribution follows the time-modulation of the electric wave vector of the incident light beam, and therefore the molecule constitutes an oscillating dipole or electric oscillator. This oscillating dipole acts as an emitter of an electromagnetic wave of the same wavelength as the incident one (λ) emitted isotropically in all directions perpendicular to the oscillator.

The angle of observation with respect to the direction of the incident light beam (θ) is called the scattering angle and provides a measure for the length scale observed in a light scattering experiment. For molecules or particles larger than 20 nm, several of these oscillating dipoles are created simultaneously within one given particle. As a consequence, some of the emitted light waves possess a significant phase difference. Accordingly, interference of the scattered light emitted from such particles leads to a nonisotropic angular dependence of the scattered light intensity. The interference pattern of intraparticle scattered light, also called particle form factor, is characteristic of the size and shape of the scattering particle. As a consequence, the form factor provides the quantitative means for the characterization of particles in very dilute solution by light scattering. For particles smaller than $\lambda/20$, only a negligible phase difference exists between light emitted from the various scattering centers within the given particle. In this case, the detected scattered intensity will be independent of the scattering angle and only depend on the mass of the particle which is proportional to the total number of scattering centers in a particle.

As a consequence of the temporal changes in interparticle positions and the corresponding temporal concentration fluctuations caused by Brownian motion, the interference pattern and the resulting scattered intensity detected at a given scattering angle also change with time. This phenomenon provides the basis for dynamic light scattering (DLS, also called quasielastic light scattering QELS or photon correlation spectroscopy PCS), an experimental procedure which yields a quantitative measure for the mobility of scattering particles in solution as characterized by their self-diffusion coefficient. The measurement involves directing a laser beam into a highly diluted sample of the dispersion and recording the scattered light on a photomultiplier at a particular angle. Most of the particle sizers used to determine the hydrodynamic size of particles in solution are based on this principle.

To quantitatively analyze the particle mobility by light scattering, it is helpful to express the scattering intensity fluctuations in terms of correlation functions. The dynamic structure factor $F_s(\mathbf{q}, \tau)$ contains all information concerning the motion of the scattering solute particle. It is the Fourier transform of the so-called van Hove autocorrelation function $G_s(\mathbf{r}, t)$:

$$F_s(\bar{q}, \tau) = \int G_s(\bar{r}, t) \exp(i\bar{q}\bar{r}) d\bar{r} \quad (3.64)$$

$$G_s(\bar{r}, t) = \langle n(\bar{0}, t) n(\bar{r}, t + \tau) \rangle_{V, T} \quad (3.65)$$

Here, $n(\mathbf{r}, t)$ is the local number density of scattering particles fluctuating with time due to Brownian motion, within a very small sub-volume of the scattering volume centered at position \mathbf{r} at a given time t . τ is the delay time of the autocorrelation function and \mathbf{q} is known as the scattering vector, whose magnitude (q) is determined by:

$$q = \frac{4\pi n_0}{\lambda} \sin\left(\frac{\theta}{2}\right) \quad (3.66)$$

n_0 corresponds to the refraction index of the sample. In principle, $G_s(\mathbf{r}, t)$ defines the probability of finding a given scattering particle at time $t + \tau$ and position \mathbf{r} , if the same particle previously at time t has been located at position $\mathbf{0}$. It should be noted that for the dynamic scattering process, only the relative distance vector $\mathbf{r} - \mathbf{0}$ as well as the time delay τ are important. The arbitrary choice of the origin of the coordinate system $\mathbf{0}$ or the starting time is unimportant. The average is taken both over the whole scattering volume and total measuring time. For an isotropic diffusive particle motion (Brownian motion or random walk), $G_s(\mathbf{r}, t)$ only depends on the distance $r = |\mathbf{r}|$, and is given as:

$$G_s(\bar{r}, t) = \left(\frac{2\pi}{3} \langle \Delta R(\tau)^2 \rangle \right)^{3/2} \exp\left(-\frac{3r(\tau)^2}{2 \langle \Delta R(\tau)^2 \rangle} \right) \quad (3.67)$$

$\langle \Delta R(\tau)^2 \rangle$ is the mean-square displacement of the scattering particle, that is, the average distance squared it travels during time τ . The scattering particle exhibits a random walk through the scattering volume, and the mean-square displacement is given by Einstein's equation (Eq. 3.25). In this case the van Hove autocorrelation function $G_s(\mathbf{r}, t)$ is a Gaussian curve with its half width given by the diffusion coefficient. Fourier transform leads to the corresponding dynamic structure factor, which is the primary quantity measured in the dynamic light scattering experiment:

$$F_s(q, \tau) = \exp\left(-\frac{q^2 \langle \Delta R(\tau)^2 \rangle}{6} \right) = \exp(-Dq^2 \tau) \quad (3.68)$$

The fluctuating signal detected by the photomultiplier at a given scattering angle is mathematically translated into an intensity autocorrelation function, using a hardware correlator: the time-dependent scattered intensity is multiplied with itself after it has been shifted by a distance τ in time, and these

products are averaged over the total measurement time. This intensity autocorrelation $\langle I(q, t)I(q, t + \tau) \rangle$ is calculated for various values of τ , ranging in a typical dynamic light scattering experiment from about 100 ns to several seconds. Here, the lower limit is given by the detector hardware, and the upper correlation time is limited by the stability of the dynamic light scattering setup and the channel number of the hardware correlator. The intensity correlation function is related to the dynamic structure factor $F_s(q, \tau)$ via the Siegert relation:

$$F_s(q, \tau) = \exp(-Dq^2\tau) = \langle E_s(q, t)E_s^*(q, t + \tau) \rangle = \sqrt{\frac{\langle I(q, t)I(q, t + \tau) \rangle}{\langle I(q, t)^2 \rangle}} - 1 \quad (3.69)$$

If the temperature T and solvent viscosity η are known, the Stokes-Einstein equation (eq. 3.30) allows to determine the hydrodynamic radius (a) of the scattering particle using the self-diffusion coefficient (D) measured by dynamic light scattering. For monodisperse samples, $F_s(q, \tau)$ is a single exponential with decay rate $\Gamma = Dq^2$, and relaxation time $1/\Gamma$. In a semi-logarithmic plot, the dynamic structure factor $F_s(q, \tau)$ is a single straight line for a monodisperse sample and a combination of two lines with different slopes for the bimodal case. The self-diffusion coefficient, and therefore the hydrodynamic radius of the scattering particles, can be determined by dynamic light scattering only in case of very dilute samples. In more concentrated samples, interactions between the scattering particles may have a strong influence on the particle mobility.

For polydisperse samples with size distribution $P(a)$, the experimentally determined self-diffusion coefficient is defined by a distribution function $P(D)$. In this case, $F_s(q, \tau)$ is not a simple single exponentially decaying function, but a superposition of several such single exponentials weighted by $P(D)$:

$$F_s(q, \tau) = \int_0^{\infty} P(D) \exp(-Dq^2\tau) dD \quad (3.70)$$

Since the particle form factor contributes to $P(D)$, for scattering particles larger than 10 nm the measured diffusion coefficient distribution $P(D)$ does not only depend on the particle size distribution itself but also on the scattering vector q . In case of non-spherical scattering particles, not only polydispersity but also non-translational particle motion like rotation or polymer segment fluctuations may cause a q -dependence of the measured apparent diffusion coefficient.

The apparent diffusion coefficient $D_{app}(q)$ is defined as:

$$D_{app}(q) = \frac{\sum n_i M_i^2 P_i(q) D_i}{\sum n_i M_i^2 P_i(q)} \quad (3.71)$$

With n_i the number density of scattering particles of species i , M_i their particle mass, $P_i(q)$ the particle form factor and D_i the corresponding self-diffusion coefficient.

The “true” average diffusion coefficient $\langle D \rangle_z$ is determined by extrapolation of the apparent diffusion coefficient towards zero q , since in this limit $R(q)=1$ for all particle species, and also non-diffusional processes like rotation or polymer segment fluctuations do not any longer contribute to the correlation function. For small particles (10 nm – 100 nm), this extrapolation is given as:

$$D_{app}(q) = \langle D \rangle_z \left(1 + K \langle R_g^2 \rangle_z q^2 \right) \quad (3.72)$$

The constant K depends both on sample polydispersity and on the particle geometry. Only for samples consisting of monodisperse spheres, $K=0$ and $D_{app}(q)=D$. With increasing q , $R(q)$ of the larger particles decays first. For this reason, the relative contribution of larger particles to the correlation function measured for a polydisperse sample in a dynamic light scattering experiment also decreases with increasing q . This leads to an increasing contribution of the smaller particles to the dynamic light scattering signal with increasing q , and correspondingly must lead to an apparent increase of the average diffusion coefficient.

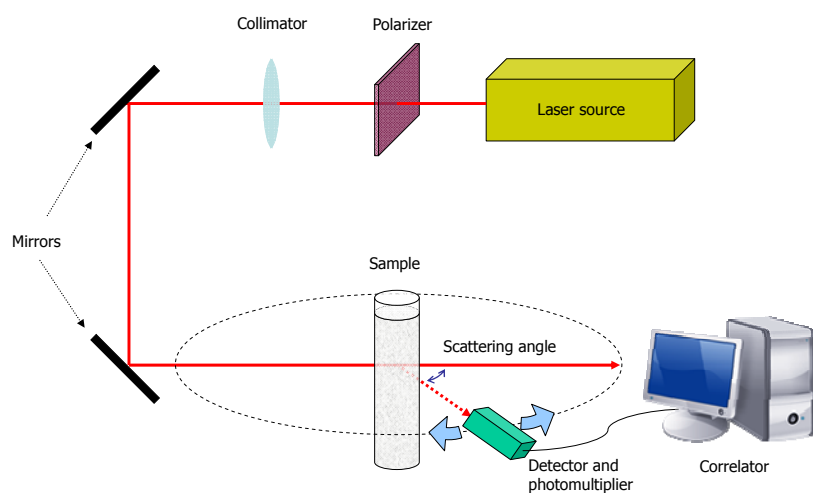


Figure 3.10 Setup for dynamic light scattering

A standard single angle light scattering setup consists of the following components (Fig. 3.10):

- The incident light source, typically a laser (gas ion, He-Ne, solid state or laser diodes)
- The light scattering cell, a cylindrical quartz glass cuvette of outer diameter between 10 and 30 mm, embedded if possible within an index matching and thermostating bath.
- The detector, either a photomultiplier tube or an avalanche photo diode (APD), and its associated optics (pinhole or optical fiber).
- The electronic hardware components associated with the detector used for signal processing (computer, hardware correlator, etc.).

In practice, the light intensity needed for a successful scattering experiment depends on the sensitivity of the optical detector, and on the scattering power of the sample itself as determined by size, concentration, and refractive index increment of the solute particles.

Chapter 4

Kinetics of Emulsion Polymerization

One of the most important characteristics of emulsion polymerization is the possibility of producing very high molecular weight polymers at rates much higher than by bulk polymerization. A first qualitative explanation to this phenomenon was presented by William Harkins in 1947.^[78] He assumed that the surfactant molecules form micelles in the continuous phase and absorb monomer molecules by diffusion from the monomer droplets (which act only as monomer reservoirs) becoming *monomer-swollen* micelles. These monomer-swollen micelles, larger in number with respect to the monomer droplets, will have a higher probability of absorbing free radicals from the continuous phase, becoming polymer particles. When a single radical is present inside the particle, the radical can grow without termination until all the monomer in the particle is consumed unless a second radical enter the particle causing immediate termination of the radicals. As the particle grows, its surface area becomes larger and adsorbs free surfactant from the continuous phase or from remaining micelles. Once the micelles are terminated, no more polymer particles are formed, and the radicals generated are captured almost completely by the existing polymer particles. The polymerization inside the particles proceeds as long as there are monomer molecules available for propagation. The monomer consumed is replenished by diffusion from the monomer droplets through the continuous phase until all monomer droplets are depleted. According to Harkins, the high molecular weight of the polymer and high polymerization rates are explained by the *compartmentalization* or segregation of radicals in the polymer particles.

Using the ideas of Harkins, Wendell Smith and Roswell Ewart proposed in 1948^[79] for the first time a quantitative model of the kinetics of emulsion polymerization. According to their model, the rate of polymerization or rate of propagation r_p can be derived from the kinetics of free radical polymerization in homogenous systems considering each polymer particle as a homogeneous polymerization reactor. The rate of propagation can be determined as follows:

$$r_p = \frac{N k_p [M]_p \bar{n}}{N_A} \quad (4.1)$$

where N is the number of polymer particles per unit volume of dispersion, k_p is the propagation rate coefficient, $[M]_p$ is the concentration of monomer inside the particles, \bar{n} is the average number of radicals per particle and N_A is Avogadro's constant.

Although the use of equation 4.1 for determining polymerization rates seems quite straightforward, the average number of radicals per particles in a given polymerization system cannot be measured directly but has to be estimated. For this purpose, Smith and Ewart proposed their famous recursion equation for describing the distribution of the number of radicals inside the polymer particles:

$$\frac{\rho}{N} N_{n-1} + k_0(n+1)N_{n+1} + \frac{k_t}{N_A v} (n+2)(n+1)N_{n+2} = \frac{\rho}{N} N_n + k_0 n N_n + \frac{k_t}{N_A v} n(n-1)N_n \quad (4.2)$$

where N_n is the number concentration of particles containing n radicals, ρ is the rate of radical capture (s^{-1}), k_0 is the rate of radical desorption (s^{-1}), k_t is the rate of termination and v is the volume of a polymer particle. The average number of radicals per particle can then be calculated from:

$$\bar{n} = \frac{\sum_{n=1}^{\infty} n N_n}{N} \quad (4.3)$$

The Smith-Ewart recursion formula can be obtained from the more general Chemical Master Equation (CME) formulation (equation 4.4), after assuming steady-state conditions:

$$\frac{dN_n}{dt} = \frac{\rho}{N} (N_{n-1} - N_n) + k_0 [(n+1)N_{n+1} - nN_n] + \frac{k_t}{N_A v} [(n+2)(n+1)N_{n+2} - n(n-1)N_n] \quad (4.4)$$

In order to obtain analytical expressions for \bar{n} from the solution of the recursion equations, Smith and Ewart considered three limiting cases:

- Case 1: The average number of radicals per particle is small ($\bar{n} \ll 1$). This situation arises when the rate of radical capture is small compared to the rate of radical desorption from the particles (i.e. very small particles). If termination takes place predominantly in the aqueous phase:

$$\bar{n} \approx m \sqrt{\frac{\rho N_A v}{2k_t}} \quad (4.5a)$$

where m is the partition coefficient of the radicals between the polymer particles and the aqueous phase. If termination takes place predominantly in the polymer particles, then:

$$\bar{n} \approx \sqrt{\frac{\rho}{2k_0 N}} \quad (4.5b)$$

The rate of radical capture was estimated using Smoluchowski's equation:

$$\rho = 2\pi D d_p [R]_w \quad (4.6)$$

where D is the diffusion coefficient of the radicals through the continuous phase, d_p is the particle diameter and $[R]_w$ is the concentration of radicals in the continuous phase.

- Case 2: The average number of radicals per particle is approximately 0.5. This situation arises when the rate of radical desorption is negligible and the rate of termination is so fast that immediate termination follows the capture of a second radical. In this case, the particles will

contain either one or zero radicals at any time, and on average, the system will contain only $\frac{1}{2}$ radical per particle.

$$\bar{n} \approx \frac{1}{2} \quad (4.7)$$

- Case 3: The average number of radicals per particle is large ($\bar{n} \gg 1$). This case is found when the rate of radical capture is large compared to the rate of radical termination, for example, when the particles are very large or the viscosity inside the particles is so large that the chains cannot easily diffuse. The average number of radicals can be approximated as:

$$\bar{n} \approx \sqrt{\frac{\rho N_A v}{2k_t}} \quad (4.8)$$

As \bar{n} increases, the kinetics of emulsion polymerization approaches the kinetics of homogeneous polymerization.

Thus, Equation 4.1 reduces the problem of emulsion polymerization kinetics to the determination of the concentration of monomer in the particles ($[M]_p$), the number of polymer particles (M) and the average number of radicals per particle (\bar{n}) which in turn depends basically on the processes of radical capture, radical desorption, radical generation, chain transfer and radical termination.

The kinetic model presented by Smith and Ewart has been the basis for much more complex analytical and numerical solutions throughout the years, but its essence still remains the same. In the following years, O'Toole^[80] and Ugelstad and coworkers^[81] were able to obtain more general analytical solutions of the recurrence formula (Eq. 4.2) under different conditions, as a function of the rates of radical capture, desorption, re-absorption and termination.

On the other hand, the concentration of monomer inside the particle strongly depends on the interaction forces between the monomer and the polymer chains, on the interfacial tension and size of the particles, and on the solubility of the monomer in the continuous phase. The number of particles depends on the processes of particle formation and particle aggregation. In summary, a precise quantitative model of the kinetics of emulsion polymerization requires the knowledge of the particle concentration, the concentration of monomer inside the particles and the mean number of radicals per particle, which in turn require the detailed knowledge of the kinetics of the physical and chemical processes listed in Table 4.1.

Table 4.1 Physical and chemical processes determining the kinetics of emulsion polymerization

Physical	Chemical
Diffusion	Initiator decomposition
Particle formation	Radical propagation
Radical capture	Radical termination
Radical desorption	Chain transfer
Swelling	
Coagulation	

4.1. Molecular diffusion

Molecular diffusion is one of the most important processes taking place in heterophase polymerization. The net molecular flux by diffusion is determined by the difference in chemical potential between two different regions, which in turn depends on the intermolecular potentials. At steady state, there is no chemical potential difference and the net molecular flux becomes zero. It is by molecular diffusion that primary radicals, monomer molecules and oligomers present in the continuous phase can reach and enter the polymer particles. Similarly, it is by molecular diffusion in polymer media that molecules present inside the polymer particles are able to reach the surface and desorb. Bimolecular reactions, such as propagation and termination, can also occur only if the reactants approach each other by molecular diffusion. If the diffusion process is slow compared to the rate of reaction, the reaction becomes diffusion-controlled. The diffusivity of a system depends on the nature and strength of the intermolecular interactions, on the kinetic energy of the molecules (associated to the temperature of the system), and on the size and concentration of the molecules. In some systems, the diffusion coefficients are extremely sensitive to the process conditions. A particular and relevant example of this situation is the diffusion in polymer media. The diffusion coefficient for small molecules (solvent or monomer) through polymer solutions in the vicinity of the glass transition are known to change by as much as six orders of magnitude with only a small change in polymer concentration.^[82] A mathematical expression relating the diffusion coefficient of a small molecule in a polymer was obtained by Vrentas and Duda^[83] using the Free-Volume Theory developed by Fujita.^[84] Free-volume theory is by far the most widely used theory for predicting diffusion coefficients in polymers and polymer solutions.

According to the free-volume theory, the diffusion of a molecule is only possible if there is enough free space or free volume surrounding the diffusing molecule to accommodate it. Free volume exists in a system because of geometrical restrictions, random thermal motion and intermolecular repulsive potentials. Even if an individual hole may not be large enough to accommodate a diffusing molecule, the cooperative motion of several neighboring molecules may allow two or more holes to merge into a single hole large enough for diffusion to occur. As the free volume of a system is reduced, the energy required by the diffusing molecule to accommodate in a new position increases, and therefore, the diffusion coefficient will decrease exponentially. According to the free-volume theory, the diffusion coefficient of a small molecule in a polymer can be obtained from the following equation:

$$D_p = D_{p01} e^{-E/k_B T} \exp\left(-\gamma \frac{(1-w_p)V_1^* + w_p \xi V_2^*}{V_{FH}}\right) \quad (4.9)$$

where the subscripts 1 and 2 represent the small molecule and the polymer respectively, E is the attractive energy between the small molecule and its polymer neighbors, D_{p01} is a pre-exponential factor, γ is a correction factor for the free-volume overlap, w_p is the weight fraction of polymer, V_i^* is

the specific critical hole free volume of the component i , ξ_v is the ratio of the critical molar volume of the small molecule jumping unit to that of the polymer jumping unit, and

$$V_{FH} = (1 - w_p)K_{11}(K_{21} + T - T_{g1}) + w_p K_{12}(K_{22} + T - T_{g2}) \quad (4.10)$$

where V_{FH} is the average hole free volume per gram of mixture, K_{ij} are parameters of the system and T_{gi} is the glass transition temperature for each component.

The Free-Volume Theory of diffusion is a macroscopic semi-empirical theory based on the motion and interaction forces between the molecules. However, if the trajectories and velocities of all the molecules in the system over a certain period of time were known, the diffusion coefficients could be directly obtained simply by using Einstein's description of Brownian motion (Equation 3.25). Therefore, as long as reliable expressions for calculating intermolecular forces are available, the diffusion coefficient of a system can be calculated from Molecular Dynamics (MD) simulation (Section 3.1.1) as follows:

$$D = \frac{1}{2n_D} \lim_{t \rightarrow \infty} \frac{\langle (r(t) - r(0))^2 \rangle}{t} = \frac{1}{2Nn_D} \lim_{t \rightarrow \infty} \frac{\sum_{i=1}^N \sum_{j=1}^{n_D} (r_{ij}(t) - r_{ij}(0))^2}{t} \quad (4.11)$$

N is the number of molecules used for the determination of the diffusivity, n_D is the number of spatial dimensions considered and r_{ij} is the position of the center of mass of the molecule i in the j -th direction. Equation 4.11 is usually referred as the Wiener-Einstein equation.

An alternative formulation of Einstein's equation was developed by Green and Kubo,^[85] where the diffusivity can be calculated as an autocorrelation function of the velocities of the molecules:

$$D = \lim_{t \rightarrow \infty} \int_0^t \langle \vec{v}(t) \cdot \vec{v}(0) \rangle dt = \frac{1}{N} \lim_{t \rightarrow \infty} \int_0^t \sum_{i=1}^N \vec{v}_i(t) \cdot \vec{v}_i(0) dt \quad (4.12)$$

Both approaches are equivalent and equally valid. As mentioned before, the use of MD simulation for the determination of diffusion coefficients relies on accurate models for describing the interaction potential between the molecules. Some of the most common models for non-polar molecules are the Lennard-Jones, Morse and Buckingham potentials. The interaction parameters of these models can be obtained from physicochemical experimental data (e.g. phase-change enthalpies), but it is also possible to estimate the parameters using semi-empirical or *ab initio* molecular modeling methods.^[86]

In order to show the dependence of the diffusion coefficient on the intermolecular forces in the system, the Buckingham interaction potential was used to calculate the molecular self-diffusion coefficients from the Wiener-Einstein expression (Eq. 4.11) using a MD simulation of an NVT ensemble as described in Section 3.1.1. In order to reduce the numerical error during the calculations, the following reduced dimensions were employed:

$$t^* = \sigma \sqrt{\frac{m}{\varepsilon}} \quad (4.13a)$$

$$D^* = \frac{D}{\sigma} \sqrt{\frac{m}{\varepsilon}} \quad (4.13b)$$

$$T^* = \frac{k_B T}{\varepsilon} \quad (4.13c)$$

$$\rho^* = \frac{\rho \sigma^3}{m} \quad (4.13d)$$

$$\alpha^* = \alpha \quad (4.13e)$$

$$m^* = \sigma^* = \varepsilon^* = 1 \quad (4.13f)$$

where m is the mass of a single molecule, and σ , ε and α are the interaction parameters of the Buckingham interaction potential:

$$\psi^B(r_{ij}) = \varepsilon \left[\frac{6}{\alpha - 6} e^{\alpha \left(1 - \frac{r_{ij}}{\sigma}\right)} - \frac{\alpha}{\alpha - 6} \left(\frac{\sigma}{r_{ij}}\right)^6 \right] \quad (3.12)$$

MD simulations were performed for small periodic simulation boxes of 64 molecules initially arranged in a cubic lattice. Up to 8 different simulations for each set of values of T^* , ρ^* and α^* were executed. When values of $\alpha^* < 14$ were considered, the time-step in reduced units (dt^*) was set equal to 0.0002, while for values of $\alpha^* \geq 14$, dt^* was set to 0.00001. 1.5×10^5 time-steps were used for equilibration of the system and 1.5×10^6 time-steps for data production. Values of α^* in the range between 10 and 15 were used, according to the values reported for several interaction parameters obtained using force field methods.^[87]

In Figures 4.1 to 4.3, the independent effects of T^* , ρ^* and α^* on the reduced diffusion coefficient D^* are presented. The behavior of the diffusion coefficient by changing the reduced temperature and keeping all other variables constant is presented in Figure 4.1. For usual values of the reduced temperature between 1 and 3, the reduced diffusion coefficient increases almost linearly with the reduced temperature. However, if lower temperature values (close to zero) are considered, it is observed that the reduced diffusivity is proportional to the square root of the reduced temperature:

$$D^*(T^*) = A_0 \sqrt{T^*} \quad (4.14)$$

where $A_0 = 0.0471$ for the conditions used in the simulation.

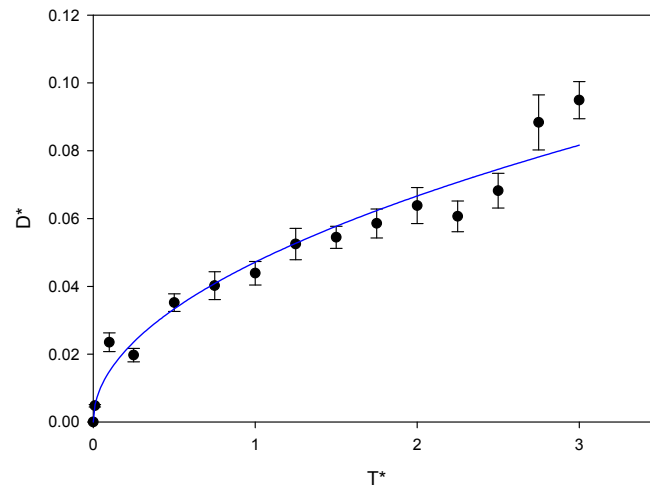


Figure 4.1 Effect of reduced temperature on reduced diffusion coefficient. $\alpha^*=11$, $\rho^*=0.3$. Data points: MD simulation. Error bars: Estimation error using MD simulation. Solid line: Best fit.

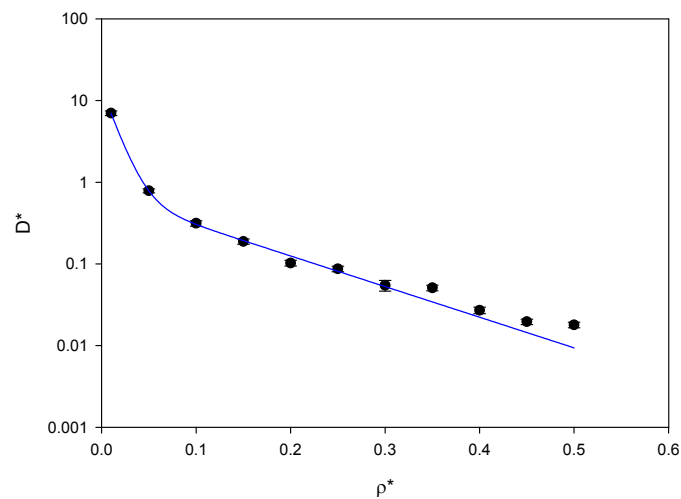


Figure 4.2 Effect of reduced density on reduced diffusion coefficient. $\alpha^*=11$, $T^*=2$. Data points: MD simulation. Error bars: Estimation error using MD simulation. Solid line: Best fit.

The effect of the reduced density on the reduced diffusion coefficient is presented in Figure 4.2. The behavior observed corresponds to a double exponential decay function for values of the reduced density between 0.01 and 0.5. If only values of the reduced density greater than 0.1 are considered, which is reasonable for condensed phases, the behavior can be represented by one single exponential decay function. The general expression obtained for the reduced diffusivity as a function of reduced density keeping all other variables constant is:

$$D^*(\rho^*) = A_1 \exp(-B_1 \rho^*) + A_2 \exp(-B_2 \rho^*) \quad (4.15)$$

where $A_1=0.705$, $A_2=13.3593$, $B_1=8.6404$, $B_2=74.0644$ for the conditions used in the simulation.

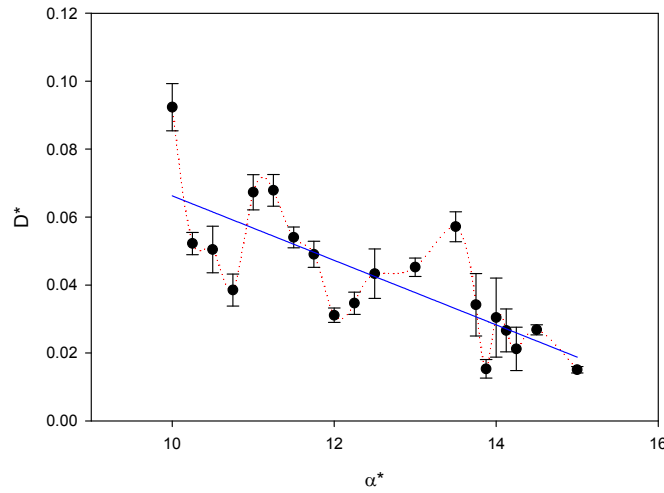


Figure 4.3 Effect of repulsion steepness on reduced diffusion coefficient. $T^*=2$, $\rho^*=0.3$. Data points: MD simulation. Error bars: Estimation error using MD simulation. Dotted line (red): Smoothed curve. Solid line (blue): Best linear fit.

Finally, the effect of the repulsion steepness of the Buckingham interaction potential (α^*) on the reduced diffusion coefficient is presented in Figure 4.3. It is observed that the reduced diffusivity is very sensitive to small variations in the value of α^* . However, there is a clear trend for decreasing the values of the reduced diffusion coefficient as α^* is increased. Although the functional dependence (Θ) of D^* on α^* may be highly nonlinear, for the range of values considered it will be approximated by a linear function as follows:

$$D^*(\alpha^*) = \Theta(\alpha^*) \approx A_3(A_4 - \alpha^*) \quad (4.16)$$

where $A_3=0.0095$, $A_4=16.9684$ for the conditions used in the simulation.

Now, taking into account all effects simultaneously, and considering one exponential decay function in the reduced density, the reduced diffusion coefficient can be approximated as:

$$D^*(T^*, \rho^*, \alpha^*) \approx A_5 \exp(-B_1 \rho^*) \sqrt{T^*} (A_4 - \alpha^*) \quad (4.17)$$

where $A_5 \approx 0.093 \pm 0.011$ is obtained from the comparison of equation 4.17 to equations 4.14 to 4.16. Using the definition of the reduced variables (Equation 4.13), it is possible to obtain an approximate expression for the diffusion coefficient as a function of the system conditions and interaction parameters:

$$D(T, \rho, \alpha, m, \sigma, \varepsilon) \approx A_5 \sigma \sqrt{\frac{k_B T}{m}} \exp\left(-\frac{B_1 \rho \sigma^3}{m}\right) (A_4 - \alpha) \quad (4.18)$$

where $A_5=0.093$, $B_1=8.6404$ and $A_4=16.9684$. Notice that although the potential well depth (ε) determines the strength of the interaction forces, the net effect on the diffusion coefficient of the molecules is apparently negligible. Now, considering that the molar volume is $V_m=N_A m/\rho$ then:

$$D(T, P, \alpha, m, \sigma) \approx A_5 \sigma \sqrt{\frac{k_B T}{m}} \exp\left(-\frac{B_1 N_A \sigma^3}{V_m(T, P)}\right) (A_4 - \alpha) \quad (4.19)$$

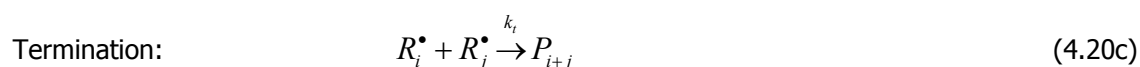
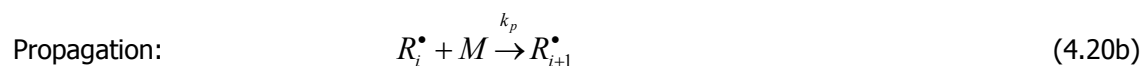
The expression in the exponential contains the effect of the free volume on the diffusion coefficient. The diffusion coefficient is therefore mainly determined by the free volume of the system, the temperature of the system, the size and mass of the molecules and the steepness of the intermolecular repulsion. Molecular modeling simulation methods as well as the model of Vrentas and Duda^[83] are perhaps the most relevant approaches for the estimation of diffusion coefficients in polymers because they consider explicitly the intermolecular forces between the polymer and the diffusion molecule. Additional information about the modeling of diffusion in polymers can be found in the review paper of Masaro and Zhu.^[88]

4.2. Diffusion-controlled polymerization kinetics

A bimolecular reaction can take place only after both molecules find each other by diffusion through the medium. If the rate of reaction is slow compared to the rate of mixing by molecular diffusion, the spatial composition of the system will be homogeneous (perfect mixing). On the other hand, if the rate of mixing by diffusion is lower than the rate of reaction, the reacting system becomes diffusion-controlled and the local spatial composition will not be homogeneous (imperfect mixing).

The most important bimolecular reactions in a polymerization process are propagation and termination. Although the energy of activation is lower for termination than for propagation reactions, the concentration of free radicals in the system is much lower than that of monomer molecules and thus the rate of termination is usually lower than the rate of propagation. Considering a termination rate coefficient of the order of 10^9 L/mol·s, the polymerization becomes diffusion-controlled if the diffusion coefficient of the radicals drops below about 10^{-10} m²/s. Due to the high viscosity of polymer media (low free volume), and to the lower mobility of oligomeric and polymeric radicals, radical diffusivities can easily reach values well below this limit, leading to diffusion control or imperfect mixing, which seriously affects the final conversion and molecular weight distribution of the polymer formed as a result of the competitive nature of radical polymerization reactions. For example, an increased rate of termination due to radical confinement ("cage" effect) reduces the rate of propagation of radicals yielding lower final monomer conversions as well as lower molecular weight polymers. On the other hand, the characteristic mixing time in a solution polymerization may decrease continually during the process due to the increase in the viscosity of the solution, causing isolation of the growing radicals and giving rise to the Trommsdorff or gel effect, and eventually, isolating also the monomer molecules so that the polymerization completely stops (glass effect).

In this section, the kinetics of diffusion-controlled polymerization are investigated using the stochastic simulation algorithm for imperfectly mixed systems (SSA-IM)^[74] described in section 3.1.3., neglecting the local spatial temperature profile that would appear as a result of the heat release during propagation, which also affects the magnitude of the diffusion coefficients. The example considered is the bulk polymerization of methyl methacrylate (MMA) up to high conversions. The reaction scheme considers the following reactions:



k_d is the rate coefficient of initiator decomposition (s^{-1}), k_p is the rate coefficient of radical propagation (L/mol·s) and k_t is the rate coefficient of radical termination by combination (L/mol·s). The initiator decomposition reaction is usually assumed to have an efficiency of reaction (f), because of geminate recombination of primary radicals. However, for SSA-IM simulations this assumption is not required.

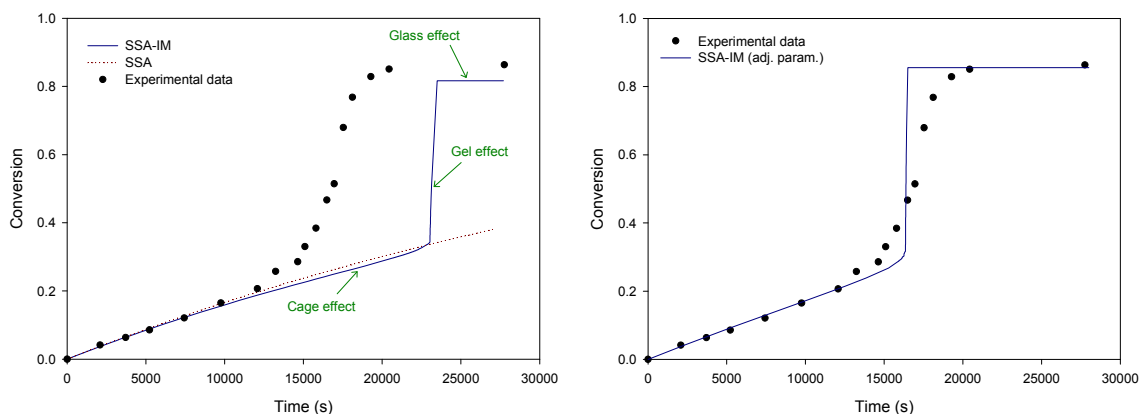


Figure 4.4 Simulation of bulk polymerization of methyl methacrylate up to high conversion. Simulation conditions: $T=323$ K; $[I]_0=0.0166$ M; $[M]_0=9.08$ M; $k_p=299$ L/mol·s; $k_t=2.91 \times 10^7$ L/mol·s; $k_d=6.74 \times 10^6$ s⁻¹; $f=1$. Left: Diffusion parameters from ref. [90]. Right: Modified diffusion parameters.

Experimental data from ref. [89]

The polymerization conditions for the simulation and the experimental data were taken from Tefera et al.^[89] The diffusion coefficients were estimated using the Free-Volume theory as presented by Vrentas and Duda,^[83] using the parameters reported by Faldi et al.^[90] for the MMA/PMMA system. The fastest species in the reactions considered are initiator molecules and primary radicals. It is assumed that the diffusion coefficients of these molecules are the same as the diffusion coefficient of MMA. The kinetic parameters were fitted from the experimental data at low conversion. The simulation results for SSA-IM (incorporating the effect of diffusion control) and for the direct SSA (assuming perfect mixing), and the experimental data are presented in Figure 4.4. For the direct SSA, a system volume of 10^{-16} L was

considered. The conversion-time curves were obtained using SSA-IM for two sets of diffusion parameters, the parameters reported by Faldi (left), and a modified set of parameters where only some of the parameters of the free-volume diffusion model were adjusted (right).

From these results, it is possible to evidence that the SSA-IM algorithm is able to describe all the effects related to mass transfer limitation in free-radical polymerization: the cage, gel and glass effects. The direct SSA and the deterministic methods (both assuming perfect mixing) are unable to describe these phenomena unless the kinetic parameters are forced to change during the polymerization either by using arbitrary breaking points or semi-empirical equations (based for example on the free-volume theory of diffusion).^[91] The SSA-IM method can be considered as the stochastic counterpart to the well-established deterministic methods used to describe diffusion-controlled polymerization reactions. The agreement between the simulation results and the experimental data adjusting some of the parameters of the diffusion model is certainly improved. Even better results are expected to be obtained if more precise models for the estimation of the diffusion coefficient of the molecules can be used, and if additional important factors are included in the algorithm, such as the segmental diffusion of the chains, the full molecular weight distribution of the polymer formed, and the mesoscopic hydrodynamic contribution to the mixing process. A very promising alternative to improve the accuracy of the stochastic algorithm for imperfect mixing is to perform multiscale simulations in which the diffusion coefficients are determined periodically for the corresponding polymerization conditions (temperature, polymer concentration, molecular weight distribution) using a lower-level Molecular Dynamics (as presented in the previous section) or Monte Carlo method.^[92] The estimated values can then be used by the higher-level SSA-IM simulation.

Further potential applications of the SSA-IM include pulsed-laser polymerization (PLP) and heterophase polymerization reactions. Stochastic simulation methods have already been proposed for the simulation of PLP experiments,^[93] but the incorporation of mass transfer effects (imperfect mixing) into the stochastic simulation will certainly help improve the accuracy in the determination of chain-dependent propagation rate coefficients. On the other hand, diffusion and mass transfer limitation phenomena are extremely important for heterogeneous polymerization processes (such as emulsion, miniemulsion, microemulsion, suspension or dispersion polymerization) where segregation and compartmentalization have a predominant effect on polymerization kinetics.

4.3. Particle formation

During *ab initio* emulsion polymerizations, the formation of polymer particles or *particle nucleation* takes place very quickly at the beginning of the process. In multi-stage emulsion polymerizations, particle formation may or may not occur, and if it does, then a bimodal or multimodal particle size distribution is obtained. A fundamental understanding of the thermodynamics, kinetics and mechanisms of nucleation processes is of great importance for the control of particle size distribution and particle morphology. The most important question that must be addressed before investigating

the kinetics of particle formation is the definition of a polymer particle. From a purely kinetic point of view, a polymer particle can be interpreted as an aggregate of monomer molecules and polymer chains such that a radical present in the aggregate can be effectively segregated from the radicals in the continuous phase. At the same time the radical is exposed to a local monomer concentration higher than that in the continuous phase. If segregation is not achieved, the radical in the molecular aggregate will react with other radicals present in the continuous phase and it will not produce a high molecular weight polymer chain and the polymerization rate will be reduced. From a thermodynamic point of view, a polymer particle can be defined as a stable new phase in the system which grows spontaneously as a result of the favorable reduction in Gibbs' free energy. The formation of polymer particles is perhaps the most difficult event to be investigated in emulsion polymerization because its characteristic time and length scales are below the sensitivity of most experimental methods available.

Different mechanisms have been proposed to explain the formation of polymer particles, including self-aggregation, cooperative aggregation, radical phase transfer and chemical reaction (Fig. 4.5). The nucleation of polymer particles can be: *homogeneous*, if only macromolecular chains in the continuous phase are present during the transition, or *heterogeneous*, if any species (polymer, surfactant, monomer, etc.) present in a different phase (seed polymer particle, surfactant micelle, monomer droplet, etc.) is involved in the transition. Therefore, the presence of interfaces is a requisite for the formation of particles by heterogeneous nucleation.

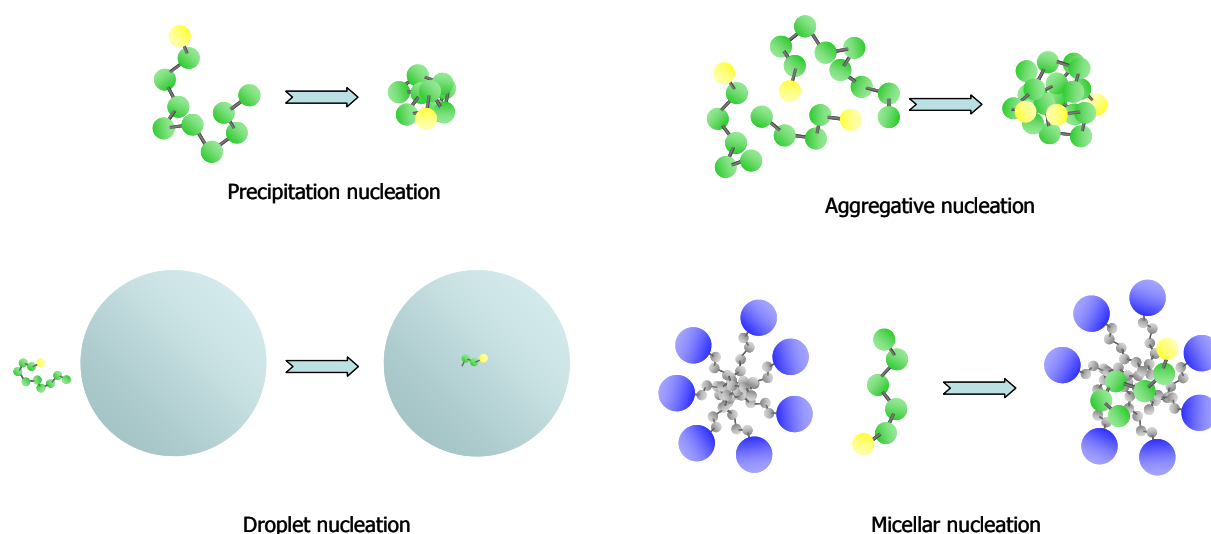


Figure 4.5 Mechanisms of particle formation in emulsion polymerization. Green spheres represent monomer units; yellow spheres: initiator-derived groups; dark blue spheres: hydrophilic moiety of the surfactant; gray spheres: hydrophobic unit of the surfactant; light blue spheres: monomer droplets

The first possible mechanism of particle formation is the collapse of a single polymer chain initially dissolved in the continuous phase. A polymer chain may be present in its coiled or dissolved state when the attraction of the molecules in the continuous phase is stronger than its own intramolecular attraction. At a certain temperature, the intramolecular forces will dominate and the chain segments will attract each other in such a way that the polymer collapses. If the temperature of the system is

kept constant, but the composition of the continuous phase is modified reducing the interaction between the macromolecule and the continuous phase to the point that the intramolecular interactions become stronger than the repulsion originated from thermal motion, the polymer will also collapse. Additionally, for a growing polymer, the addition of a new monomer unit to the chain will increase the intramolecular attraction, and unless the solvent-segment interaction is stronger than the segment-segment attraction, the chain will reach a certain length at which the intramolecular attraction overcomes the thermal repulsion forces and the chain collapses. Since thermal motion exerts a fluctuating force on the chain, the length at which the chain collapses may vary around a certain average critical chain length. This type of single-chain particle formation mechanism is usually called *precipitation particle formation* and was suggested by Fitch and Tsai^[94] and improved some years later by Ugelstad and Hansen.^[95] According to the Hansen-Ugelstad-Fitch-Tsai (HUFT) theory, the rate of particle formation can be determined by:

$$\frac{dN_1}{dt} = 2fk_d[I] \left(1 + \frac{k_{tw}[M\cdot]_w}{k_p[M]_w} + \frac{k_c N}{k_p[M]_w} \right)^{1-j_{cr}} \quad (4.21)$$

where N_1 is the number concentration of new particles, f is the initiation efficiency factor, k_d is the rate coefficient of initiator decomposition, k_{tw} is the rate coefficient of radical termination in water, k_p is the rate coefficient of radical propagation, k_c is the rate coefficient of radical capture by particles, N is the total number concentration of particles and j_{cr} is the critical chain length for precipitation.

An alternative mechanism of homogeneous particle formation consists in the simultaneous interaction of different macromolecules causing a multi-chain collapse. This mechanism is known as *aggregative nucleation*. It is evident that the rate of nucleation in this case will depend on the amount and length of the polymer chains present in the continuous phase relative to their solubility, that is, on the *supersaturation* of the polymer. This mechanism can be described by the theory of homogeneous nucleation developed by Becker and Döring,^[96] presently known as *Classical Nucleation Theory* (CNT). From a thermodynamic point of view, nucleation is characterized by the necessity to overcome a certain energy barrier by means of thermal fluctuations. This energy barrier or activation energy represents the free energy of formation of a critical particle and strongly depends on the specific conditions of the system. Tauer and Kühn developed a modeling framework for aggregative nucleation in emulsion polymerization processes, based on CNT.^[18] The model allows the estimation of the chain length of the nucleating oligomers, the number of chains per nucleus, the diameter of the nucleus, the total number of nuclei formed and the rate of nucleation, using the activation energy of nucleation as the only adjustable parameter. According to the CNT, the rate of particle formation by aggregation of oligomers of chain length j can be calculated as:^[18]

$$\frac{dN_{1,j}}{dt} = \frac{2D_{w,j}}{\nu_w} \left(\frac{\pi\rho_w N_A}{6M_w} \right)^{2/3} \exp\left(-\frac{\Delta G_{\max}}{k_B T} \right) \quad (4.22)$$

$$\Delta G_{\max} = \frac{\pi\sigma^3}{3} \left(\frac{4jM_m}{\rho_p N_A k_B T \ln S_j} \right)^2 \quad (4.23)$$

where $D_{w,j}$ is the diffusion coefficient of the oligomers in water, v_w is the molar volume of water, ρ_w is the density of water, M_w is the molecular weight of water, σ is the interfacial tension between the nucleus and water, M_m is the molecular weight of a monomer unit, ρ_p is the density of the polymer and S_j is the supersaturation of the oligomer of length j , given by the ratio of concentration (C_j) to solubility, which in turn is obtained using the Flory-Huggins interaction parameter (χ):

$$S_j = \frac{M_m C_j}{\rho_p} \left(\frac{j^2(\chi-1) + 2j}{j(1-\chi) - 1} \right) \quad (4.24)$$

It is also possible to consider particle formation as the result of the aggregation of oligomers of different chain lengths. In this case, the total supersaturation of the oligomers forming the aggregate can be expressed as:

$$S = \prod_{j=1}^J S_j^{m_j} \quad (4.25)$$

where m_j is the number of oligomers of length j forming the aggregate. According to the CNT, the free energy of formation for this cluster is:

$$\Delta G = -kT \sum_{j=1}^J m_j \ln(S_j) + \sigma(4\pi)^{1/3} \left(\frac{3M_m}{\rho_p N_A} \right)^{2/3} \left(\sum_{j=1}^J j m_j \right)^{2/3} \quad (4.26)$$

where σ is the interfacial tension oligomer/water, M_m is the molecular weight of a monomer unit and ρ_p is the density of the polymer particle. Therefore, the change in free energy by adding an additional oligomer of size i is:

$$\left(\frac{\partial G}{\partial m_i} \right)_{j \neq i} = -kT \ln(S_i) + \frac{2i\sigma}{3} (4\pi)^{1/3} \left(\frac{3M_m}{\rho_p N_A} \right)^{2/3} \left(\sum_{j=1}^J j m_j \right)^{-1/3} \quad (4.27)$$

The concentration of oligomers in the aqueous phase can be obtained from the kinetics of polymerization in water. A new stable particle is formed as soon as $\left(\frac{\partial G}{\partial m_i} \right)_{j \neq i} \leq 0$, that is, when

$$\frac{1}{i} \ln(S_i) \geq \frac{2\sigma}{3kT} (4\pi)^{1/3} \left(\frac{3M_m}{\rho_p N_A} \right)^{2/3} \left(\sum_{j=1}^J j m_j \right)^{-1/3} \quad (4.28)$$

Equation 4.28 implies that the energy of activation for the nucleation of a particle will strongly depend on the size and amount of oligomers forming the precursor and the size and concentration of the

oligomer which reaches the critical nucleus size. Therefore, there will not be a single unique value of the activation energy of particle nucleation. The noise and variability of the nucleation process is increased by this effect. The drawback of this approach, however, is that the interfacial tension between the nucleus and the continuous phase is a strong (and usually unknown) function of the size of the nucleus. Therefore, the use of Eq. 4.28 may result questionable.

On the other hand, the precipitated polymer aggregate can grow by subsequent absorption (*swelling*) and polymerization of monomer or by the incorporation of additional chains or clusters of chains into the particle. The aggregation of polymer cluster proceeds until the particles are sufficiently stabilized by adsorbed surfactant (from solution, monomer droplets or micelles) or by ionic groups incorporated to the chains from ionic primary radicals or as a result of side reactions of the radicals. The growth of polymer particles via aggregation of polymer clusters or precursors has been called *coagulative nucleation*, in spite that it is not a nucleation process. In fact, the so-called "coagulative nucleation" is not a mechanism of particle formation, but a colloidal aggregation process determining the size and number of particles in the system.

In a typical emulsion polymerization process, the concentration of the monomer in the continuous phase can be several orders of magnitude larger than the concentration of polymer chains in the continuous phase. For this reason, the probability of the formation of polymer particles by homogeneous nucleation without the intervention of monomer molecules is very low. Monomer-polymer association occurs when the chains are still dissolved in the continuous phase, and thus, heterogeneous nucleation necessarily should take place. Additional molecules such as surfactant molecules, initiators, chain-transfer agents, etc. can also associate with the polymer chains and participate in the heterogeneous mechanism of particle formation. In this case, it is important to consider two additional factors: the interaction between the macromolecules and the additional molecules, and the interaction between the molecules and the continuous phase. If the additional chemical species are attracted more strongly to the macromolecules than to the molecules of the continuous phase, then the collapse of the polymer chains will take place more easily. Perhaps the most important chemical species involved in heterogeneous nucleation are amphiphilic molecules because they contain a lyophobic moiety that interacts strongly with the polymer chains while their lyophilic moiety interacts with the continuous phase reducing the interfacial tension of the particle. Surfactants facilitate nucleation by lowering both the interfacial tension and the free-energy barrier thus, leading to faster rates of particle formation. The effect of the amphiphile on the nucleation process will depend also on the concentration of surfactant in the continuous phase. The lyophobic interaction of surfactant molecules is so strong that they are subject to their own phase separation process, which is called *micellization*. Micelles (or surfactant aggregates) are formed after reaching certain saturation in the continuous phase denominated the *critical micellar concentration* (cmc). If a radical is captured by a micelle or a monomer-swollen micelle, segregation of the radical takes place and thus, a new particle is formed. This mechanism of particle formation is called *micellar nucleation*.^[97]

Not only molecularly dissolved monomer but also aggregates of monomer molecules (droplets) can be involved in the formation of polymer particles via capture (absorption or adsorption) of macromolecules, oligomers or primary radicals from the continuous phase. This capture process, which is in principle the aggregation of radicals or chains to monomer droplets, is usually referred as *droplet nucleation*. Although droplet nucleation has been considered to be more relevant for miniemulsion polymerization than for emulsion polymerization, the association of radicals and chains with very small aggregates of monomer molecules (nanodroplets) formed by *spontaneous emulsification*^[98] might be the most important mechanism of particle formation in emulsion polymerization. At first sight, the determining step for the formation of new particle by droplet nucleation is the capture of a primary radical or a growing chain; however, there is also another effect that must be considered: the energy release during the propagation of the radical. In typical emulsion polymerization systems, water-soluble initiators are used for the creation of new chains and thus, the water-soluble initiator fragments at the end of the chains prefer to stay close to the interface than buried inside the particle. Even if the initiator fragments are not soluble in water, propagation will very probably take place while the radical is still diffusing from the surface to the center of the particle. During the propagation reaction, the double bond of the monomer is broken and a new bond between the growing chain and the monomer is formed, releasing a large amount of energy. If the radical is buried inside the particle this energy will be dissipated to the surrounding molecules causing a net increase in the temperature of the particle. However, if the radical is on the surface or close to it, this energy may be used by the radical to escape from the particle. Considering that the energy barrier for the desorption of a monomer unit is E_{des} and the heat released during the propagation reaction is $-\Delta H_p$, then the chain length of the radical for which at least half of the radicals "survive" propagation inside the particles is:

$$z_{1/2} = -\frac{\Delta H_p}{E_{des}} \quad (4.29)$$

If the chain length of the radical is less than $z_{1/2}$, then the radical will be more probably desorbed from the particle (or droplet). If the chain length is greater than $z_{1/2}$, the radical will more probably continue inside the particle. The minimum chain length required to almost completely avoid desorption as a consequence of a propagation event can be approximated as twice the value of $z_{1/2}$:

$$z_{min} = 2z_{1/2} = -\frac{2\Delta H_p}{E_{des}} \quad (4.30)$$

For chain lengths below z_{min} the radical can be continuously captured by droplets or particles but desorbed upon propagation, and thus the kinetics of polymerization will basically correspond to that of a homogeneous process. Once this chain length is attained, the droplet containing the radical can be properly considered as a polymer particle. Although the idea of a critical chain length for particle formation was already considered in the HUFT theory of precipitation nucleation, the underlying

mechanism is completely different. According to the initial results of Fitch and Tsai,^[99] the critical chain length for chain precipitation in the emulsion polymerization of methyl methacrylate (MMA) with sulfate or sulfonate end-groups is on the order of 65 to 75 units, which is a very reasonable result for a polymer collapse process. However, the critical chain length for particle formation estimated from experimental kinetic data of the emulsion polymerization of MMA at 80°C has been found to be on the order of 10 units.^[97] Following the CNT for aggregative nucleation, the critical chain length for MMA emulsion polymerization at 50°C is 11.^[18] According to Eq. 4.30, for MMA at 50°C the minimum chain length for particle formation is 13 ($\Delta H_p = -56$ kJ/mol,^[100] $E_{des} = 8.98$ kJ/mol^[101]). In the case of styrene, at 70°C the experimental critical chain length was found to be 5.^[97] According to the CNT, the critical value for styrene at 50°C is 6,^[18] and using Eq. 4.30, for styrene at 60°C the calculated minimum chain length is 6 ($\Delta H_p = -73$ kJ/mol,^[100] $E_{des} = 24.89$ kJ/mol^[101]). For vinyl acetate at 80°C, the experimental critical chain length is 20,^[44] while the calculated value at 50°C using the CNT framework is 22, and employing Eq. 4.30 at 60°C the critical chain length is 18 ($\Delta H_p = -88$ kJ/mol,^[100] $E_{des} = 10.11$ kJ/mol^[101]). In general, the experimental critical values observed are too low for a polymer precipitation or collapse process. Let us consider for example the critical chain length of styrene: at 70°C the critical length is only 5 monomer units. For this chain length, there is no physically possible single-chain conformation that can completely isolate the radical from the continuous phase, which is required by the definition of a particle presented above. On the other hand, if the chain is surrounded by other chains or by individual monomer molecules, the segregation of the radical is possible. In addition, the probability of finding a particle conformed only of polymer chains is extremely low compared to the probability of finding a particle formed by monomer molecules and polymer chains. For these reasons, the idea of a droplet nucleation mechanism controlled by the enthalpy of propagation seems to be quite reasonable. According to this mechanism, the size of the droplet also plays an important role especially for smaller droplets because the energy barrier of desorption is reduced with decreasing size due to the positive contribution of the Laplace pressure to molecular desorption:

$$E_{des} = E_{nc} + \Delta\mu + \frac{2V_m\gamma}{r_d} \quad (4.31)$$

where E_{nc} is the contribution of non-conservative forces, $\Delta\mu$ is the difference in chemical potential of the oligomer between the aqueous phase and the droplet or particle, V_m is the molecular volume of the oligomer, γ is the interfacial tension between the droplet or particle and water, and r_d is the radius of the droplet or particle.

In the case of small droplets, the minimum chain length required for particle formation may be some units longer than for larger droplets. Even if the radical is not close to the surface, the dissipation of the released energy through the droplet or particle may lead to the desorption of some monomer units, and if the droplet is small enough, this could result in the complete disintegration of the droplet.

A similar argument can be proposed for the formation of particles by micellar nucleation. A swollen micelle can be considered a very small droplet stabilized by a surfactant layer. Even though the surfactant layer can reduce the Laplace pressure effect and can also increase the energy barrier for desorption, the propagation of a radical (especially primary radicals) inside the micelle might still lead to the desorption of the radical. This was evidenced experimentally by Harkins using X-ray diffraction.^[78] In these experiments, Harkins found that the micelles absorbed styrene before polymerization increasing the thickness of the micelles by 7.2 Å. Just after polymerization of the monomer by the action of the X-rays, the thickness of the original micelle was restored indicating that the polymer formed abandoned the micelle and appeared in the aqueous phase. Once the radical is desorbed, it can more easily swell molecular monomer or associate with small monomer droplets and adsorb free surfactant molecules rather than enter the micelle again, depending on the relative concentration of monomer and surfactant in the system. As a result of these effects, micellar nucleation should not be a significant mechanism of particle formation in emulsion polymerization, as it has been demonstrated experimentally using on-line conductivity measurements.^[102]

Using the CNT approach, the first "stable" molecular clusters of monomer are formed at supersaturation values between 5 - 6, containing between 60 and 80 molecules per cluster and with a diameter of about 2.75 – 3 nm. Even larger molecular aggregates are formed close to the source of monomer, where the relative supersaturation values are even higher. The concept of stability in this case is referred to the stability to cluster dissociation, and not to cluster aggregation. These droplets formed by the association of molecularly dissolved monomer units are much smaller than those formed by *comminution* techniques such as mechanical stirring or the application of ultrasound, and can grow further by the incorporation of additional monomer units present in the continuous phase or by coalescence with other droplets. This process of *spontaneous emulsification* has been observed in oil-water systems in the absence of any stabilizer compound. The colloidal stability of the droplets formed by spontaneous emulsification is a matter of further investigation.^[103]

In conclusion, in an emulsion polymerization process different mechanisms of particle formation can take place simultaneously, but their relevance will depend strongly on the composition and conditions of the system. Under typical emulsion polymerization conditions, the formation of particles as a result of the heterogeneous aggregation of growing chains and individual monomer units or small monomer droplets is perhaps the most probable mechanism of particle formation.

4.4. Radical capture

In an emulsion polymerization process the simultaneous high molecular weight and high polymerization rate is only possible to achieve if the polymer particles can contain an odd number of radicals. In this case, at least one single radical will always survive to termination which will continue propagating until all the monomer in the particle is depleted. The presence of odd numbers of radicals inside the particles is possible thanks to the transfer of the activity of single radicals from the

continuous phase to the polymer particle (*radical capture*), or from the polymer particle to the continuous phase (*radical desorption*). The free radicals transferred from one phase to the other can be *primary radicals* (generated after the separation of paired electrons) or *growing chains* (formed after the propagation of primary radicals) of any length.^[19,104] The phase-transfer process of a radical takes place when a radical reaches the interface between the polymer particle and the continuous phase and its kinetic energy is high enough to overcome the resistance to transfer at the interface.

Different mechanisms have been proposed as rate-determining steps in order to describe the kinetics of radical capture by polymer particles:

- Collisional mechanism. The limiting-step for the absorption of radicals is assumed to be the ballistic collision between the radicals and the polymer particles. In this case, the rate of radical capture is proportional to the surface area of the polymer particles.^[94,105]
- Diffusion-controlled mechanism. Given that both radicals and particles are suspended in a continuous phase of water molecules, it is likely improbable that they can follow perfect ballistic trajectories without colliding with water molecules, resulting in a change in their directions and velocities. As a result of the multiple collisions with the continuous-phase molecules, the overall displacement of the radicals and particles is not ballistic but diffusional. For diluted dispersions of polymer particles, the rate of collision by diffusion is given by Smoluchowski equation.^[79] In this case, the rate of radical capture depends linearly on the particle diameter. Considering that not every radical-particle collision leads to a radical absorption event, and that not every absorbed radical reacts inside the particle affecting the kinetics of polymerization, a rate-reduction factor or an *absorption efficiency* factor is included in the model.^[95]
- Colloidal mechanism. Penboss et al.^[106] considered that the polymer particles are electrostatically-stabilized polymer colloids and used the DLVO theory to determine the rate of radical absorption by colloidal aggregation. The resulting dependence of the rate of radical capture to the size of the particles was found to be approximately linear. Cheong and Kim^[107] performed the simulation of surfactant-free emulsion polymerization over electrostatically-stabilized seed particles, and showed that when highly charged seed particles are used, the electrostatic repulsion resulting from the electrical charge of seed particles reduces the absorption rate of the growing oligomeric radical.
- Surfactant displacement mechanism. Yeliiseva^[108] considered that the rate-determining step for radical capture is the displacement of enough surfactant molecules of the stabilizing layer around the particles. The rate of radical capture will therefore depends on the amount of surfactant adsorbed around the particle, on the strength of the interaction between the surfactant and the polymer chains at the interface of the particle, and on the size of the radical. Although the surface density of surfactants and its adsorption strength depend on the curvature of the particle, in general, the size of the particles will have a negligible effect on the rate of radical capture. The presence of a surfactant layer acts as an energy barrier for the absorption process. However, if the energy barrier is not enough, the effect is negligible.

- Propagation-controlled mechanism. Maxwell and coworkers^[109] proposed that the rate-determining step is the growth of the radicals in the continuous phase up to a certain critical chain-length after which the capture process is imminent. According to this model, only oligomeric radicals of a critical chain length can enter the particles, and these radicals do not participate in any other reaction. Entry is independent of particles size and charge.

The mechanism of radical capture in emulsion polymerization has been a matter of controversy for many years. There is plenty of experimental results supporting or contradicting each of the mechanisms proposed, and there is until now, no agreement regarding which is the "correct" mechanism of radical capture, although the diffusional and propagational are the most currently accepted mechanisms.

The rate of radical capture (ρ , radicals/s·part.) assuming a diffusion-controlled mechanism is given by:

$$\rho = 2\pi D_w d_p N_A [R]_w F \quad (4.32)$$

where D_w is the diffusion coefficient of the radicals in water, d_p is the diameter of the particles, $[R]_w$ is the molar concentration of radicals in the continuous phase and F represents the absorption efficiency factor that describes the degree to which absorption is lowered compared to irreversible capture, which is given by:^[95]

$$F = \frac{1}{\left(\frac{D_w}{K_{Req} D_p (X \coth X - 1)} \right) + W'} \quad (4.33)$$

where $X = \frac{d_p}{2} \sqrt{\frac{k_p [M]_p + k_{tp} (n/v_p)}{D_p}}$ and K_{Req} is the equilibrium partition coefficient of radicals

between the particles and water, W' is the potential energy barrier analogous to Fuchs' stability factor, D_p is the diffusion coefficient for the radicals inside the particle, k_p is the propagation rate constant, $[M]_p$ is the monomer concentration in particles, n is the number of radicals per particle, N_A is Avogadro's number and v_p is the particle volume.

A different expression for the efficiency factor was proposed by Nomura:^[17]

$$F = \frac{k_p [M]_p + k_{tp} (n/v_p)}{k_o + k_p [M]_p + k_{tp} (n/v_p)} \quad (4.34)$$

where k_o is the overall radical desorption rate constant for a particle.

On the other hand, the rate of radical capture assuming a propagation-controlled mechanism is:

$$\rho = \frac{N_A k_{pw}}{N} [IM_{z-1}] [M]_w \quad (4.35)$$

where k_{pw} is the propagation rate constant in the aqueous phase, $[M]_w$ is the monomer concentration in the aqueous phase and N is the concentration of particles in the dispersion. By substituting the steady-state concentration of $(z-1)$ -mer radicals $[IM_{z-1}]$, the approximate expressions for ρ and the initiator efficiency, f_{entry} are:

$$\rho = \frac{2N_A k_d [I]}{N} \left\{ \frac{\sqrt{k_d [I] k_{tw}}}{k_{pw} [M]_w} + 1 \right\}^{1-z} = \frac{2N_A k_d [I]}{N} f_{entry} \quad (4.36)$$

$$f_{entry} = \left\{ \frac{\sqrt{k_d [I] k_{tw}}}{k_{pw} [M]_w} + 1 \right\}^{1-z} \quad (4.37)$$

where $z \approx 1 + \text{int}(-23 \text{ kJ/mol} / (RT \ln[M_{sat,w}]))$ is the critical chain length for irreversible capture.

There are still some unresolved issues regarding the mechanism of radical capture. For the propagation-controlled mechanism, for example, no single value of z can provide a perfect fit to all the data.^[17,30] Additionally, it has been evidenced that any kind of species present in the aqueous phase can enter the particles.^[19] Therefore, not only radicals but also initiator molecules or any other type of molecule present in the aqueous phase can be absorbed by the particles. Initiator-derived radicals with only one monomer unit have also a significant contribution on the rate of capture in particles. Even though the capture of radical chains with chain length $j < z$ are thermodynamically not favored, their concentration in the aqueous phase is greater than that of radicals with $j \geq z$, and thus, the frequency of particle-radical collisions is considerable higher.^[110] Moreover, due to side reactions of the radicals in water, different primary radical species ($\cdot\text{OH}$, $\text{SO}_4\cdot$, $\text{C}\cdot$) can be present with correspondingly different thermodynamic properties.

Although the functional dependence of the entry rate coefficient on the particle diameter is very different for the various models, it is quite intriguing that all of them have been successfully validated with experimental data^[111-113] Unfortunately, there are no direct measurements of radical capture (i.e., data free of model assumptions), so it is not possible to test the free-radical-capture model unambiguously;^[114] it is always necessary to perform indirect measurements from the overall kinetics of emulsion polymerization. Sood and Awasthi^[115] demonstrated that depending on the experimental conditions, the particle size dependency of the entry rate coefficient determined using indirect methods might not be reflected on the measured entry rate, and thus erroneous conclusions might be obtained from experimental results. Given the experimental difficulties for the precise observation of radical entry, a different approach to study the mechanism of radical capture is proposed based on the simulation of the Brownian motion of primary radicals generated in the continuous-phase of dispersions of colloidal polymer particles using the Monte Carlo Random Flight (MCRF) method (section 3.1.2). One main advantage of Brownian Dynamics simulation is that the capture rate coefficients can be easily determined based on the well-established mechanistic equations of Brownian motion, and in addition, radical capture kinetics can be determined in a reliable way without the

interference of competitive events such as radical desorption, propagation, termination and additional radical reactions.

The probability density distribution of the time interval for entering a radical to a particular polymer particle is given by the most probable distribution:^[116]

$$P(t) = \frac{1}{\tau} e^{-\frac{t}{\tau}} \quad (4.38)$$

The capture time τ , defined as the time elapsed between the radical generation and its capture by the particles, can be determined using BD simulation for each radical generated in the simulation cell as depicted in Figure 4.6. Then, the capture rate coefficient and the rate of capture are calculated using equations 4.39 and 4.40, respectively:^[67]

$$k_c = \frac{N_A}{N \langle \tau \rangle} \quad (4.39)$$

$$\rho = k_c [R^\bullet] = \frac{N_A}{N} \frac{[R^\bullet]}{\langle \tau \rangle} \quad (4.40)$$

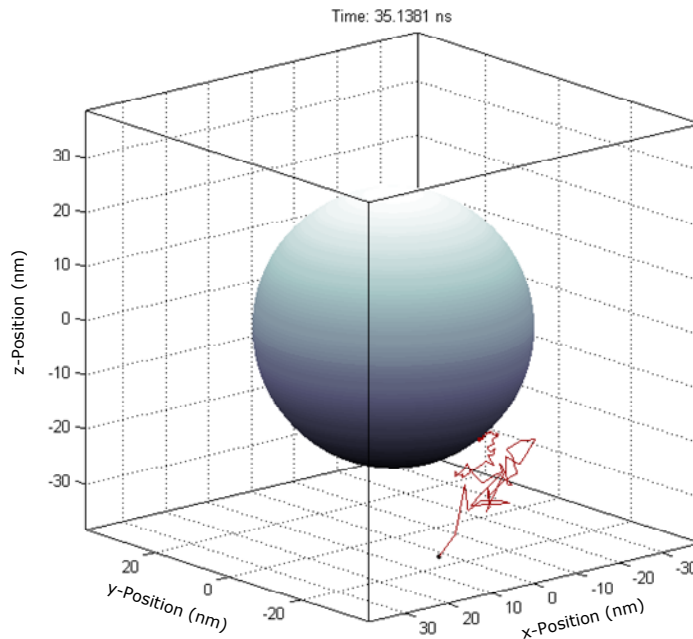


Figure 4.6 Brownian trajectory followed by a radical between generation and capture by a particle

As a first approximation, no interaction forces involving polymer particles, radicals and water molecules are considered explicitly in the system. This assumption facilitates the comparison of the simulation results with the established model described by Smoluchowski equation. In principle, this simplified model is best suited for dispersions of hydrophilic particles since in this case the interaction forces can safely be neglected. It is possible to consider interaction forces during BD simulations

either by incorporating additional forces in Langevin's equation (Eq. 3.26), or by considering energy barriers for radical capture. The capture process is assumed irreversible and is the only event considered during the simulation. This assumption is very important because it allows the determination of *actual* capture rate coefficients and not *net* or *apparent* capture rate coefficients which are the case when additional competitive events such as radical desorption, propagation or termination are present. Unless an energy barrier for capture is present, the absorption of radicals by polymer particles is determined by the collision between a radical and a particle. Radicals are assumed spherical and the diffusion of radicals in water is assumed to follow the Stokes-Einstein equation (Eq. 3.30). The temperature and the volume of the system remain constant during each simulation run. By repeating the simulation for a large number of radicals, each one generated in a random position in the aqueous phase, the lifetime distribution of the radicals until collision with a particle can be determined. The accuracy in the determination of the capture rate coefficient is improved by increasing the number of radicals considered in the calculation. For 1000 radicals, the standard deviation in the determination of the capture rate coefficient was found to be of the order of 3%.

According to Smoluchowski,^[117] the collision rate coefficient between small radicals and large particles is:

$$k_c = 2\pi D_w d_p N_A \quad (4.41)$$

This means that there is a linear relationship between the particle diameter and the term k_c/D_w . The collision rate coefficient between primary persulfate radicals and polymer particles was determined under different simulation conditions with large variations in the size and number concentration of the particles (and therefore in the polymer volume fraction of the dispersion) and in the diffusion coefficient of the primary radicals. The parameters used in the simulations are summarized in Table 4.2. The values of k_c/D_w obtained by MCRF simulation are presented in Fig. 4.7 as a function of the particle diameter and the particle number concentration (expressed in number of particles per cubic meter of dispersion). In the left graph, the x -axis represents the particle size and the dashed lines correspond to contour lines of constant particle number concentration. In the right graph, the x -axis is the particle number concentration and the dashed lines represent constant particle diameter data. Solid lines correspond to the values predicted by Smoluchowski's equation.

Table 4.2 Parameters used in the MCRF Simulation

Parameter	Value (or Range)
Radical diameter*, d_r (nm)	0.5262
Radical mass, m_r (g)	1.594×10^{-22}
Temperature, T (K)	353
Particle diameter, d_p (m)	$2.0 \times 10^{-8} - 5.0 \times 10^{-6}$
Number concentration, N (part/m ³)	$1.44 \times 10^{14} - 7.21 \times 10^{21}$
Diffusion coefficient, D_r (m ² /s)	$1.0 \times 10^{-11} - 1.0 \times 10^{-7}$
Polymer volume fraction**, ϕ_p	$6.545 \times 10^{-7} - 5.236 \times 10^{-1}$

* Assuming the size of the persulfate radical as the size of a sulfuric acid molecule.

** The upper limit of the volume fraction was selected based on the maximum packing ratio for a simple cubic structure.

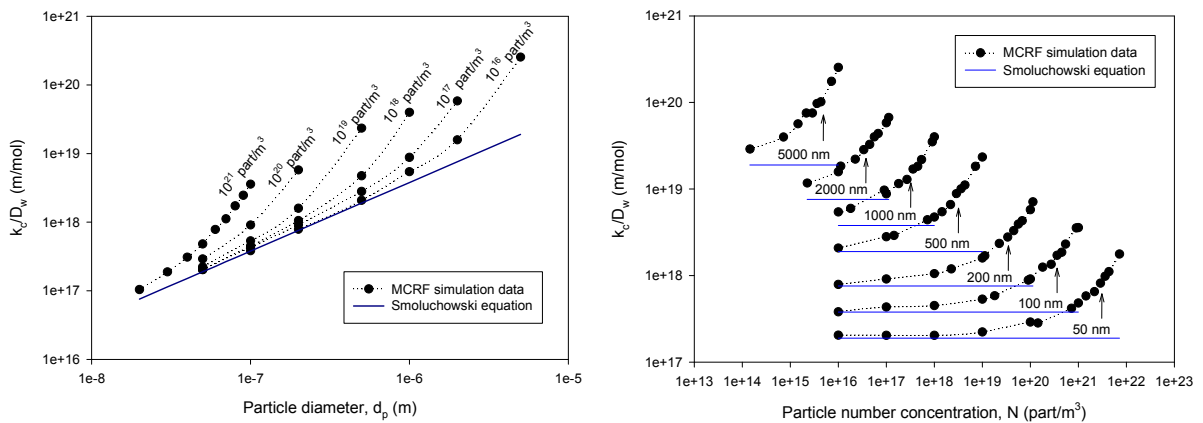


Figure 4.7 Ratio of collision rate coefficient to diffusion coefficient vs. particle diameter and particle number concentration.

According to Smoluchowski's equation (Eq. 4.41), the linear relationship between k_c/D_w and d_p is expected to have a slope equal to $2\pi N_A$ (solid line in Fig. 4.7 left). However, large deviations in the value of k_c/D_w with respect to the ideal behavior predicted by Eq. 4.41 are evidenced. In Fig. 4.7, it is observed that the higher the particle number concentration and the larger the particle size, the larger the deviation from ideality. Since the polymer volume fraction increases with increasing particle number concentration and particle size, the previous results suggest that the volume fraction of the particles in the dispersion has a great influence on the rate coefficient for the capture of primary radicals, which is not taken into account by the Smoluchowski equation. This conclusion is not surprising given the fact that in the derivation of Smoluchowski's equation for diffusion-controlled reactions, the concentration of the particles in the dispersion is assumed extremely low (i.e. only one particle dispersed in an infinite medium), so the particles are not perturbed by the presence of neighboring particles. Therefore, the Smoluchowski equation is expected to work well only at very low particle concentrations.

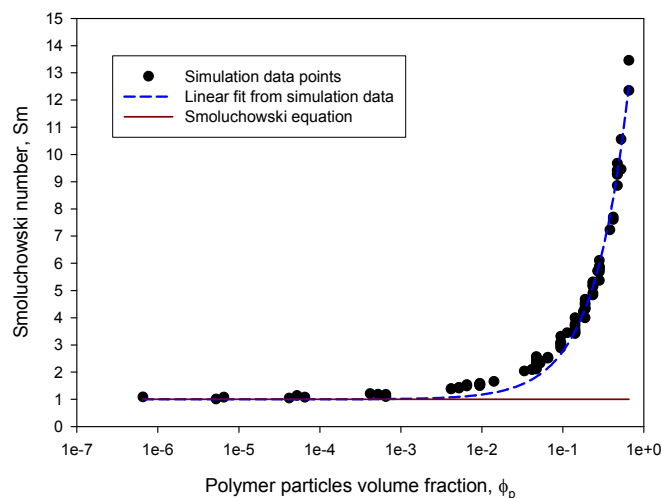


Figure 4.8 Smoluchowski number as a function of polymer particles volume fraction

The ratio between the collision rate coefficient obtained by MCRF simulation and the ideal rate coefficient given by Smoluchowski's equation was plotted against the volume fraction of polymer particles in the dispersion ϕ_p (Fig. 4.8). This ratio has been designated as the dimensionless *Smoluchowski number* (Sm):

$$Sm = \frac{k_c}{2\pi D_r d_p N_A} \quad (4.42)$$

At very low volume fractions of polymer particles the simulation successfully predicts the collision rate coefficient obtained with the Smoluchowski equation ($Sm=1$), while for concentrated polymer dispersions (volume fractions $> 0.1\%$) the Smoluchowski number, and therefore the capture rate coefficient, presents a linear dependence with respect to the volume fraction of polymer particles in the dispersion. This is consistent with the results obtained by Rzepiela et al.,^[118] who found that the rate of aggregation of colloidal particles obtained by simulation always exceeds the value predicted by Smoluchowski theory for fast aggregation, and only for volume fractions below about 0.1% the discrepancy is small. The behavior of the Smoluchowski number can be summarized as follows:

$$Sm = \nu\phi_p + 1 \quad (4.43)$$

where $\nu \approx 17.95$ is a dimensionless constant obtained for the system under the particular conditions considered in the simulation. The regression coefficient for the fit of Equation 4.41 to the data obtained by MCRF simulation was found to be 98.19%. In addition, since for a dispersion of spherical particles

$$\phi_p = \frac{\pi N d_p^3}{6} \quad (4.44)$$

the following expression can be obtained from Eq. 4.42 to 4.44:

$$k_c = 2\pi D_r N_A \left(\frac{\nu\pi N d_p^4}{6} + d_p \right) \quad (4.45)$$

The available radical capture mechanisms predict different dependences of the entry rate coefficient on the particle diameter according to the general model $k_c \propto d_p^a$, where k_c is the capture rate coefficient and a is a functional parameter with a value of 2 for the collision model, 1 for the diffusion and colloidal models, and 0 for the propagational model. It is therefore interesting to point out that when the collision rate coefficient is expressed as a function of particle diameter (Eq. 4.45), depending on the range of values for the number concentration and size of the particles, different functional dependences of the rate coefficient on the particle diameter can be observed, ranging from a linear to a fourth-power relationship. This means that the effect of polymer volume fraction on

collision kinetics under diffusion-controlled conditions could explain the different results obtained during the experimental determination of radical capture kinetics in emulsion polymerization.

Table 4.3 Experimental data used for radical capture model identification

Reference Data	Particle number concentration range (part/m ³)	Particle size range (nm)	Polymer volume fraction range	<i>a</i> (fitted from Eq. 4.45)	<i>a</i> (reported value)
Asua and de la Cal ^[105]	9.8×10 ¹⁸ – 4.9×10 ¹⁹	94 – 154	4.26×10 ⁻³ – 9.37×10 ⁻²	1.43 – 2.34	0 – 1.75*
López de Arbina ^[106]	4.0×10 ¹⁶ – 3.0×10 ¹⁷	79 – 117	1.03×10 ⁻⁵ – 2.52×10 ⁻⁴	1.00	1
Liotta ^[107]	2.0×10 ¹⁸ – 2.0×10 ¹⁹	93 – 215	8.42×10 ⁻⁴ – 1.04×10 ⁻¹	1.17 – 2.08	2**

* A feasible region for the simultaneous estimation of the parameters for the entry and exit models was reported.

** Only integer values of *a* were evaluated (0, 1 and 2).

Experimental data previously used to determine the best model of radical entry are presented in Table 4.3, showing the corresponding particle number concentration, particle size and polymer volume fraction ranges considered in the experiments. The values of particle number concentration are expressed in number of particles per cubic meter of latex dispersion; therefore, these values may vary from the corresponding number concentrations per unit volume of water, especially at high polymer volume fractions.

Different values of particle diameter and particle number concentration (in the ranges shown in Table 4.3) were used in Equation 4.39, assuming a value of $D_r = 1 \times 10^{-9}$ m²/s, to calculate capture rate coefficients. These coefficients were fitted to the general model $k_c \propto d_p^a$, obtaining a value for the parameter *a* at each particle number concentration. The reported best fit value of *a*, as well as the range of values of *a* obtained using Eq. 4.45 are also presented in Table 4.3. As can be seen in Table 4.3, the kinetic model obtained from the MCRF simulation satisfactorily explains the different results, depending on the experimental conditions. The precise determination of the radical capture mechanism can be reliable only if a wide range of values for the polymer volume fraction, from highly diluted (<<0.1%) to concentrated (>10%) dispersions, is considered.

According to the Stokes-Einstein equation (Eq. 3.30), the system temperature affects the diffusion coefficient directly by the term kT , but also indirectly by the viscosity of the medium. The influence of temperature on viscosity for liquids is usually expressed in the form:

$$\eta = Ae^{B/T} \quad (4.46)$$

where for pure water, $A=6.404 \times 10^{-3}$ cP and $B=1418$ K.^[119] From equations 4.45 and 4.46, the capture rate coefficient as a function of the system temperature is:

$$k_c = \frac{2}{3} \frac{d_p}{d_r} \frac{RT}{A} \left(1 + \frac{\nu \pi N d_p^3}{6} \right) e^{-B/T} \quad (4.47)$$

Up to this point, every radical-particle collision was considered as a successful radical capture event. However, interaction forces, interfacial tensions, the presence of stabilizer molecules at the surface of the polymer particles and many other physical and chemical effects may lead to an increase in free

energy during radical capture, and thus, to the existence of an energy barrier for radical capture. In these cases, only a fraction of the radicals colliding with the particles will be effectively captured (capture efficiency) and the other will just bounce. When a radical is not captured by a particle because of the energy barrier, the radical will remain close to the particle surface and therefore it will have a very high probability of hitting the same particle again, leading to a series of multiple collisions in a very short time before the radical goes away from the particle surface.^[120] BD simulations were performed for the same system, but this time varying the system temperature between 278 and 353 K, and the magnitude of the energy barrier between 0 and 50 kJ/mol. The effect of the magnitude of the energy barrier on the capture efficiency is presented in Figure 4.9, and the effect of the energy barrier at different temperatures on the capture rate coefficient is presented in Figure 4.10.

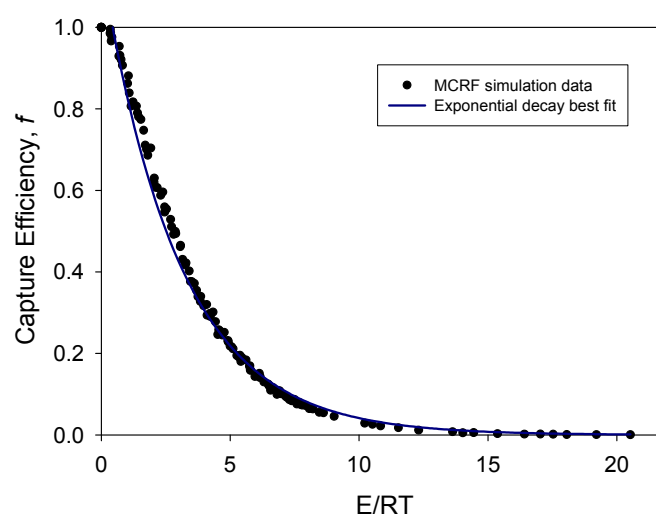


Figure 4.9 Effect of energy barrier on capture efficiency.

The radical capture efficiency (f) defined as the fraction of collisions leading to radical capture with respect to the total number of radical-particle collisions depends strongly on the energy barrier that a radical must overcome to get inside a polymer particle. Only if the energy of the collision, calculated as the sum of the kinetic energies of the radical and the particle, is higher than the energy barrier for radical capture, the collision leads to a successful capture. Therefore, the capture efficiency is expected to behave according to Equation 3.40d, that is, to show an exponential decay with respect to E/RT , where E is the magnitude of the energy barrier for radical capture.

BD simulation results varying the magnitude of the energy barrier (Figure 4.9 and 4.10) clearly evidence that the capture efficiency f decays exponentially with E/RT , while the radical capture coefficient remains almost constant until certain “apparent” threshold energy (E^*) is reached, and then it shows the expected exponential decay. As stated before, this behavior is explained by the very high probability of a repeated collision after any radical-particle collision not leading to successful capture. The magnitude of the apparent threshold energy observed under the conditions of the simulation is approximately $10 RT$, corresponding to a capture efficiency of about 0.04. This means that a radical hits the same particle on average 25 times before going away unless radical capture

occurs. It is important to remark that in this case, parallel competitive reactions of the radical, such as propagation, chain transfer or termination, have been neglected. The effect of an energy barrier on the capture rate coefficient can be expressed as:

$$k_c = \begin{cases} k_{c0} & , E < E^* \\ k_{c0} e^{-\frac{(E-E^*)}{3RT}} & , E \geq E^* \end{cases} \quad (4.48)$$

where k_{c0} , the capture rate coefficient in the absence of energy barriers, is given by Equation 4.47, and E^* is the magnitude of the apparent threshold energy which is expected to be a function of the radical and particle diameters.

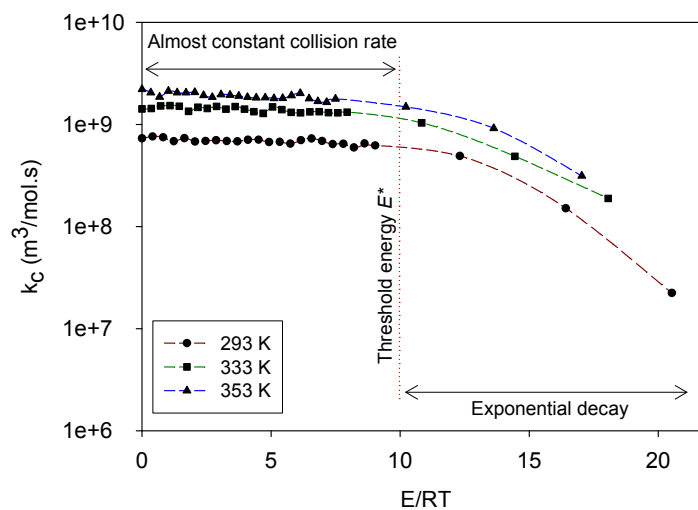


Figure 4.10 Effect of temperature and energy barrier on capture kinetics. Data points are the results obtained by BD simulation. Dotted lines are smoothed curves.

4.5. Radical desorption

The process of radical desorption can be regarded as the opposite to radical capture. In this case, a free radical is transferred from the interior of the particles to the continuous phase. The mechanism by which this transfer takes place is also similar: the radical must reach the particle surface and then it must overcome the barrier for desorption exerted by the interface. In general, desorption will result in a decrease in the concentration of radicals in the particles and hence cause the rate of polymerization to decrease. For many important emulsion polymerization systems, exit is a major (or the only) cause of the loss of free-radical activity inside a particle.

Ugelstad et al. in 1967^[81] proposed that the rate of radical desorption was inversely proportional to the surface of the particle, but quantitative results were not possible at that time. Nomura, Harriot and Litt almost simultaneously suggested that the chain transfer to monomer inside the particles and

the subsequent desorption of the radicals into the aqueous phase was responsible for the different kinetic behavior in the emulsion polymerization of vinyl acetate, and not the high water solubility of the monomer.^[101] Nomura and coworkers, aware of the necessity of estimating quantitatively the rate coefficient for radical desorption from the particles for the prediction of rates of emulsion polymerization, developed the first quantitative model of radical desorption. They continued improving this model during more than one decade. Asua et al.^[121] complemented the model of desorption by considering the fate of the radicals in the aqueous phase. Further improvements of the model have been proposed by considering the layer of stabilizer around electrosterically stabilized polymer particles as an additional resistance to the desorption process.^[122,123]

The diffusion-controlled mechanism for radical desorption is widely accepted right now, but there are minor differences regarding the mathematical treatment of the problem leading to different expressions for the rate of radical desorption. However, all of them predict the same inverse dependence on the surface area of the particles. Some of these differences are caused by a lack of consensus regarding the definition of radical desorption. Different concepts of radical desorption have been used previously in the literature. In this work, the following own definitions are used:

- *Simple radical desorption:* Simple radical desorption is the result of the diffusive motion of the radicals when no reactions are considered inside the polymer particles. In this definition, the fate of the radicals after desorption is not considered. The rate coefficient of simple radical desorption (k_0), also known as maximum desorption rate coefficient, is determined by the velocity at which the radical diffuses out of the particle and is a function of the particle size (d_p) and the diffusion coefficient of the radical inside the polymer particle (D_p):

$$k_0 = \lambda \frac{D_p}{d_p^2} \quad (4.49)$$

where λ is a constant with a value of 60.^[101]

- *Equilibrium radical desorption:* The equilibrium desorption of a radical takes into account the different solubility of the radicals between the polymer particles and the aqueous phase. In this case, radicals are assumed to reach an equilibrium distribution between the bulk aqueous phase and the polymer particles, represented by the partition coefficient. In this definition, competitive reactions involving the radicals are neglected, and the fate of the radicals in the bulk aqueous phase is not considered. The rate coefficient of equilibrium radical desorption (k_0^*) can be related to the simple radical desorption rate coefficient by:

$$k_0^* = \frac{k_0}{\left(1 + K_{eq} \frac{D_p \delta_w}{D_w \delta_p}\right)} \quad (4.50)$$

where D_w is the diffusion coefficient of the radical in the aqueous phase, K_{eq} is the partition coefficient of the radical between the polymer particle and the aqueous phase, δ_w is the thickness of the stagnant layer in the aqueous phase and δ_p is the thickness of the diffusion layer in the polymer phase. The equilibrium radical desorption can also be considered from a

kinetic point of view as the simple radical desorption in the presence of an energy barrier for desorption, originated by the difference in chemical potential of the radical between both phases and by the presence of surfactant layers around the particles:

$$k_0^* = k_0 e^{-\frac{E_{des}}{k_B T}} \quad (4.51)$$

in very good agreement with experimental data.^[101]

- *Net radical desorption:* The net desorption of a radical occurs when the radical escapes the polymer particle after surviving the competitive reactions taking place inside. The possibility of radical re-absorption and re-desorption is not considered. The rate coefficient of net radical desorption (K_D) is determined by:

$$K_D = (k_{regen} + \rho) \cdot \frac{k_0^*}{k_0^* + \sum_i k_{i,p}} \quad (4.52)$$

where $k_{i,p}$ is the rate of the i -th reaction involving radicals and k_{regen} is the rate of generation of desorbing radicals inside the particle. Possible sources of radical generation are the decomposition of oil-soluble initiators or chain transfer reactions inside the particles.

- *Effective radical desorption:* A radical is considered to be effectively desorbed from the particle only after it reacts in the aqueous phase. This definition accounts for the fact that desorbed radicals which diffuse through the aqueous phase may be reabsorbed by a polymer particle and continue reacting therein, without significantly affecting the kinetics of emulsion polymerization. The rate coefficient of effective radical desorption is (k_{des}):

$$k_{des} = k_{regen} \cdot \frac{P_w(1-P_p)}{1 - (1-P_w)(1-P_p)} \quad (4.53)$$

where $P_p = \frac{\sum_i k_{i,p}}{k_0 + \sum_i k_{i,p}}$ is the probability of reaction of the radical inside the particles and

$$P_w = \frac{\sum_i k_{i,w}}{k_{abs} + \sum_i k_{i,w}}$$

is the probability of reaction of the radical in the continuous phase.

The model of equilibrium radical desorption was developed by Nomura and coworkers, and it has been widely used to describe radical desorption in heterophase polymerization. However, the underlying assumptions involved in the derivation of this model may not be fulfilled by a radical desorption process in a real emulsion polymerization system. The theory of mass transfer by Fickian diffusion through stationary films may not be suitable for describing radical desorption because in this case the radicals are present in a very low concentration inside or around the particles, and therefore it is not possible to have radical concentration profiles around the particles or to observe stationary boundary layers for the transfer of radicals.^[115] Nomura and Harada were aware of this situation when they presented the model.^[124] Now, if the concentration of radicals inside the particles is compared to

the concentration of radicals in the bulk of the aqueous phase, it is clear that the latter cannot be neglected as is also assumed in this model.

On the other hand, the equilibrium radical desorption model considers that a radical is desorbed only until it reaches the bulk of the aqueous phase. However, immediately after the radical abandons the particle surface, it is able to react with other molecules present in the aqueous phase (i.e. monomer, chain transfer agents, other radicals), or to re-enter the particle. All these events are possible even in the boundary layer surrounding the particle, as was demonstrated by Thickett and Gilbert^[40] who reported chain transfer and termination reactions taking place in the stabilizer layer outside the particle. Therefore, the radical is desorbed just after abandoning the particle surface (as is assumed by the simple desorption model) and not after abandoning the boundary layer. A very clear evidence of the failure of the boundary layer model was presented by Grady.^[125] He calculated the thickness of the stationary layer around the polymer particles and found that increasing the volume fraction of particles the boundary layers of neighbor particles begin to overlap, and around a volume fraction of 15% the mass transfer boundary layer of the particles occupy the whole aqueous phase volume. Considering the traditional equilibrium model, this means that in polymer dispersions with volume fractions above 15% it is impossible to observe radical desorption since the radicals will never abandon the boundary layers of the particles, and this is evidently not the case.

The equilibrium radical desorption model has been successfully used because it is able to explain the effect of the hydrophobicity of the radicals on the desorption rates. However, this effect can also be explained using energy barriers for phase transfer in the simple radical desorption model (Equation 4.51) instead of assuming equilibrium radical concentration profiles and using radical partition coefficients.

Similarly to the capture process, the probability of overcoming the interfacial energy barrier depends on the nature and length of the free radical. As the chain length or hydrophobicity increases, the probability of overcoming the energy barrier is reduced exponentially. For this reason, the transfer of the radical activity to a smaller molecule increases the rate of radical desorption from the polymer particles. Although this effect is especially important for monomers such as vinyl acetate, vinyl chloride and ethylene, for more hydrophobic monomers such as styrene it cannot be neglected.

The rate at which any given molecular species abandons a particle depends on the concentration and the diffusion coefficient of the molecule inside the particle, on the size of the particle, on the magnitude of the energy barrier for desorption and on the rate of competitive processes that consume the molecules before they leave the particle. The diffusion coefficient inside the particle is closely related to the size and shape of the diffusing molecule and the magnitude of intermolecular forces acting on the molecule. The energy barrier for desorption depends basically on the chemical potential of the molecule between the polymer particle and the continuous phase, which includes the interfacial free energy involved in the process.

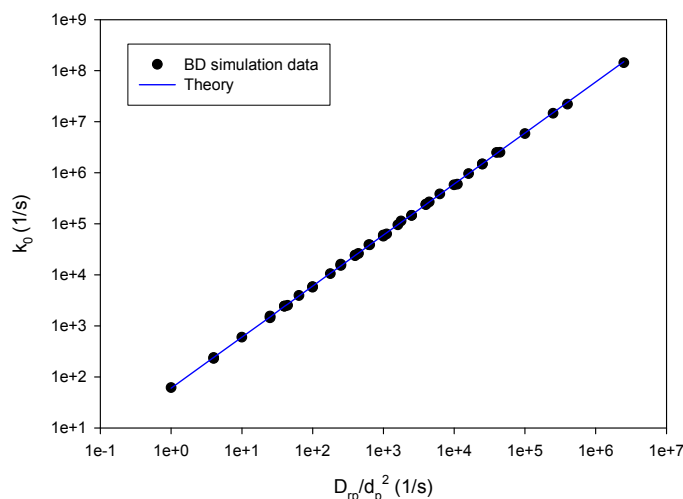


Figure 4.11 Linear regression of BD simulation results for simple radical desorption rate coefficients as a function of D_r/d_p^2 . Data points represent BD simulation results. Solid line corresponds to the theoretical results obtained using Equation 4.49.

In this section, simple radical desorption rate coefficients are obtained from the simulation of the Brownian motion of radicals inside the particles using a variable time-step MCRF method for BD simulation, similar to the method used for estimating radical capture by polymer particles. Figure 4.11 presents the rate coefficients of simple radical desorption obtained from BD simulations performed under the homogeneous distribution assumption for different particle diameters and radical diffusion coefficients. Notice that the desorption rate coefficients are estimated using average values of desorption time obtained from many single-radical simulations (usually between 2000 and 20000 simulations). In Figure 4.11, the linear regression of the simple desorption rate coefficient as a function of D_r/d_p^2 for the complete set of simulation data is presented. The fitted value of the slope for the simulation data was 57.14, in very good agreement with the value of 60 predicted by the theoretical model.^[101]

In many situations, the polymer particles are not perfectly uniform as was assumed above. This is the case, for example, of structured particles. In these cases, analytical expressions for the calculation of simple desorption rates are difficult to obtain, whereas they can be easily estimated using BD simulation. The system conditions for BD simulation are selected in such a way that the radicals are generated uniformly in both phases, generated only in the shell or generated only in the core of the particle. It is assumed that there is no energy barrier for the exchange of radicals through the different interfaces (core-shell and shell-continuous phase).

In the first case, core/shell polymer particles composed of a hard and a soft polymer are considered. The particle size is kept constant at $d_p = 100$ nm, and the diffusion coefficients for the hard and soft polymer phases are assumed to be $D_{hard} = 10^{-12}$ m²/s and $D_{soft} = 10^{-9}$ m²/s respectively. This range of values can be observed during the transition of a monomer-polymer solution from the amorphous to the glassy state.^[83,90,92] The simulations were run for both cases: hard core/soft shell and soft

core/hard shell, varying the volume fraction of the soft polymer phase (ϕ_{soft}). The results obtained are summarized in Figure 4.12 and compared to the rate coefficients for homogeneous particles of hard or soft polymer of similar size calculated with equation 4.49.

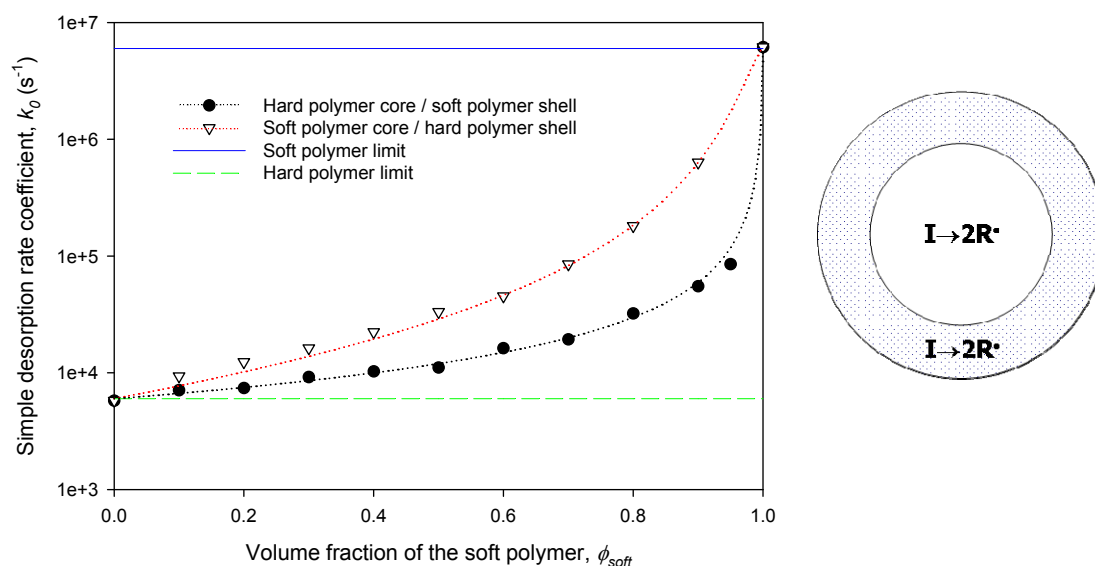


Figure 4.12 Simple desorption in core/shell particles. Simulation conditions: $d_p = 100$ nm, $D_{hard} = 10^{-12}$ m²/s and $D_{soft} = 10^{-9}$ m²/s. Dotted lines: Best fit using equation 4.54

Figure 4.12 shows that the simple desorption rate coefficient increases with an increase in the volume fraction of the soft polymer. In addition, the average desorption rate coefficient in a core/shell particle is strongly determined by the nature of the core material. For this reason, a particle with a given volume fraction of the soft material in the core presents a simple desorption rate coefficient always higher than that of a particle with the same composition but with the hard material in the core. A general empirical equation that can be used to fit both sets of data is the following as a function of the volume fraction of the soft material (ϕ_{soft}) is:

$$k_0 = \frac{a + b\phi_{soft}}{1 + c\phi_{soft} + d\phi_{soft}^2} \quad (4.54)$$

where the soft material can form either the core or the shell of the particle. The following parameters were obtained for the hard core/soft shell particles: $a = 6000$, $b = 0$, $c = -0.999$, $d = 0$. On the other hand, the parameters obtained for the soft core/hard shell were: $a = 6000$, $b = 2863$, $c = -1.974$, $d = 0.9751$.

A second case of desorption in core-shell morphologies is observed when the radicals are generated predominantly in the shell. This is the case of a monomer layer around a polymer particle or the encapsulation of a non-solvent by a polymer shell (hollow particles). In Figure 4.13 the results obtained, varying the volume fraction of the shell, are presented using the following conditions: $d_p = 100$ nm, $D_c = 10^{-12}$ m²/s and $D_s = 10^{-9}$ m²/s.

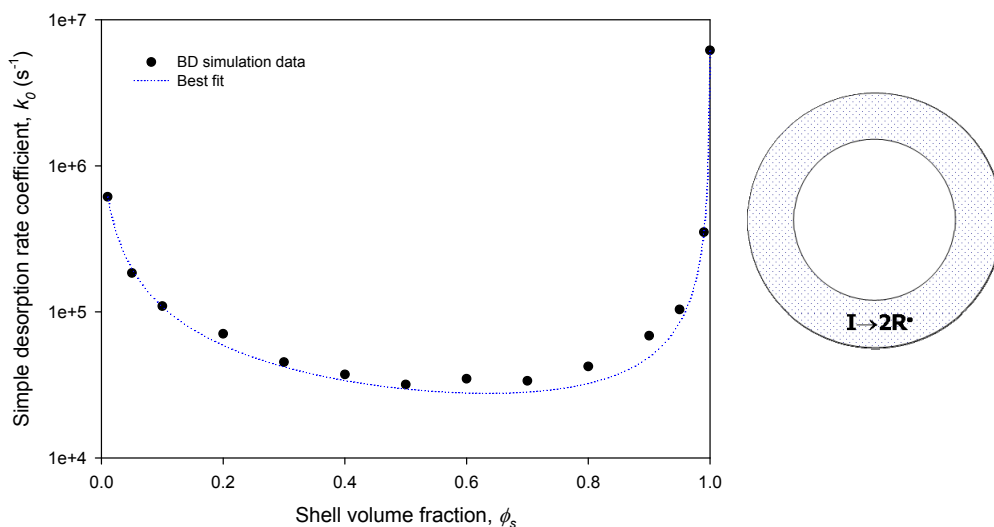


Figure 4.13 Simple desorption of radicals generated exclusively in the soft shell. Simulation conditions: $d_c = 100$ nm, $D_c = 10^{-12}$ m²/s and $D_s = 10^{-9}$ m²/s. Dotted line: Best fit using equation 4.54

The data presented in Figure 4.13 can also be fitted using equation 4.54. The fitted parameters obtained are: $a = 1321960.5$, $b = -888759$, $c = 115.41$ and $d = -116.34$. The behavior observed in Figure 4.13 is very interesting: the simple desorption rate coefficient initially decreases, then reaches a plateau and finally increases with an increasing volume fraction of the shell. Additionally, when the volume fraction of the shell is close to zero, the desorption rate is high and its value do not tend to the desorption rate coefficient for a homogeneous particle made only with polymer from the core. The reason for this is basically that when the shell volume fraction is reduced the radicals are generated closer to the particle surface, and this effect is more important than the increase in the volume fraction of the core with a smaller diffusion coefficient. This limiting situation is very similar to the case where the radicals are captured from the continuous phase. An increase in the volume fraction of the shell causes two opposite effects. On one hand, the radicals are generated closer to the center of the particle, and therefore the diffusion paths and average diffusion times before desorption are increased. On the other, the proportion of material of the shell increases (soft material in this example) and thus the overall diffusion becomes faster. For low shell volume fractions (<20%) the first effect dominates; for intermediate compositions (20% - 80%), both effects cancel out each other and an almost constant desorption rate coefficient is obtained; for high shell volume fractions (>80%) the second effect is more important and the desorption rate coefficient increases until the value for a homogeneous soft particle is reached.

When the radicals are generated mostly in the core of the particle, the shell acts basically as a barrier for radical desorption. There are several practical examples, but perhaps the most representative case is the presence of a surfactant layer around the particle. In this case, the radicals are generated uniformly in the polymer core while there is no radical generation in the shell. BD simulations for particles with $d_p = 100$ nm, $D_c = 10^{-12}$ m²/s and $D_s = 10^{-9}$ m²/s are presented in Figure 4.14.

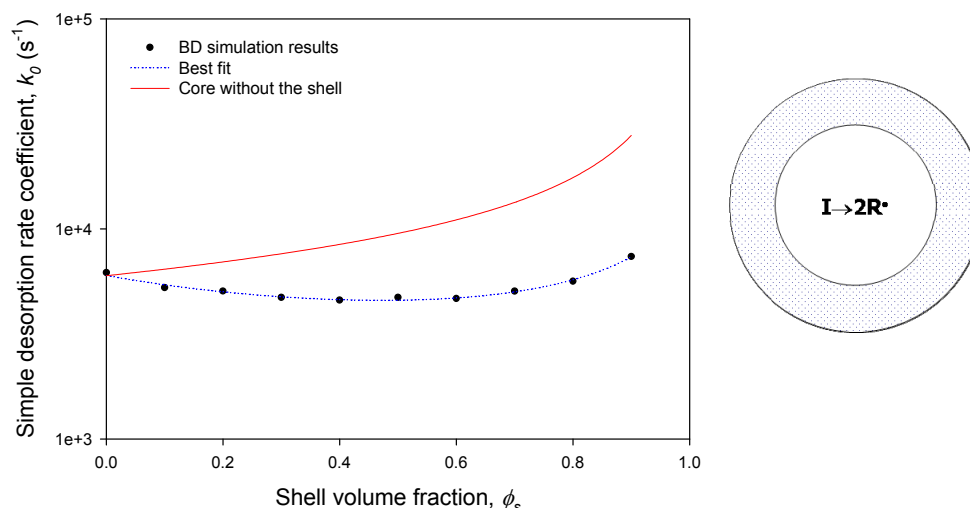


Figure 4.14 Simple desorption of radicals generated exclusively in the hard core. Simulation conditions: $d_c = 100$ nm, $D_c = 10^{-12}$ m²/s and $D_s = 10^{-9}$ m²/s. Dotted line: Best fit using equation 4.54. Solid line: Simple desorption rate coefficient of particles without any shell having the same size as the core of core-shell particles with a shell volume fraction ϕ_s .

Fitting the results of BD simulation using equation 4.54, the following parameters are obtained: $a = 6000$, $b = -3236.3$, $c = 0.6157$, $d = -1.4017$. In this case, the simple desorption rate coefficient remained almost constant for a wide range of shell volume fractions (0% - 80%). Just as in the previous example, the same two opposite effects are observed. When the volume fraction of the shell increases, the radicals are also generated closer to the center of the particle increasing the diffusion paths for desorption, whereas the increase in the proportion of soft polymer increases the average diffusion coefficient of the radical. In the present example both effects are equally important for almost the whole range of shell volume fractions and this is why the desorption rate coefficient is relatively constant. However, a slight decrease followed by an increase in desorption rates is observed. Comparing desorption rate coefficients for this type of core-shell particles with desorption rate coefficients expected only for the particle cores (in the absence of the shell), it is observed that the presence of the shell acts as a barrier for desorption. The thicker the shell, the larger the decrease in the desorption rate of the particle. Additional examples of the application of Brownian Dynamics Simulation to the estimation of simple radical desorption kinetics in emulsion polymerization are presented in ref. [126].

4.6. Monomer swelling

Another important physical phase-transfer process taking place in an emulsion polymerization is the swelling of polymer particles. The swelling of a polymer is the process by which the molecules of a good solvent for the polymer strongly attach to the macromolecular chain. By means of this process, polymer particles can grow to sizes much larger than their original unswollen sizes.^[127] With a very few exceptions (e.g. acrylonitrile, vinyl chloride), the monomer is a good solvent for the polymer, and

therefore, it can swell the polymer particles. Swelling takes place as a result of the diffusion through the aqueous phase of individual molecules or clusters of molecules to the surface of polymer particles and the subsequent absorption when the interfacial energy barrier is surpassed. Given that the diffusion through the continuous phase can be a limiting factor for many solvents, for any given solvent the higher is the solubility of the solvent in water, the faster will be the rate of swelling.^[128]

From a thermodynamic point of view, the driving force for the swelling of a polymer by a solvent is the free energy of polymer-solvent mixing which has both entropic and enthalpic components. At equilibrium, the change in free energy becomes zero, and therefore:

$$\Delta G_{mix} = \Delta H_{mix} - T\Delta S_{mix} = 0 \quad (4.55)$$

Using the Flory-Huggins approach to describe the enthalpy and entropy of mixing, and including an additional term for the change in surface free energy of the particle, the *Morton-Kaizermann-Altier (MKA) equation* for crosslinked particles is obtained:

$$\frac{\Delta\mu}{RT} = \ln(1 - \Phi_p) + \Phi_p \left(1 - \frac{1}{P_n}\right) + \chi\Phi_p^2 + b \frac{V_m \rho_p}{M_C} \left(\Phi_p^{1/2} - \frac{\Phi_p}{2}\right) + \frac{2V_m \gamma \Phi_p^{1/3}}{r_0 RT} \quad (4.56a)$$

which becomes:

$$\ln \Phi_m = \left(\frac{1}{j} - 1\right) \Phi_p - \chi\Phi_p^2 - b \frac{V_m \rho_p}{M_C} \left(\Phi_p^{1/2} - \frac{\Phi_p}{2}\right) - \frac{2\bar{V}_m \gamma}{RT r_p} \quad (4.56b)$$

where Φ_p and Φ_m are volume fractions of polymer and monomer inside the particle, χ is the Flory-Huggins interaction parameter between polymer and monomer and is a function of concentration, V_m is the partial molar volume of the monomer, γ is the interfacial tension between the particle and the surrounding medium, r_0 is the unswollen particle radius, r_p is the swollen particle radius, b is a crosslinking parameter ($b=0$ uncrosslinked, $b=1$ crosslinked), ρ_p is the density of the polymer and M_C is the average molecular weight between crosslinks. The last term in Equation 4.56 represents the resistance because of the creation of new surface area upon swelling. The origin of this resistance is the pressure difference between the interior of the particle and the continuous phase (*Laplace pressure*), which is proportional to the radius of curvature and the interfacial tension of the particle. For this reason, larger particles swell to a larger extent and also swell initially faster.^[129] The Laplace term also indicates that larger objects in coexistence with smaller ones will grow in size at the expense of the smaller objects, which have a tendency to dissolve. This effect is known in colloid science as *Ostwald ripening*. The dissolution of emulsion droplets can be retarded or even prevented if the droplets contain a substance which is insoluble in the continuous phase. In this case, the decrease in size increases the chemical potential of the insoluble compound inside the smaller drops and generates a force counteracting Ostwald ripening. Even a small amount of a water-insoluble

compound is able to stabilize towards degradation by diffusion. In order to prepare stable emulsions, it is necessary that this compound have a high degree of water insolubility.^[130]

Even if the monomer and the polymer are miscible in all proportions in bulk, only a limited amount of monomer can enter a latex particle from the monomer saturated aqueous phase.^[95] Each particle can swell only to the extent where the free energy of mixing and the surface energy change on swelling exactly compensate each other and there is a well-defined swelling equilibrium. In emulsion systems the presence of emulsifier greatly lowers the interfacial tension and allows a substantial amount of swelling.^[131] For crosslinked particles, the swelling capacity is strongly reduced and depends inversely on the degree of crosslinking.^[132]

The experimental values of swelling are much lower than described by the classical MKA equation. Antonietti et al.^[133,134] observed a pronounced dependence on the swelling ratio on particle size. In order to explain this phenomenon, the authors presented a modified description that considered size-relevant effects using an additional swelling pressure term, which increases with the curvature of the particle size and counteracts swelling. The MKA equation cannot be trusted to accurately predict the concentration of monomer inside a particle as a function of the particle radius.^[40] The corrected equation for swelling equilibrium presented by Kaspar,^[135] is the following:

$$\ln \Phi_m = \left(\frac{1}{j} - 1 \right) \Phi_p - \chi \Phi_p^2 - b \frac{V_m \rho_p}{M_C} \left(\Phi_p^{1/2} - \frac{\Phi_p}{2} \right) - \frac{\bar{V}_m}{RT} \left(\frac{2\gamma}{r_p} + \Delta\Pi \right) \quad (4.56c)$$

where $\Delta\Pi$ is the swelling pressure.

The volume fraction of monomer in the particle can be expressed as a function of the number of molecules in the particle (nm):

$$\Phi_p = 1 - \Phi_m = \frac{N_A v_{p0}}{n_m V_m + N_A v_{p0}} \quad (4.57)$$

where v_{p0} is the volume of the unswollen particle.

From a molecular point of view, monomer or solvent molecules are continuously absorbed by or desorbed from the polymer particles. If the rate of molecular absorption per particle is larger than the rate of desorption, swelling takes place, otherwise *deswelling* occurs. Thus, swelling (or deswelling) is simply the result of the balance between the absorption and desorption of molecules. At steady state, the rates of desorption and absorption are exactly the same, and thus, there is no net change in the number of molecules inside the particles. The ratio of the concentration of molecules inside the particle to the concentration of molecules in the continuous phase is the steady-state partition or steady-state partition coefficient (K_{ss}). Since the rates of desorption and absorption depend on the diffusion coefficients inside the particles and in the continuous phase, respectively, they are determining factors for the steady-state distribution of the molecules in the system.

The effect of the diffusion coefficients on the steady-state partition coefficient in dispersions of polymer particles is investigated using BD simulation. A system composed of a 10% volume fraction dispersion of spherical particles (100 nm in diameter) is considered. The diffusion coefficient of the continuous phase (D_w) was considered to be 10^{-9} m²/s, while the diffusion coefficient inside the particles (D_p) was varied between 5×10^{-11} and 1×10^{-8} m²/s. Although the upper limit of 1×10^{-8} m²/s may seem too high compared to real values, it was used in order to consider also the case where $D_p > D_w$. The initial concentration of the species was assumed to be uniform and identical between the particles and the continuous phase. No energy barriers for phase transfer of the molecular species were considered. Under these conditions, the system was allowed to equilibrate for 2000 ns, and then, the steady-state partition coefficient between the particles and the continuous phase was calculated as:

$$K_{ss} = \frac{[M]_p}{[M]_w} = \frac{1 - \phi_p}{\phi_p} \cdot \frac{n_p}{n_w} \quad (4.58)$$

where n_p and n_w are the number of molecules present in the particle and continuous phase. The results obtained are presented in Figure 4.15.

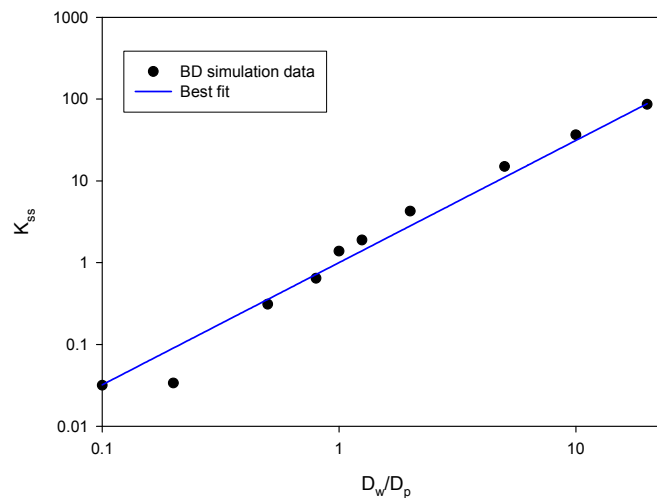


Figure 4.15 Steady-state partition coefficients as a function of the ratio between diffusion coefficients.

Solid line: Best fit using equation 4.59

From these results, it can be concluded that the molecules tend to accumulate in the phase where they present the lowest diffusion coefficient. This is reasonable because the fastest molecules will cross the interface more frequently causing an accumulation in the phase of lowest mobility. The effect of the ratio of diffusion coefficients on the steady-state partition coefficient of the system can be expressed approximately as:

$$K_{ss} \approx \left(\frac{D_w}{D_p} \right)^\beta \quad (4.59)$$

where β is positive and its value depends on the geometry of the system, for example, on the volume fraction of the particles in the dispersion. According to the expressions obtained for irreversible absorption and desorption of molecules, a value of $\beta=1$ would be expected. However, for the dispersion of spherical particles under the conditions considered, it is found that $\beta \approx 1.6$. This deviation is caused by the fact that a single molecule at the interface can be absorbed and desorbed several times before diffusing to the center of the particle or to the bulk of the continuous phase, which is not considered by the models of irreversible phase transfer, giving rise to different effective diffusion paths for phase transfer. It is important to notice that under these conditions, only when the diffusion coefficients in both phases are identical (and in the absence of energy barriers), the concentration of the molecular species in each phase is the same. The simultaneous effect of volume fraction and diffusion coefficients on the steady-state partition coefficient for monodisperse spherical particles is presented in Figure 4.16. It can be noticed that the value of β (steepness of the slope in the y - z plane) decreases as the volume fraction of particles decreases. In the limit of infinitely diluted dispersions, β tends to 1. The functional dependence of the steady-state partition coefficient on the volume fraction and the diffusion coefficients ratio is quite complex. For this reason, numerical methods such as BD simulation are advantageous for the detailed investigation of molecular mass transfer phenomena.

In the previous examples, no activation energies for phase transfer were considered. If there is an energy barrier for absorption, the molecules accumulate on the continuous phase. Similarly, if there is an energy barrier for desorption, the molecules will concentrate inside the particles. This effect on the steady state can be expressed in the following way:

$$K_{ss} = \left(\frac{D_w}{D_p} \right)^\beta \exp\left(-\frac{E_a^{abs} - E_a^{des}}{3RT} \right) \quad (4.60)$$

where $E_a^{abs} \geq 0$ is the activation energy of the absorption process, $E_a^{des} \geq 0$ is the activation energy for the desorption process. In Figure 4.17 the results of BD simulation for the simultaneous absorption and desorption for different activation energies are presented, assuming that $D_w = D_p$. These results can be well described using Equation 4.60, which represents the distribution of the molecules once steady-state has been reached, that is, when the total rate of absorption is equal to the total rate of desorption. From equation 4.60, it can be inferred that:

$$r_{abs} = \hat{k} D_w^\beta [M]_w f_{abs} \quad (4.61a)$$

$$r_{des} = \hat{k} D_p^\beta [M]_p f_{des} \quad (4.61b)$$

where \hat{k} is a common rate coefficient for the reversible absorption/desorption process and f is an efficiency factor given by:

$$f_{abs} = \exp\left(-\frac{E_a^{abs}}{3RT}\right) \quad (4.62a)$$

$$f_{des} = \exp\left(-\frac{E_a^{des}}{3RT}\right) \quad (4.62b)$$

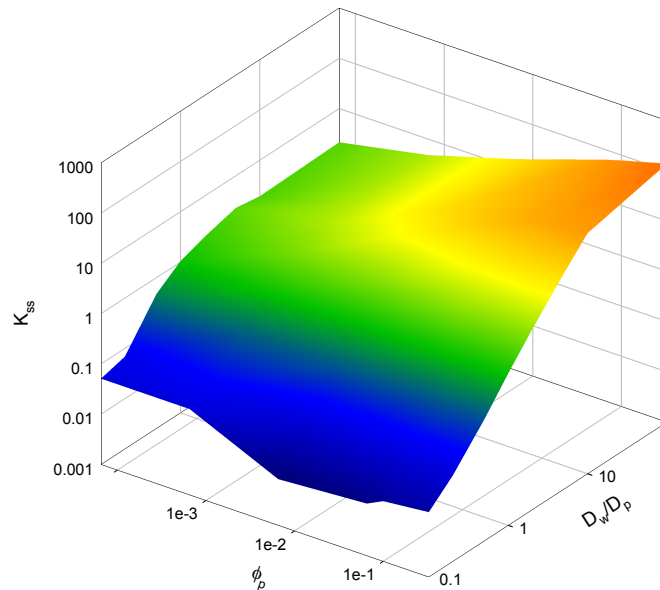


Figure 4.16 Steady-state partition coefficients as a function of the ratio between diffusion coefficients and the volume fraction for monodisperse spherical particles.

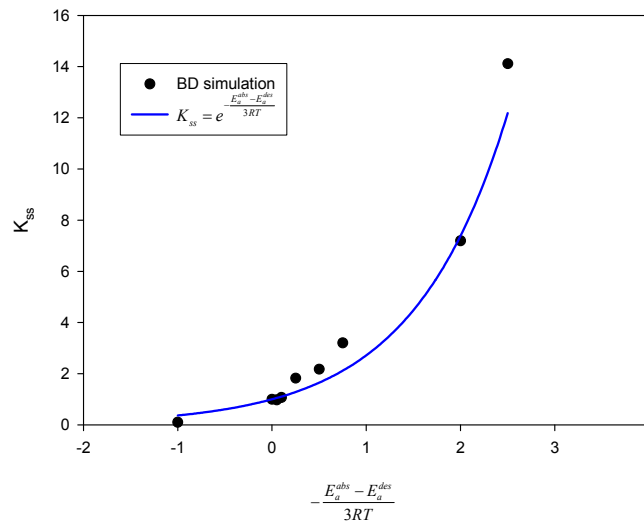


Figure 4.17 Effect of activation energies for phase transfer on the steady-state distribution coefficient

The degree of swelling (Q), which is the ratio between the volume of the particles and their initial volume, is defined as:

$$Q = \frac{v_p}{v_{p0}} = \frac{\phi_p}{\phi_{p0}} = \left(\frac{d_p}{d_{p0}} \right)^3 = \frac{1}{\Phi_p} = \frac{1}{1 - \Phi_m} \quad (4.63a)$$

The diffusion coefficients can be estimated using the free volume theory model of Fujita,^[84] or can be obtained from MD simulation or equation 4.19. In any case, the diffusion coefficients will depend on the composition of each phase, the temperature of the system and the density (or the free volume). The volume fraction of particles in the dispersion is related to the volume of the particle by $\phi_p = v_p N_p$, and the volume fraction of monomer inside the particles is $\Phi_m = 1 - \Phi_p$. The concentration of monomer inside the particles is

$$[M]_p = \frac{1 - \Phi_p}{\Phi_p V_m} \quad (4.64)$$

and therefore,

$$Q = 1 + [M]_p V_m \quad (4.63b)$$

and at steady state:

$$Q_{ss} = 1 + [M]_{w,ss} K_{ss} V_m \quad (4.65)$$

The monomer concentration in the continuous phase can be assumed to be constant and equal to the saturation concentration, or it can be obtained from a mass balance if the system is below saturation.

The rate of swelling of a single particle is given by:

$$\frac{dv_p}{dt} = \frac{M_M (r_{abs} - r_{des})}{\rho_M \tilde{N}_p} = \frac{M_M}{\rho_M N_p N_A} \frac{\Delta n_p}{\Delta t} \quad (4.66)$$

where v_p is the volume of a particle, M_M is the molecular weight of the monomer or swelling agent, ρ_M is its density, \tilde{N}_p is the number concentration of particles, N_p is the total number of particles in the system, and Δn_p is the change in the total number of molecules in the polymer phase during a time interval Δt .

In the following example, BD simulation is used to investigate methyl methacrylate swelling dynamics and equilibrium in a dispersion of uncrosslinked poly(methyl methacrylate) particles, assuming zero activation energies for absorption and desorption. Different amounts of monomer were added to the system, assuming that all the monomer is solubilized in the continuous phase. The simulation conditions are summarized in Table 4.4.

Table 4.4 Simulation conditions for the BD simulation of MMA swelling of PMMA particles

Parameter	Value
Temperature	45°C
Unswollen particle diameter	50 nm
Initial particle volume fraction of the dispersion	12.5%
Monomer molecular weight	100.12 g/mol
Monomer molecular diameter	0.7063 nm
Diffusion coefficient of monomer in water	3×10^{-9} m ² /s
MMA/PMMA interaction parameter	0.6
Monomer molar volume	0.111 L/mol
Amount of monomer added to the dispersions	0.08 – 2.40 L monomer/L particles

The dynamics of monomer swelling obtained are summarized in Figure 4.18. The time required to reach steady state in all cases considered was approximately the same, around 300 ns. If activation energies were considered, the equilibration times would have been much longer. In addition, a limited solubility of the monomer in the continuous phase will also slow down the rate of monomer swelling. According to the MKA equation (Eq. 4.56) the equilibrium degree of swelling should have been the same for all cases, independently of the relative amount of monomer. However, the degree of swelling is observed to increase by increasing the amount of monomer added. This can be explained by the fact that the Flory-Huggins entropic term included in the MKA equation was obtained considering that the polymer is dispersed in pure monomer. Thus, the equilibrium swelling value obtained from Eq. 4.56 should correspond to the limit obtained for very large volume ratios of monomer to polymer.

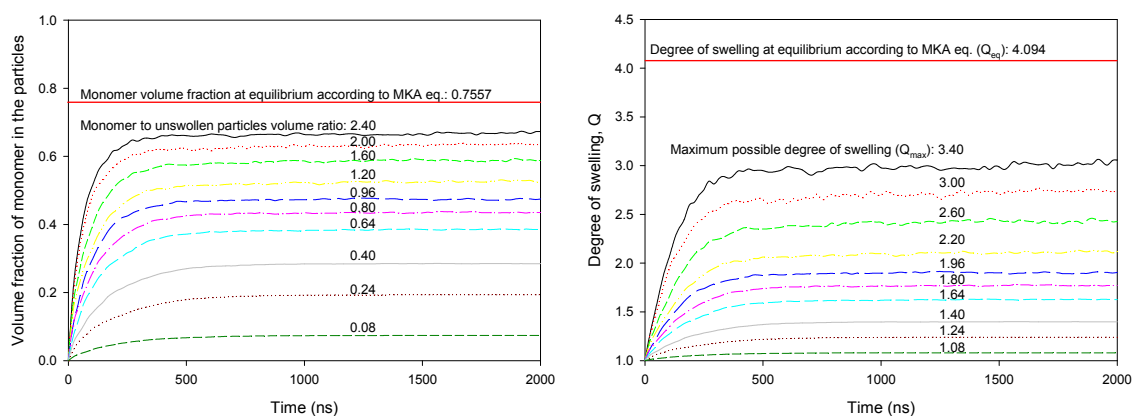


Figure 4.18 Monomer swelling dynamics: Monomer volume fraction in the particles (left) and degree of swelling (right). Each line represents the swelling behavior of a single particle for different amounts of monomer added to the dispersion.

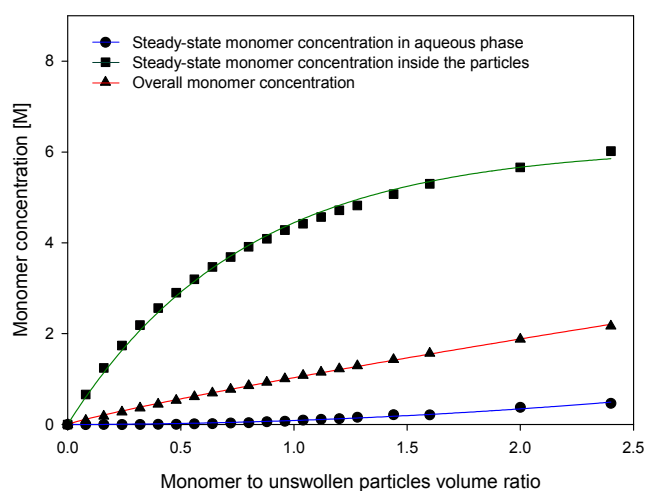


Figure 4.19 Overall monomer concentration and steady-state monomer concentration inside the particles and in the continuous phase as function of the amount of monomer added.

Figures 4.19-4.21 show the properties of the system obtained after swelling steady-state has been reached. In Figure 4.19 the overall monomer concentration and the steady-state concentration of monomer inside the particles and in the continuous phase are plotted as a function of the volume ratio of monomer to particles in the dispersion. For low amounts of monomer added (below 0.5 monomer-to-particles volume ratio), practically all the monomer is absorbed by the particles. For larger amounts of monomer, the swelling capability of the particles is reduced and the monomer begins to accumulate in the continuous phase. As the amount of monomer is increased, the concentration of monomer inside the particles also increases until a saturation concentration of monomer is reached beyond which no more monomer can be absorbed. Above 0.5 volume ratio, the molecular mobility inside the particles is large enough to have significant desorption rates, and for this reason, accumulation of monomer in the continuous phase can be observed.

Figure 4.20 shows the behavior of the steady-state swelling coefficient and the steady-state monomer partition coefficient as a function of the monomer added. The steady-state swelling coefficient increases almost linearly for low amounts of monomer, but then, as a result of saturation of monomer inside the particles, the increase in swelling begins to slow down. As long as there is an excess of swelling agent in the system, the MKA equation can be used to calculate the limiting equilibrium degree of swelling. For the example considered, this corresponds to a value of $Q_{eq}=4.094$. On the other hand, the steady-state monomer partition coefficient is observed to decrease initially very sharply with increasing monomer concentration, and then it decreases slowly until a certain limiting value is reached. The values of the steady-state partition coefficient are also plotted in Figure 4.21 as a function of the ratio of the diffusion coefficient of monomer in water to that in the particles. The behavior observed can be fitted using equation 4.59 and using a value of $\beta \approx 1.66$.

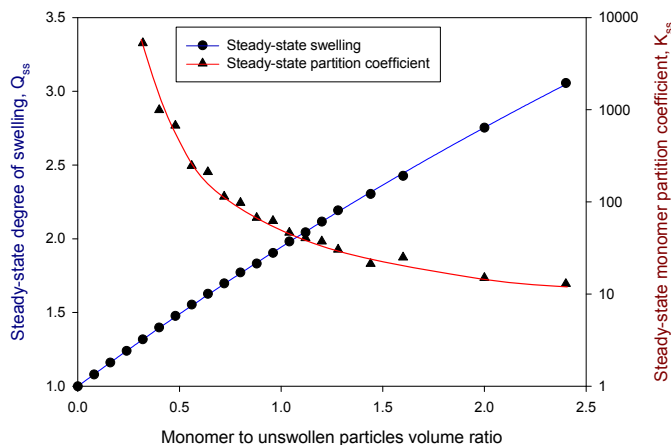


Figure 4.20 Steady-state degree of swelling and steady-state monomer partition coefficient as a function of the amount of monomer added

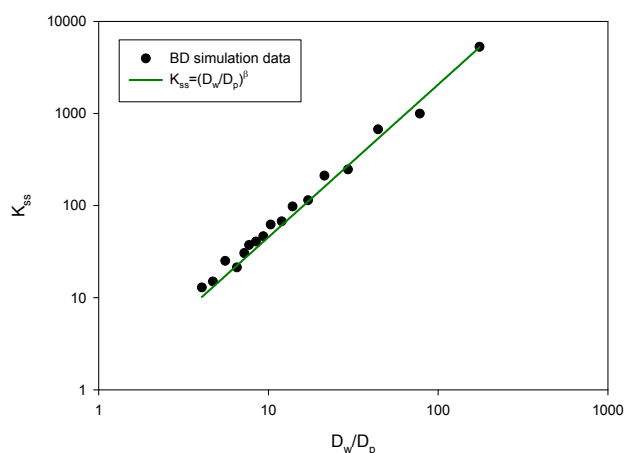


Figure 4.21 Steady-state monomer partition coefficient as a function of the ratio of diffusion coefficients for the MMA/PMMA swelling example.

The molecular picture used to simulate the dynamics of monomer swelling in emulsion polymerization satisfactorily predicts a maximum concentration of monomer inside the particles even though there is monomer available in the continuous phase, as has been evidenced experimentally. From the simulation results, the expected saturation concentration of monomer in the particles is about 6.1 M, in very good agreement with the experimentally determined value of 6.6 M.^[97] It was also possible to describe the dynamic behavior of the system under non-equilibrium conditions, while this information cannot be obtained using the MKA approach. It is also observed that during the simulations the steady-state conditions are reached very quickly (<300 ns) while in practice, the time required to reach steady-state can be in the order of hours. This can be explained by the fact that no energy barriers for absorption or desorption were considered during the simulations. In the presence of energy barriers the equilibration times will increase exponentially with the magnitude of the barriers, but as long as the difference in energy barrier between absorption and desorption remains constant, the steady-state partition coefficients obtained will be the same. The molecular approach presented

here is a very good alternative for the prediction of non-equilibrium monomer concentration inside polymer particles in emulsion polymerization, and can be very useful in systems where the swelling equilibrium assumption is not valid, for example, in monomer-starved semi-batch processes. This approach can be used to investigate the non-equilibrium uptake of any other type of molecule, such as primary radicals, oligomers, solvents, or any other compound.

4.7. Colloidal aggregation

In emulsion polymerization, colloidal aggregation is one of the most important factors determining the size and size distribution of the particles. Chung-li et al.,^[31] for example, found that the rate of swelling of latex particles was too slow to account for the rate of particle growth, and that colloidal aggregation played an important role in particle growth. There are two types of colloidal aggregation of polymer particles: coagulation and coalescence. During coagulation the total surface of the particles remains constant whereas during coalescence the total particle surface decreases as a result of the migration of the chains trying to minimize the free energy of the system. However, coagulation can be considered as the first step in the coalescence process, and it will be the only type of colloidal aggregation discussed in this section.

The coagulation theory of colloidal particles is based on a balance of the repulsive and attractive forces between the particles. When the repulsive forces are stronger than the attractive, the particles are stable and do not coagulate; if the attractive forces are stronger, then particle aggregation (coagulation or flocculation) takes place. Flocculation can be regarded as a reversible aggregation process whereas coagulation is irreversible. The nature of the interparticle forces responsible for the stabilization of the colloidal particles can be classified into: electrostatic, steric and electrosteric.

The theory of electrostatic stabilization of colloidal particles is called the DLVO (*Deryaguin-Landau-Verwey-Overbeek*) theory after the scientists who developed it. The DLVO theory relies on the consideration of both electrostatic forces and van der Waals forces. The principle of electrostatic stabilization is the presence of a net electric charge at the surface of the particles (Figure 4.22). Around these charges, a well-defined layer (*Stern layer*) of ions of opposite sign to that of the surface ions (counter-ions) is formed. In addition, as a result of electrostatic interactions and thermal motion of the molecules, a non-uniform diffuse second layer develops around the particles which is composed mainly of counter-ions, but may contain also ions of the same sign as the surface (co-ions). This layer, called the diffuse electrical layer, can be described mathematically by the *Poisson-Boltzmann equation*. The theory of electrical double layers at interfaces is also called the *Gouy-Chapman* theory. When two different colloidal particles electrically charged at their surfaces with ions of the same sign approach each other, they will experience a net repulsion force as a result of the interaction between the ions located at their diffuse layers. If the net interaction potential between the particles is repulsive and larger than the kinetic energy of the collision, they will not coagulate.

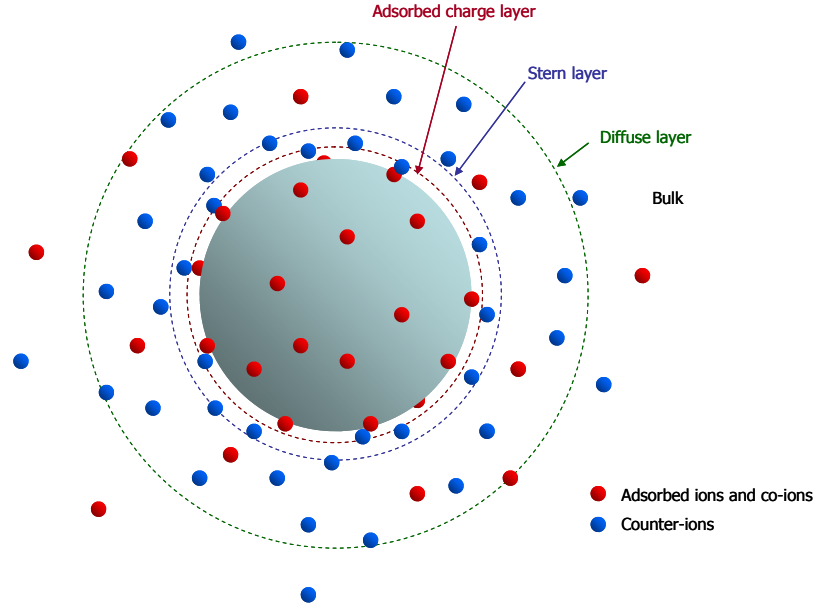


Figure 4.22 Ionic layers around a colloidal particle

The electrostatic stability of a colloidal system depends not only on the magnitude of the electrical charge surface density of the particles but also on the dielectric properties of the medium, on its ionic strength, on the valence of the ions in the double layer, on the size of the particles, and on the temperature of the system (only slightly). The total interaction potential between two spherical particles charged by a single type of ions at the surface can be determined using the DLVO equation:

$$\psi^{DLVO}(r) = \frac{32\pi k_B T d_p \rho_\infty \gamma^2}{\kappa^2} \exp(-\kappa r) - \frac{Ad_p}{12r} \quad (4.67)$$

where ρ_∞ is the number density of ions in the bulk continuous phase, d_p is the diameter of the spheres, A is the Hamaker constant, r is the minimum distance between the surface of the particles, κ is the reciprocal of the Debye length, given by:

$$\kappa = \sqrt{\frac{\rho_\infty e^2 z^2}{\epsilon \epsilon_0 k_B T}} \quad (4.68)$$

and γ is obtained from the Gouy-Chapman theory as:

$$\gamma = \tanh\left(\frac{ze\Psi_0}{4k_B T}\right) \quad (4.69)$$

where z is the valence of the ions at the surface, e is the charge of the electron, ϵ is the relative permittivity, ϵ_0 the permittivity of vacuum and Ψ_0 is the electrostatic potential at the surface of the spheres.

Electrically stabilized colloidal dispersions are very sensitive to the addition of electrolytes. If the concentration of ions in the solution increases, the thickness of the diffuse layer (*Debye length*)

decreases as a result of both entropic and electrical screening effects, leading to a reduction in the repulsive potential. On the other hand, colloid particles dispersed in organic media (low dielectric constant) cannot be electrically stabilized because the electrostatic forces become extremely short-ranged. In these cases, steric stabilization is recommended. Steric stabilization is imparted by non-ionic amphiphilic molecules (usually polymeric molecules). The lyophobic moiety of the amphiphiles will adsorb on the surface of colloidal particles, while its lyophilic moiety will be extended in the continuous phase. When two sterically-stabilized particles approach each other, the concentration of the lyophilic segments of the amphiphile in the continuous phase between the particles begins to increase and the concentration of solvent decreases. The difference in local solvent concentration around the particles results in an increase in the osmotic pressure and a net flow of solvent towards the interaction zone (Figure 4.23). At the same time, the increased concentration of the polymer segments leads to a reduction in the configurational entropy of the chains causing repulsion between the particles. Both effects (osmotic and entropic) restore the chemical potential equilibrium by separating the particles. The efficiency of steric stabilization relies on the solubility of the lyophilic moiety of the stabilizer in the continuous phase. Since the solubility is temperature-dependent, sterically-stabilized colloidal dispersions are very sensitive to the temperature of the system.

The third type of stabilization, electrosteric stabilization, is the combination of the two previous mechanisms. In this case the colloidal particles can be made stable to the presence of electrolytes thanks to the steric repulsion, and to changes in temperature thanks to the electrostatic interaction. Electrosteric stabilization can be achieved simply by using a mixture of stabilizers (one electrostatic and one steric), or by using only one single type of stabilizer, like for example, *polyelectrolytes*. In particular, polyelectrolytes grafted to the polymer particles offer an extraordinary stability to the presence of electrolytes.^[136]

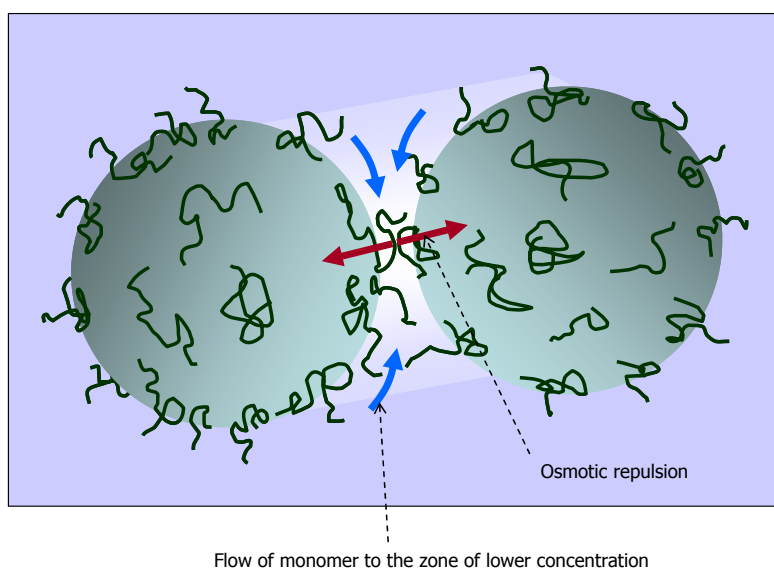


Figure 4.23 Principles of steric stabilization

If the repulsion potential between the particles were infinite, the particles would be stable forever. However, since the repulsion potentials are finite, there is always the probability of particle

aggregation depending on the thermal fluctuations of the system. The rate of particle coagulation will be a function of the frequency at which the particles encounter each other and of the probability of coagulation at each collision. In the absence of a repulsive potential, the particles aggregate at the same rate at which they encounter by diffusion through the continuous phase. This rate is called the *Brownian collision rate*, or the *Smoluchowski fast coagulation rate*:

$$r_{coag}^{fast} = 8\pi D_p d_p N = \frac{8k_B T N}{3\eta} \quad (4.70)$$

where D_p is the diffusion coefficient of the particles, d_p is the diameter of the particles, N is the concentration of particles per unit volume of dispersion and η is the viscosity of the continuous phase. In the absence of stabilizer, coagulation proceeds very rapidly even in fairly dilute dispersions.

In the presence of a net repulsion potential or energy barrier, *slow coagulation* takes place at a rate depending on the magnitude of the barrier. In general, the rate of slow coagulation can be expressed as:

$$r_{coag}^{slow} = \frac{r_{coag}^{fast}}{W} \approx r_{coag}^{fast} \exp\left(-\frac{\psi_r}{k_B T}\right) \quad (4.71)$$

where ψ_r is the net repulsion energy barrier (maximum value of the interaction energy curve), and W is the *Fuchs stability ratio* $W \approx \exp\left(\frac{\psi_r}{k_B T}\right)$.

Given that, in the absence of particle formation, $\frac{dN}{dt} = -r_{coag}^{slow} N$, the number of particles in the dispersion can be obtained from:

$$N(t) = \frac{N_0}{1 + \frac{8k_B T N_0}{3\eta W} t} \quad (4.72)$$

The molecular mechanism of particle aggregation is basically the same as that of radical capture or molecular absorption: the collision between two different entities after they diffuse towards each other following random walk trajectories. Brownian Dynamics (BD) can be used for the simulation of fast and slow particle aggregation. Rzepiela^[118] used BD to simulate the aggregation of colloid particles and found that for concentrated systems the fast coagulation rate is even faster than predicted by Eq. 4.70, in agreement to the results obtained for radical capture.^[67] It is possible to include interaction forces, either by solving the Langevin equation for Brownian motion including the interaction force term or by considering the activation energy for aggregation equal to the interaction potential energy between the particles. A very important consideration during the simulation of particle aggregation is that the particles form clusters as they aggregate. The new entity, the cluster of particles, will behave

as a single, larger Brownian entity. Therefore, instead of simulating the Brownian motion of each particle independently, all the particles in the cluster will follow the same trajectory and will have the same velocity.

In this Section, Brownian Dynamics is used to simulate the fast and slow aggregation of colloid particles in polymer dispersions. The conditions considered are summarized in Table 4.5. Fast particle aggregation is obtained by neglecting both electrostatic and van der Waals interaction potentials.

Table 4.5 Simulation conditions for the simulation of particle aggregation

Parameter	Value
Temperature	80°C
Initial particle diameter	50 nm
Initial particle number concentration	10^{20} part/m ³
Particle density	1.06 g/cm ³
Water viscosity	3.55×10^{-4} Pa·s
Surface potential of the particles	10 mV
Average valence at the surface	3
Ionic concentration	0.01 M
Hamaker constant	0.58×10^{-21} J

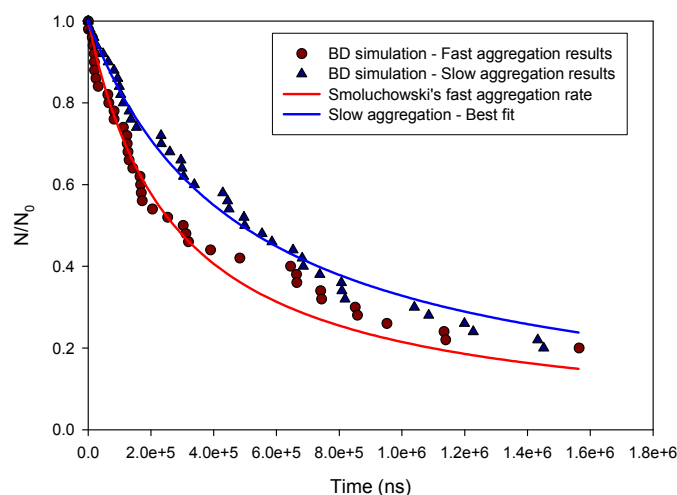


Figure 4.24 Kinetics of particle aggregation

In Figure 4.24 the kinetics of slow and fast aggregation are compared. Fast particle aggregation results obtained using BD simulations are in good agreement with Smoluchowski fast coagulation equation (Eq. 4.61), especially at the beginning of the simulation. The example presented considered a relatively diluted polymer particle dispersion (0.65% solids), and thus, significant deviations from Eq. 4.61 were not expected. On the other hand, slow aggregation was simulated considering both electrostatic and van der Waals interactions. The surface potential considered for the particles corresponds to an interaction energy of 4.8×10^{-21} J, while the van der Waals interaction corresponds to 5.8×10^{-22} J. The results obtained by simulation were fitted to Eq. 4.62, and a value of $W=1.784$ was obtained, corresponding to a net repulsion energy of $\psi_r=2.82 \times 10^{-21}$ J. This value is about four times larger than the difference between the electrostatic and the van der Waals interactions basically because of many-particle long-range electrostatic interactions. An example of the time evolution of

the system during particle aggregation for a representative volume of 6.4×10^{-17} L is presented in Figure 4.25. In this figure it is possible to observe the formation and growth of clusters of particles as a result of the colloidal aggregation of particles.

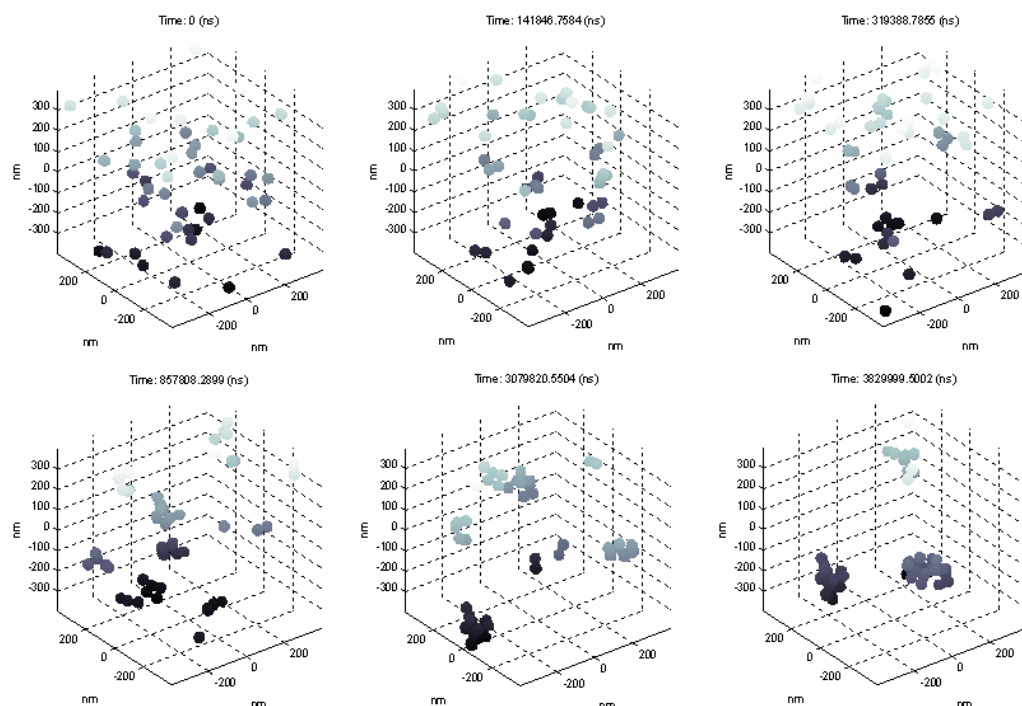


Figure 4.25 Evolution of particle aggregation. Colors indicate the relative z-position.

4.8. Particle morphology development

Polymer particles are mixtures of polymer and monomer segregated in a non-solvent continuous phase. The polymer-monomer mixture may be composed of one single type of polymer or different types of polymers depending on the monomers used and on the polymerization conditions (monomer feed rates, order of addition, etc.). Usually, the intermolecular interaction between chains of the same monomer is much stronger than the attraction between chains of different polymers. If the mobility of the chains is high enough, phase separation may occur inside the particles. Phase separation inside polymer particles can be considered to take place by a nucleation-like mechanism, where small aggregates or clusters of one single type of polymer are formed. These small clusters may diffuse inside the particle and collide with other clusters or individual polymer chains, and following a mechanism similar to that of particle aggregation, the polymer clusters grow inside the particle. The motion of the clusters inside the particles is determined by van der Waals interaction forces between the different clusters and the continuous phase, by the viscous drag force opposing to motion, and by random forces as a result of the thermal motion of the molecules in the system. The simulation of particle morphology development can therefore be performed using a coarse-grained version of

Brownian dynamics (BD) simulation. For systems with high polymer mobility, the final particle morphology will correspond to the “equilibrium morphology”, that is, the morphology that minimizes the free energy of the system. The expression for the free energy should consider the contribution of all the surfaces in the system. The surface free energy can be expressed in general as:

$$G_{surf} = \sum_{\alpha=1}^{p-1} \sum_{\beta=\alpha+1}^p \gamma_{\alpha\beta} A_{\alpha\beta} \quad (4.73)$$

where p is the total number of phases in the system, $\gamma_{\alpha\beta}$ is the interfacial tension between phases α and β , and $A_{\alpha\beta}$ is the total interfacial area between phases α and β . If the polymer mobility is reduced the equilibrium morphology might not be attained or it will be reached after very long times. These non-equilibrium particle morphologies are kinetics- or diffusion-controlled morphologies. When the diffusion of the chains is high enough to allow nucleation, but not enough to allow cluster aggregation, a bicontinuous phase structure may be formed. This phenomenon is known as *spinodal decomposition*. For systems where the polymer phases are in their glassy state or for crosslinked polymer networks the mobility of the chains is strongly reduced and the particle morphology is determined almost exclusively by the order of incorporation of polymer chains into the particle.

González-Ortiz and Asua developed a mathematical model for the simulation of particle morphology development in emulsion polymerization taking into account cluster nucleation, polymerization, polymer diffusion and cluster migration.^[137] The model takes into account only the effect of van der Waals interaction forces and drag forces. This is a simplified version of Langevin Dynamics simulation, where the random forces are neglected. Using this model, they were able to predict the morphology of polystyrene/poly(methyl methacrylate) composite particles in very good agreement with experimental observations. The results obtained by González-Ortiz and Asua clearly shows the potential of computer simulation for predicting the development of the particle morphology in composite systems, and for this reason a particular simulation example of particle morphology development will not be presented.

Recently, Stubbs and Sundberg^[138] presented a decision tree for determining the final particle morphology in composite polymer particles. They show how simulation methods can be used to predict the particle morphology development in any particular system. For that purpose, they used the UNHLATEX™ EQMORPH and KMORPH software developed by Sundberg’s group at the University of New Hampshire.

Chapter 5

Multiscale Stochastic Simulation

5.1. Multiscale Integration in Heterophase Polymerization

The basic definition of heterogeneous polymerization is the presence of more than one phase at some moment during the reaction process. In a typical emulsion polymerization the following phases may be found: an aqueous phase (continuous phase) which may contain dissolved ions and molecules, a monomer phase segregated as droplets in a wide range of sizes, micelles or surfactant aggregates, polymer particles and even polymer clusters inside the particles. The size of each segregated phase in a typical emulsion polymerization may vary from a few angstroms (molecular aggregates) to some millimeters (macroscopic monomer drops). All these separate phases are clusters or aggregates of molecules, and all of them are correspondingly subjected to the processes of diffusion, aggregation (including absorption) and dissociation (including desorption). This is graphically presented in Figure 5.1.

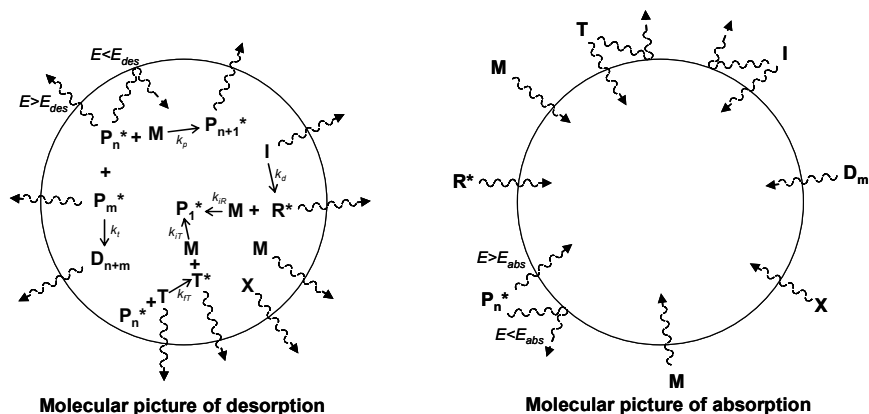


Figure 5.1 Molecular picture of the processes of desorption and absorption of molecules by a segregated phase. The transfer of any molecule through the interface is possible only if the energy (E) of the molecule is higher than the barrier for transfer (E_{des} for desorption, E_{abs} for absorption). M: Monomer, I: Initiator, R*: Primary radical, T: Chain transfer agent, T*: Transfer-derived radical, P_n^* : Polymer radical, D_m : Dead polymer, X: Any other molecule.

The main factors determining the diffusion, dissociation and aggregation of clusters and individual molecules are the magnitude and direction of intermolecular forces acting between neighboring molecules. Because of this, it would be possible to get a complete picture of heterophase

polymerization using molecular dynamics simulation; however, the computational requirement of performing a simulation for reasonable time and length-scales is extremely high and at present, such a task is practically not viable. Much larger time and length scales can be reached using Brownian Dynamics as it was exemplified in the previous Chapter for many different processes taking place in emulsion polymerization. However, these methods are not enough to simulate processes at an industrial scale. For these purposes, stochastic kinetic Monte Carlo or deterministic numerical integration of differential equations can be used. Although deterministic methods offer fast estimations of average values, stochastic methods can handle the variability of the process.

In general, polymeric systems are difficult to simulate because of the wide spectrum of time and length scales characterizing their dynamics and structure.^[92] If the scale of the simulation is increased in order to observe slower dynamics, the fast dynamics at lower scales must be either neglected or approximated. Depending on the type of approximation and its accuracy, the results obtained in the simulation can or cannot represent the real process. In this sense, a suitable multi-scale simulation algorithm capable of simultaneously considering all relevant dynamics would be desirable.

Multiscale simulation can be defined as the enabling technology of science and engineering that links phenomena, models and information between various scales of complex systems.^[139] Growth in a number of critical technological areas, such as nanotechnology, biotechnology and microscale systems, would be accelerated and catalyzed by a new multiscale modeling and computational paradigm.^[140] A very important aspect of multi-scale modeling is the processing and exchange of information between the different scales. Linking widely different scales has been based on two general modeling strategies: a "parallel" and a "serial" strategy. In the parallel approach, different-scale techniques are implemented simultaneously in the same computational domain that is decomposed appropriately. However, the serial approach has been used more extensively.^[141] In this approach, lower-scale models require information about the state of the system (temperature, velocity, composition, etc.) which is determined at a higher scale, while at the same time the upper-scale model requires parametric and structural information of the system obtained at the lower scale. Therefore, top-down and bottom-up information exchange procedures must be clearly defined.^[141-143] In the top-down procedure, a suitable grid decomposition method based on the distribution of states of the corresponding system scale must be used, while in the bottom-up procedure, the integration of the lower-scale results must be performed. The challenge is the seamless coupling between the various models while meeting conservation-laws, numerical convergence and stability.

5.2. Multiscale Stochastic Simulation of Seeded Emulsion Polymerization

In this section, two approximations to the modeling of secondary particle nucleation in emulsion polymerization based on multi-scale simulation are presented. The system considered is similar to that presented by Ferguson et al.^[34]: the semi-batch surfactant-free emulsion polymerization of vinyl

acetate in the presence of monodisperse polystyrene seed latex, initiated by a water-soluble initiator (potassium persulfate) at 80°C. This particular system is very interesting to investigate because:

- Vinyl acetate and styrene do not copolymerize. In fact, the presence of free styrene monomer inhibits the polymerization of vinyl acetate.
- These monomers have very different solubility in water. Vinyl acetate is hydrophilic (0.5 M) while styrene is hydrophobic (4.3×10^{-3} M).
- Their polymers are incompatible. Therefore, polymer phase separation is expected.

The first approach for multi-scale simulation is based on two simulation scales: the microscopic and colloidal scales. The microscopic scale is simulated using the kinetic Monte Carlo (kMC) algorithm (Section 3.1.3), whereas the colloidal scale is considered using Brownian Dynamics simulation (Section 3.1.2). A multiscale model is developed to simulate the molecular weight distribution of polymers in the aqueous phase during the whole polymerization time in the presence of radical-capturing polymer particles.^[144] For a monomer-starved feed addition policy, it is possible to assume that the monomer concentration in the aqueous phase is constant, that the monomer concentration in the polymer particles is low enough to give rise to a high viscosity inside the particles (therefore negligible radical desorption rates), and that the particles grow at the rate of monomer addition. The presence of surfactant in the system can be incorporated in this model by considering an increase in the concentration of monomer in the continuous phase. The following competitive events are simulated by kMC: Initiator decomposition in the aqueous phase, radical capture by polymer particles, and propagation and termination by recombination reactions in the aqueous phase. Additional events such as chain transfer reactions or termination by disproportionation can be easily included in the formulation of the kMC, but they are considered negligible in this example. The key state variables at the microscopic scale are the chain length distribution and concentration of polymer in the aqueous phase. The kinetic coefficients used for the chemical reactions were taken from ref. [34]. The capture rate coefficients are periodically calculated by lower-scale Brownian Dynamics simulations of the system. The calculations were performed assuming a negligible energy barrier for radical capture.

Table 5.1 Parameters used for the first example of multiscale kMC-BD simulation for the semi-batch seeded emulsion polymerization of vinyl acetate

Parameter	Value	Parameter	Value
Temperature (°C)	80	Simulation volume (l)	1×10^{-14}
Seed volume fraction (%)	0.01 – 10	Seed particle diameter (nm)	10-500
Seed polymer density (g/ml)	1.044	Water density (g/ml)	0.972
Poly(vinyl acetate) density (g/ml)	1.15	Aqueous monomer concentration (mol/l)	0.3
Monomer feed rate (mol/l·s)	3×10^{-4}	Initiator efficiency	0.9
Initial initiator concentration (mol/l)	1×10^{-3}	Initiator decomposition rate coefficient (s ⁻¹)	8.6×10^{-5}
Propagation rate coefficient (l/mol·s)	1.29×10^4	Termination rate coefficient (l/mol·s)	1.13×10^{10}
Primary radical molar volume (l/mol)	0.046	Primary radical molar mass (g/mol)	96.16
Monomer unit molar volume (l/mol)	0.075	Monomer unit molar mass (g/mol)	86.09
Water viscosity (cP)	0.355	Particle size tolerance for BD simulation triggering	5%

Radical capture kinetic coefficients can be easily estimated with BD simulation, by determining the average time required by a radical generated in the aqueous phase to enter a polymer particle (Section 4.3). When the size of the polymer particles changes above a certain tolerance value in the kMC simulation, a BD simulation of radical capture under the new conditions is triggered. The capture rate coefficients for every chain length of the radicals are calculated and given back to the kMC model, to continue the upper-scale simulation. In Table 5.1., the full set of conditions and parameters used during the multiscale kMC-BD simulation is presented. In all cases the final polymer volume fraction was 20%.

Figure 5.2 shows an example of the multiscale integration in the kMC-BD simulation. Whenever the particle size is increased above the tolerance value of 5%, a BD simulation is triggered and the capture rate coefficients are updated. This can be seen in Figure 5.2 as “jumps” in the value of the rate coefficient. In this example, an increase of at least one order of magnitude in the capture rate coefficient between the start and the end of the simulation is observed.

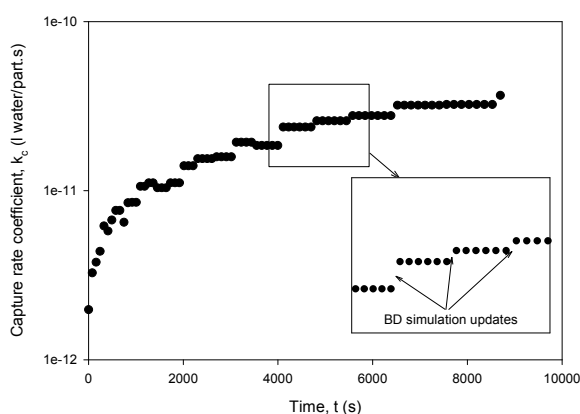


Figure 5.2 Periodic determination of the capture rate coefficient of primary radicals by BD simulation.

Seed particle size: 100 nm; seed volume fraction: 0.1%.

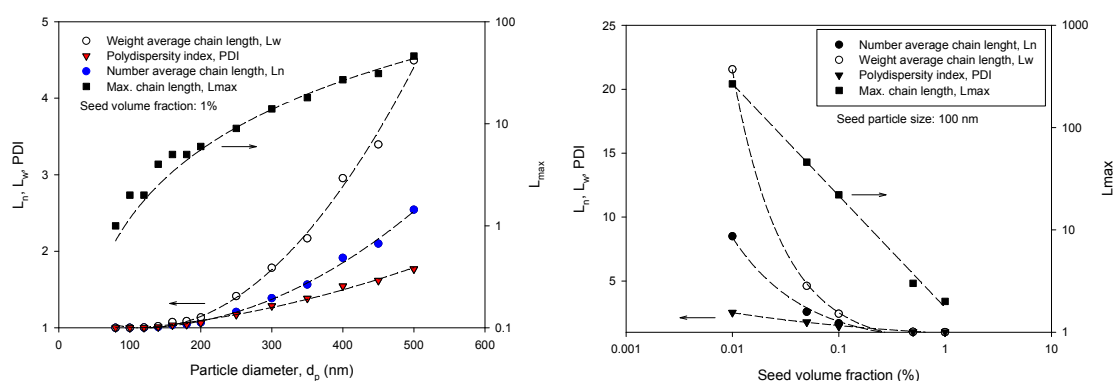


Figure 5.3 Number average chain length (L_n), Weight average chain length (L_w), Polydispersity Index (PDI) and Maximum chain length (L_{max}) of the radicals formed in the aqueous phase for different particle size and volume fraction of the initial seed. The dashed lines represent best fit curves.

The effects of the competition between aqueous phase propagation and radical capture by polymer particles are clearly seen in Figure 5.3. The chain length of the polymer formed in the aqueous phase increases as the initial seed particle size increases (for a constant volume fraction) or the volume fraction of the initial seed decreases (for a constant particle size). That is, the degree of polymerization in the aqueous phase increases as the rate of radical capture decreases. An additional effect observed is the increase in the polydispersity of the polymer formed in water as the rate of radical capture decreases. This result reflects the fact that smaller radicals are captured by the particles more easily than the larger ones. Therefore, the larger radicals can grow even further in the aqueous phase increasing the polydispersity of the system. For the particular case considered, radical propagation in the aqueous phase is practically suppressed when initial seed particles smaller than 80 nm at seed volume fractions higher or equal than 1% are used. These results are, however, somehow optimistic since no energy barrier for the capture of radicals and no radical desorption were considered.

In the second approach, the dynamics of radicals around or inside a single structured polymer particle are simulated using also a kMC-BD multiscale approach, but in this case, a BD simulation will be performed around one single particle achieving a spatial resolution of the motion of the radicals, while all other processes are periodically incorporated by means of the kMC approach. In this case, not only radical absorption but also desorption are considered assuming energy barriers determined by non-conservative forces and by the chemical potential difference of the radicals between the particle and the continuous phase. In addition, radical desorption induced by the propagation of the growing chain and chain transfer to monomer are incorporated into the model, and the particles are assumed to be swollen by monomer before starting the polymerization. New particle formation is assumed to take place according to the model presented in Section 4.3. According to this model, the growing chains in the continuous phase can be absorbed by the monomer-swollen seed polymer particles or by small monomer droplets formed by spontaneous emulsification. Under these monomer-rich conditions the radicals propagate and a large amount of energy is released. If the chain length is below a certain critical value, the energy released during propagation overcomes the energy barrier for desorption and the chain will return to the continuous phase. If the critical chain length is reached inside a seed polymer particle, new particle formation does not take place. Since the time-scale that can be covered by BD simulation is relatively short compared to the total polymerization time, the simulation is performed only up to the first 400 seconds of the reaction. In order to investigate secondary particle formation this time is enough given that secondary nucleation, if ever takes place, is observed at the beginning of the process. In fact, since the existing polymer particles are continuously growing, the probability of radical capture increases with polymerization time and thus the probability of particle formation is reduced. The parameters and conditions used in the simulation are summarized in Table 5.2. In a first case, the radicals are generated by thermal decomposition of initiator molecules which are assumed to be uniformly distributed in the continuous phase. A second set of simulation data was obtained using the same conditions of Table 5.2, but assuming that hydrophilic radicals are generated by a redox reaction between one hydrophilic reducing agent located in the continuous phase and one

hydrophobic oxidizing agent present inside the polymer particles.^[145] In this way, the locus of radical formation can be restricted to the surface of the particles. A third set of simulation data was obtained using the same parameters and assuming that the radicals are generated by the thermal decomposition of *inisurf* molecules, that is, initiators with surface activity that are mainly located at the surface of the particles. The simulation results for all three situations are presented in Figure 5.4.

Table 5.2 Parameters used for the second example of multiscale kMC-BD simulation for the seeded emulsion polymerization of vinyl acetate

Parameter	Value	Parameter	Value
Temperature (°C)	80	Simulation volume (l)	2×10^{-18} - 9×10^{-15}
Seed volume fraction (%)	5 – 40	Seed particle diameter (nm)	100 – 1000
Particle number concentration (#/l)	4×10^{14} – 4×10^{17}	Aqueous monomer concentration (mol/l)	0.5
Monomer concentration inside the particles (mol/l)	7.5	Initial initiator concentration (mol/l)	1×10^{-3}
Initiator decomposition rate coefficient (s ⁻¹)	8.6×10^{-5}	Propagation rate coefficient (l/mol·s)	1.29×10^4
Chain transfer to monomer rate coefficient (l/mol·s)	2.32	Termination activation energy (J/mol)	2000
Primary radical diameter (nm)	0.526	Primary radical molar mass (g/mol)	96.16
Monomer unit diameter (nm)	0.664	Monomer unit molar mass (g/mol)	86.09
Chemical potential difference (J/mol)	10110	Non-conservative energy barrier (J/mol)	2000
Enthalpy of propagation (J/mol)	88000	Minimum chain length for particle formation	18
Radical diffusion coefficient in water (m ² /s)	1.4×10^{-9}	Radical diffusion coefficient inside the particles (m ² /s)	1×10^{-11}
Final simulation time (s)	0.42 – 390		

According to the simulation results, the probability of secondary particles formation decreases by increasing the seed volume fraction of the latex for a given seed particle size, and increases by increasing the seed size for a constant seed volume fraction. This is caused by the increased chain length of the polymers that can be achieved in the continuous phase, as it was shown in Figure 5.3. On the other hand, it is possible to clearly evidence the influence of the locus of radical generation on the probability of secondary nucleation. When a hydrophilic/hydrophobic redox initiation system is used, it is observed a complete suppression of secondary particle formation for seed volume fractions above 20% for a seed particle size of 500 nm, and for 20% volume fraction seed latexes, secondary nucleation is suppressed for seed particle sizes below 1 μ m. In the case of the *inisurf*, the probability of particle formation is greatly reduced compared to normal initiators. Although both the redox initiator and the *inisurf* produce radicals close to the surface of the particles, the use of the redox system allowed a larger reduction in secondary particle formation compared to the *inisurf*. This result can be explained by the fact that the rate of radical generation in the redox system is much higher than for the thermal decomposition of the *inisurf*, leading to a higher concentration of radicals around the particles and to a larger number of termination events. Even though secondary nucleation is further suppressed with the redox system, the rate of polymerization can also be reduced and shorter chains may be produced. However, this multi-scale simulation approach showed that the control of

the locus of radical generation is an excellent strategy for the control of secondary particle formation during the synthesis of structured particles by seeded emulsion polymerization.

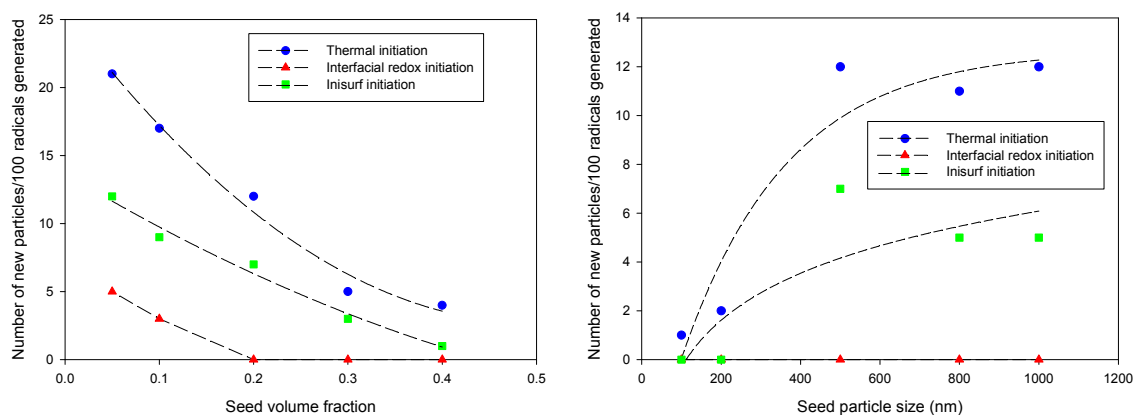


Figure 5.4 Number of new particles formed per 100 radicals as a function of the seed volume fraction for a seed latex of 500 nm in particle size (left) and as a function of the seed particle size for a seed latex of 20% volume fraction (right). Blue circles: Generation of radicals by thermal decomposition of water-soluble initiator. Red triangles: Radical generation by redox interfacial reaction between a hydrophilic reducing agent and a hydrophobic oxidizer. Green squares: Radicals generated by the thermal decomposition of an inisurf. Dashed lines: Fitted curves.

The experimental evidence of the success of this idea was presented by Soltan-Dehghan et al.^[146] for the synthesis of structured polystyrene/poly(vinyl acetate) polymer particles. They used a two-stage polymerization process to prepare PS/PVAc nanocomposite polymer particles with a core-shell morphology in an emulsifier-free emulsion polymerization system, employing 2,2-azo bis(2-amidino propane) dihydrochloride as an inisurf initiator. The particle diameter of the polystyrene seed used was around 300-400 nm, which is clearly beyond the limiting value of 150 nm obtained by Ferguson et al.^[44] for this particular system.

Chapter 6

Conclusions

The most important conclusion of the present work is that heterophase polymerization can be considered as a complex multi-scale stochastic process with at least seven different relevant scales: macroscopic, mesoscopic, microscopic, colloidal, macromolecular, molecular and atomistic scales. For that reason, a very accurate description of this type of process requires the adequate integration of all these relevant scales, that is, requires the use of suitable multiscale dynamic simulation methods.

In order to obtain a more complete picture of emulsion polymerization, the most relevant physical and chemical processes were investigated using different modeling strategies at the corresponding scales. The processes investigated include: diffusion, chemical reaction under diffusion control, particle formation, radical capture, radical absorption, monomer swelling and particle aggregation.

Molecular diffusion was investigated using Molecular Dynamics simulation and considering Buckingham-type interatomic pair interaction potentials. It was possible to obtain an analytic expression (Eq. 4.18) for describing the simulation results, where the diffusion coefficient of the molecules is proportional to the square root of the absolute temperature of the system, inversely proportional to the molecular mass (according to Graham's law), and depends exponentially on the density of system (in agreement with the free-volume theory) and decreases almost linearly on the steepness of the repulsive forces. In the results obtained, the magnitude of the interaction energy did not show a direct influence on the value of the diffusion coefficient.

For the investigation of diffusion-controlled polymerization reactions, a modified stochastic simulation algorithm was proposed which is able to incorporate imperfect mixing effects into the kinetic Monte Carlo scheme. In this method, the simulation volume is not an input parameter, but it is calculated at every step according to the diffusivity of the reacting species. By means of this modified stochastic simulation algorithm, denoted as SSA-IM (Fig. 3.7), it was possible to describe mass transfer limitation effects (cage effect, gel effect and glass effect) in a typical bulk polymerization of MMA.

A new model of particle formation based on the experimental observations of Harkins^[78] and Tauer^[18,98,103] was presented. According to Tauer's observations, the formation of polymer particles is an aggregation process which involves not only the polymer chains but also monomer molecules and droplets and any other molecule with a certain affinity with the polymer (e.g. surfactant molecules). It is for this reason that the most probable source of polymer particle formation comes from the interaction between growing polymer chains and small monomer droplets formed by the process of

spontaneous emulsification. However, given that the propagation of the radicals is a highly exothermic reaction, the chain length of the growing radical and the size of the aggregate are the limiting factors for the proper formation of a polymer particle. If the radical is too small, as well as the polymer-monomer aggregate, the energy released during a propagation step can be enough to promote the desorption of the radical into the continuous phase. For longer chains and larger aggregates, the thermal dissipation of the energy avoids the propagation-induced desorption of the radical.

The investigation of radical dynamics (absorption-desorption) in emulsion polymerization was performed using Brownian Dynamics simulation, achieving a precision which cannot be matched with the available experimental methods. In the case of radical absorption or radical capture, it was found that for very dilute polymer dispersions the rate of capture is in excellent agreement with Smoluchowski's equation (Eq. 4.41). However, for concentrated dispersions ($>0.1\%$) the rate of radical capture deviates significantly from Smoluchowski's equation. This deviation is represented by the dimensionless Smoluchowski number, and it was found to increase almost linearly with respect to the volume fraction of the particles (Eq. 4.43). According to these results, the dependence of the capture rate coefficient on the particle size ranges from a linear to a fourth order dependence depending on the volume fraction of particles in the system. This explains why different models of radical capture have been satisfactorily validated using experimental data.

In the case of radical desorption, Brownian Dynamics (BD) simulation allowed a more precise determination of the desorption rate coefficient in excellent agreement with theoretical expressions. BD simulation has been shown to be a very useful method for the determination of radical desorption kinetics especially when more complex but also more realistic situations are considered, like for example, in core-shell particles, in particles with radial monomer gradients, or for non-spherical polymer particles.

It has been also evidenced that absorption/desorption dynamics and equilibrium are strongly affected by the presence of energy barriers for the mass transfer across the surface of the particles. Furthermore, the behavior described by BD simulation is not exclusive of the radicals but can be extended to all the molecules present in the system, including for example, the monomer molecules. Therefore, the swelling dynamics and equilibrium of polymer particles by monomer can also be described by this approach.

Finally, it has also been shown that multiscale dynamic simulation methods can be successfully used for the investigation of the kinetics of emulsion polymerization. In particular, these methods were used to investigate the synthesis of structured polymer particles by semi-batch seeded emulsion polymerization as a representative case study. The results obtained in the simulation were used to find optimal conditions for the suppression of secondary nucleation in emulsion polymerization. It was demonstrated that by controlling the locus of radical generation at the surface of the particles it is possible to greatly reduce the probability of secondary particle formation in seeded emulsion polymerization systems. These conditions were successfully tested by combining Brownian Dynamics

simulation with kinetic Monte Carlo simulation, and they could not be obtained with traditional modeling techniques used in emulsion polymerization.

There are still enormous possibilities for the investigation and exploration of multi-scale integration in heterogeneous polymerization systems, involving different combination of scales ranging from the atomistic to the macroscopic scale. Hopefully, these ideas can be used to obtain an even more complete understanding of all the mechanisms taking place in heterophase polymerization at all relevant length scales, and also, that the fast increase in computational power can allow very soon to perform faster simulations and to span more easily a wider range of time scales.

Appendix A

Experimental Examples

A.1 Chemicals and Equipment

The chemicals used for the synthesis of polymer particles in the following examples are summarized in Table A.1.

Table A.1 Chemicals employed in the experimental examples

Chemical Product	Supplier	Purification procedure
Deionized water		Taken from a Seral purification system (PURELAB Plus).
Methanol (MeOH)	Merck	Used as received
Styrene (St)	Aldrich	Distilled under reduced pressure
n-butyl Methacrylate (n-BMA)	Aldrich	Purified with Al ₂ O ₃
Vinyl acetate (VAc)	Aldrich	Distilled under reduced pressure
Methyl Methacrylate (MMA)	Röhm	Distilled under reduced pressure
Divinyl benzene (DVB)	Alfa Aesar	Washed with NaOH (10%) aqueous solution
Potassium peroxydisulfate (KPS)	Fluka	Used as received
Azobisisobutyronitrile (AIBN)	Fluka	Recrystallized from methanol
Sodium dodecyl sulfate (SDS)	Fluka	Used as received
Poly(vinyl pyrrolidone) (PVP)	Acros	Used as received
K29-32: 58.000 g/mol average molecular weight		
Poly(vinyl alcohol) (PVOH)	Aldrich	Used as received
98% Hydrolized, 13.000 – 23.000 g/mol molecular weight		
Aerosol OT 100 (AOT)	Acros	Used as received
Sodium bicarbonate (NaHCO ₃)	Acros	Used as received
Ruthenium tetraoxide (RuO ₄)		Prepared before use by the reaction of ruthenium trichloride (Acros) and sodium hypochlorite (Acros).
Phosphotungstic acid (PTA)	Acros	Used as received

In these experiments, three different types of reactors were employed. The polymer seeds were prepared by batch emulsion or dispersion polymerization in jacketed glass reactors of 250 mL using 45° pitch-blade stirrers. The temperature in these reactors is regulated using a Fisherbrand FBH604 thermostat (Fisher Scientific, Germany). The system also includes a vertical condenser and a line of nitrogen used for inertization. The semi-batch polymerization of the following stages was performed with a Chemspeed A100 Miniplant automatic station (Chemspeed Technologies, Switzerland), using a glass or a stainless steel reactor of 100 mL. The temperature inside the reactor and in the jacket and the flowrate of two liquid feeds are controlled by the AutoSuite Software supplied by Chemspeed.

Second-stage polymerizations by swelling or pre-swelling methods were carried out in a rotating thermostat (VLM, Germany) with a capacity of 24 test tubes. The seed latex, fresh monomer and initiator are weighed in test tubes and sealed with Teflon before being placed in the thermostat.

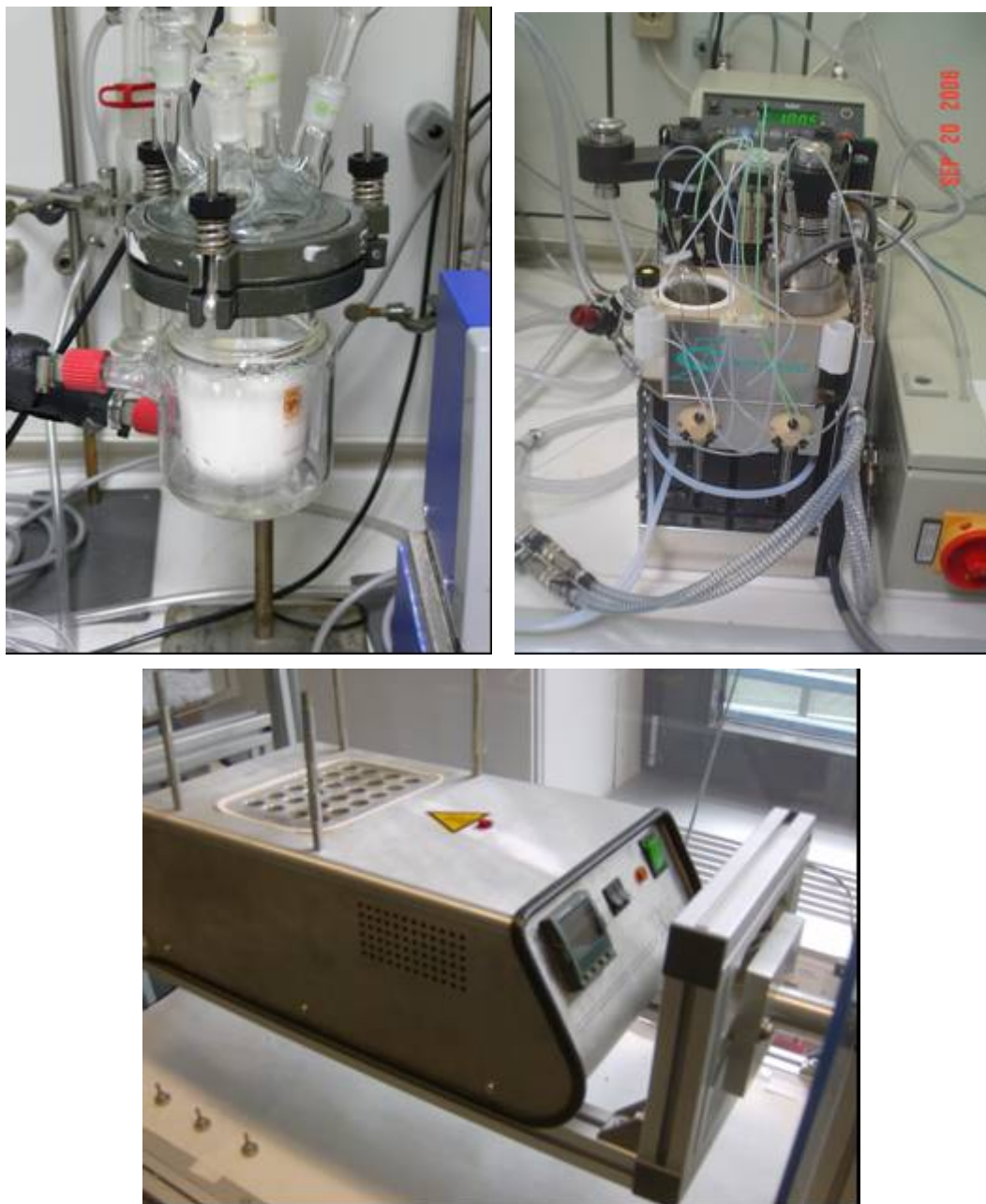


Figure A.1 Polymerization reactors: Batch reactor (top left), semi-batch automatic reactor (top right), rotating thermostat (bottom)

Solids content analyses were performed with a HR73 Halogen Moisture Analyzer (Mettler-Toledo, Switzerland). The measurement of average particle size (intensity-weighted diameter) of the latexes by Dynamic Light Scattering (DLS) was carried out in a NICOMP 380 particle sizer (Particle Sizing Systems, USA) at a fixed scattering angle of 90° with a laser power of 35 mW. Transmission electron microscopy (TEM) images were obtained using a Zeiss EM 912 Omega microscope (Carl Zeiss, Germany) operating at 100 kV and the samples were placed on the grids via suspension preparation.

Suitable staining techniques with Ruthenium tetroxide (RuO_4) and/or Phosphotungstic acid (PTA) were used when required. Optical light microscopy images were obtained with a Keyence VH-X digital microscope (Keyence, Japan). Ultrasonication was performed using a Branson Digital Sonifier W-450D (Branson Ultrasonics, USA).

A.2 Polystyrene/Poly(*n*-butyl Methacrylate) core-shell particles

Preparation of the seed particles (D01.1-10):

0.002 g of NaHCO_3 , 0.3 g of SDS and 190 g of deionized water were added to a 250 mL glass reactor. The stirring rate was set to 300 rpm. The system was purged with nitrogen for 15 minutes before the addition of 18.5 g of styrene. After monomer addition, the temperature of the thermostat was set to 80°C. 15 minutes after the polymerization temperature was reached, a solution of 0.27 g of KPS in 10 g of deionized water was added to the reactor. After some minutes, when turbidity was observed, the nitrogen flow was stopped. The polymerization proceeded for 24 hours. The final product obtained was a monodisperse latex of 150 nm in particle size and a solids contents of 8.51%, corresponding to a particle number concentration of 4.54×10^{16} part/L. The final monomer conversion calculated gravimetrically was 97.7%.

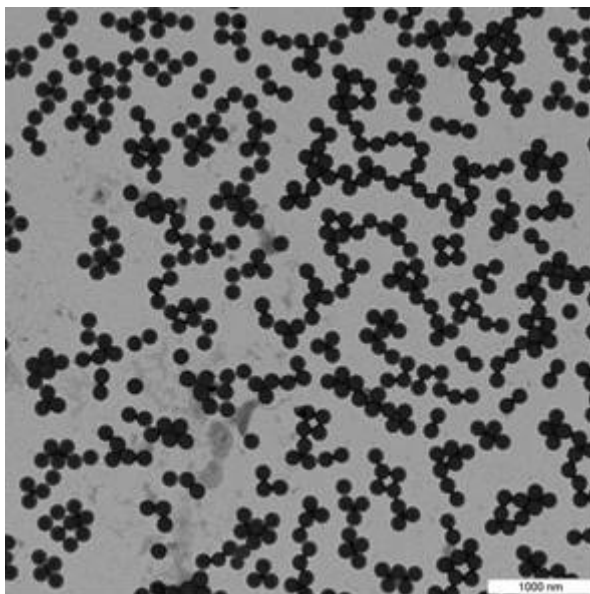


Figure A.2 Transmission electron micrograph of latex D01.1-10

Second stage polymerization (A028):

The second-stage polymerization was carried out in the automatic semi-batch reactor. 30 g of the seed latex previously prepared (D01.1-10) were used. In one feed vessel, 0.05 g of KPS were dissolved in 5 g of deionized water. In the second feed vessel, 5 g of n-BMA were added. The system was purged with nitrogen before starting the addition. The stirring speed was set to 150 rpm and the reactor temperature was set to 80°C. 15 minutes after reaching the reaction temperature, the monomer and the initiator solution were added to the reactor at flowrates of 0.0333 mL/min and

0.0297 mL/min, respectively. After 1 hour, the addition was stopped and the reaction continued for another 2 hours. The final average particle size obtained was 180 nm and the final solids content was 12.24%. The monomer conversion of the second stage was 86.4% and the particle number concentration was 3.78×10^{16} part/L. No secondary nucleation was observed, and a soft shell of poly(*n*-butyl methacrylate) was formed around the polystyrene seed as observed in Fig. A.3.

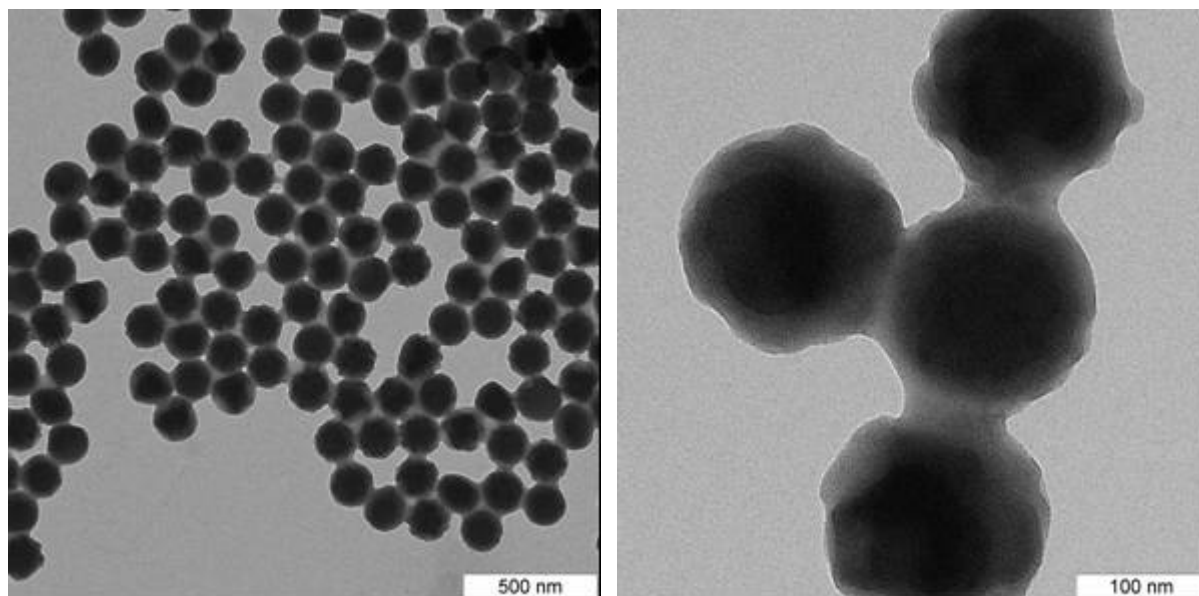


Figure A.3 Transmission electron micrographs of latex A028

A.3 Polystyrene/Poly(Vinyl Acetate) structured particles prepared by multi-stage emulsion polymerization

Preparation of the seed (A010):

0.36 g of SDS and 35 g of deionized water were added to a glass reactor of 100 mL, installed in the Chemspeed automatic station. 20 mL of styrene were added to the feed vessel #1, and a solution of 0.135 g of KPS in 5 g of deionized water was added to the feed vessel #2. The stirring rate was set to 300 rpm. 15.3 g of styrene were added to the reactor at a flowrate of 0.85 mL/min. After monomer addition, the temperature set point was set to 70°C. 5 minutes after reaching the polymerization temperature, 2.55 g of initiator solution were added at a flowrate of 0.51 mL/min. The polymerization proceeded for 4 hours. The final product was a polymer latex of 73.6 nm in diameter and 30.16% solids. The particle number concentration was 1.363×10^{18} part/L, and the monomer conversion was >99%.

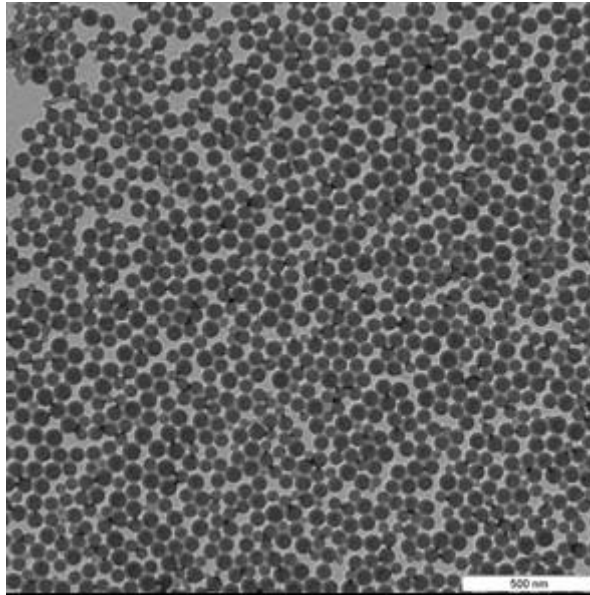


Figure A.4 Transmission electron micrograph of latex A010

Second-stage vinyl acetate polymerization (A011):

20 g of the previous seed latex (A010), 0.023 g of NaHCO_3 and 17.5 g of deionized water were added to a glass reactor of 100 mL, installed on the Chemspeed station. 17 g of vinyl acetate were charged in feed vessel #1, and a solution of 0.131 g KPS in 5 g of deionized water was prepared in feed vessel #2. The stirring rate was fixed in 300 rpm and the reaction temperature was set to 70°C. 5 minutes after reaching this temperature, the continuous addition of monomer and initiator solution was started. 12 g of VAc were added at a flowrate of 0.071 mL/min, while 2.55 g of initiator solution were added at a rate of 0.51 mL/min. The total polymerization time was 4 hours, including 1 hour of post-reaction after finishing monomer addition. A latex of 99.6 nm in diameter and 33.13% solids was obtained. The final number of particles was 6.099×10^{17} part/L. The conversion of vinyl acetate in this stage was 89%, and the expected final particle size at 100% conversion was 100.8 nm.

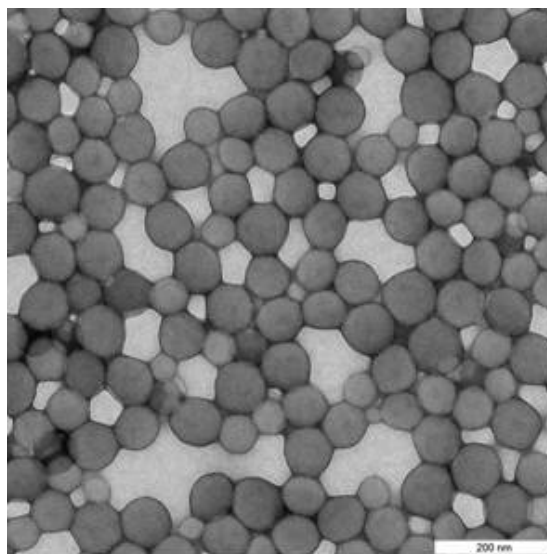


Figure A.5 Transmission electron micrograph of latex A011

Third-stage styrene polymerization (A012):

25 g of the previous latex (A011) and 17.5 g of deionized water were added to a glass reactor of 100 mL installed on the Chemspeed automatic station. 11 mL of styrene were added to the feed vessel #1, and a solution of 0.134 g of KPS in 5 g of deionized water was added to the second feed vessel. The stirring speed was set to 300 rpm and the temperature set point to 70°C. After reaching polymerization temperature, 8.55 g of monomer were added at a rate of 0.0528 mL/min and 2.55 g of initiator solution were added at 0.51 mL/min. After 4 hours of polymerization, a polymer latex of 111.1 nm in size and 24.5% solids was obtained. The corresponding particle concentration was 3.25×10^{17} part/L, and the expected particle size was 112.3 nm.

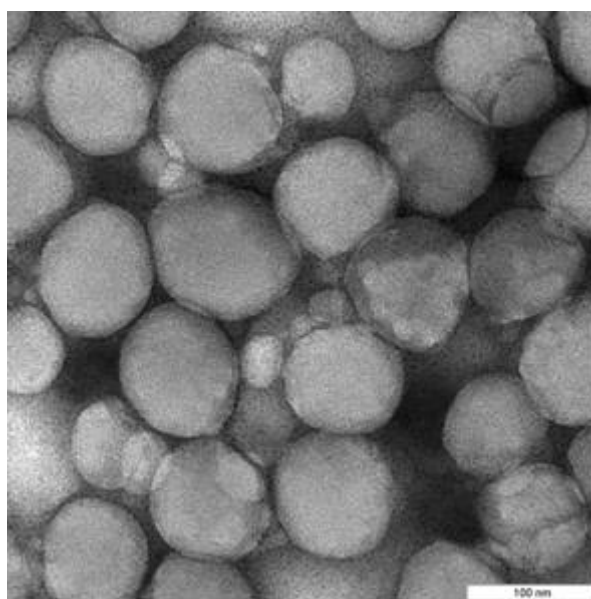


Figure A.6 Transmission electron micrograph of latex A012

Fourth-stage vinyl acetate polymerization (A014):

40 g of the previous latex (A012) and 0.007 g of NaHCO_3 were added to a glass reactor of 100 mL installed on the Chemspeed station. 7.5 g of vinyl acetate were added to feed vessel #1, and 0.04 g of KPS in 5 g of deionized water were added to feed vessel #2. Stirring rate was set to 300 rpm and reactor temperature to 70°C. After reaching polymerization temperature, 3.745 g of VAc were added at 0.02 mL/min. and 2.52 g of initiator solution were added at 0.51 mL/min. After 4 hours and 20 minutes of reaction, a 22.29% solids bimodal polymer latex was obtained with peaks at 62.6 nm (4.7%) and 122.6 nm (95.3%). The final solids content is low due to the formation of coagulum. The expected particle size in the absence of secondary nucleation was 123.1 nm. This example demonstrates the tendency of vinyl acetate to generate secondary polymer particles even for relatively small (~110 nm) polymer particles.

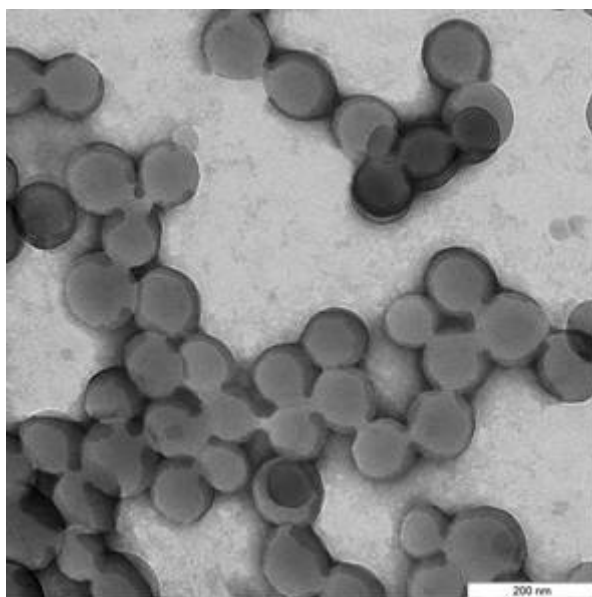


Figure A.7 Transmission electron micrograph of latex A014

A.4 Micron-sized Polystyrene/Poly(Vinyl Acetate) composite particles

Micron-sized seed particles preparation (D06.1-05):

10 g of PVP K30 were slowly dissolved in 119.24 g of methanol, and added to a glass reactor of 250 mL after complete dissolution. The stirring rate was set to 100 rpm, and nitrogen was supplied to the reactor to purge the system. After 15 minutes, a solution of 0.5 g of AOT in 30 g of methanol was added to the reactor and allowed to mix for additional 15 minutes. A monomer mixture of 27 g of styrene and 3 g of DVB was added and the temperature of the thermostated bath was set to 55°C. 15 minutes after the reaction temperature has been reached, a solution of 0.26 g of AIBN in 10 g of methanol was added to the reactor and the stirring rate was raised to 200 rpm to achieve a faster mixing, and decreased again to 100 rpm after 1 minute. After 40 hours of reaction, the temperature was raised to 70°C to reduce the amount of unreacted monomer. After 5 hours at 70°C, a monodisperse product with an average size of 1.4 μm was obtained, with a solids content of 20.61%. The number concentration of particles was 1.07×10^{14} part/L.

Transfer to water (D06.1-05W):

77.18 g of deionized water were added to 250 g of the previous dispersion (D06.1-05), and the mixture was distilled by vacuum at 300 mbar and 50°C. 110.86 g of methanol were removed, and the final solids content of the latex obtained was 26.73%. The new particle number concentration was 1.72×10^{14} part/L.

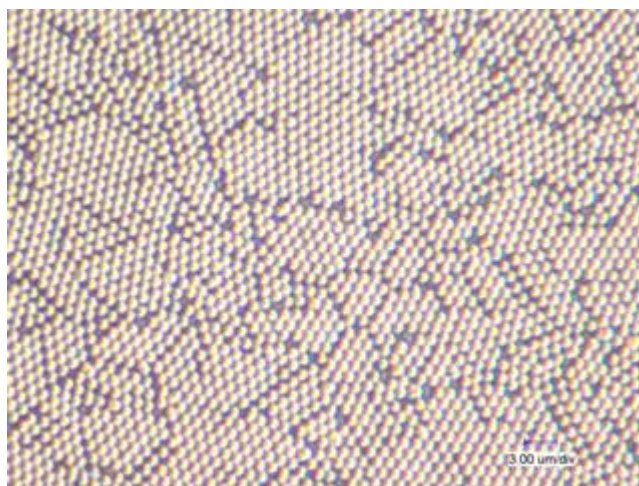


Figure A.8 Optical microscope image of latex D06.1-05W

Second-stage vinyl acetate polymerization (D06.2-2):

To 4 g of the previous latex (D06.1-05W), 2.8 g of deionized water were added. The resulting dispersion was mixed with a solution of 0.015 g of AIBN in 1.2 g of vinyl acetate. The system was sonicated using various pulses of 30 seconds at 50% power. The sonicated dispersion was placed in a 20 mL test tube and taken to the rotating thermostat, previously set to 80°C. The reaction proceeded for 5 hours. Composite polymer aggregates in sizes ranging from around 20 to 50 μm were obtained as can be observed in Fig. A.9. These composites correspond to polystyrene particles dispersed in a soft polymer matrix of poly(vinyl acetate).

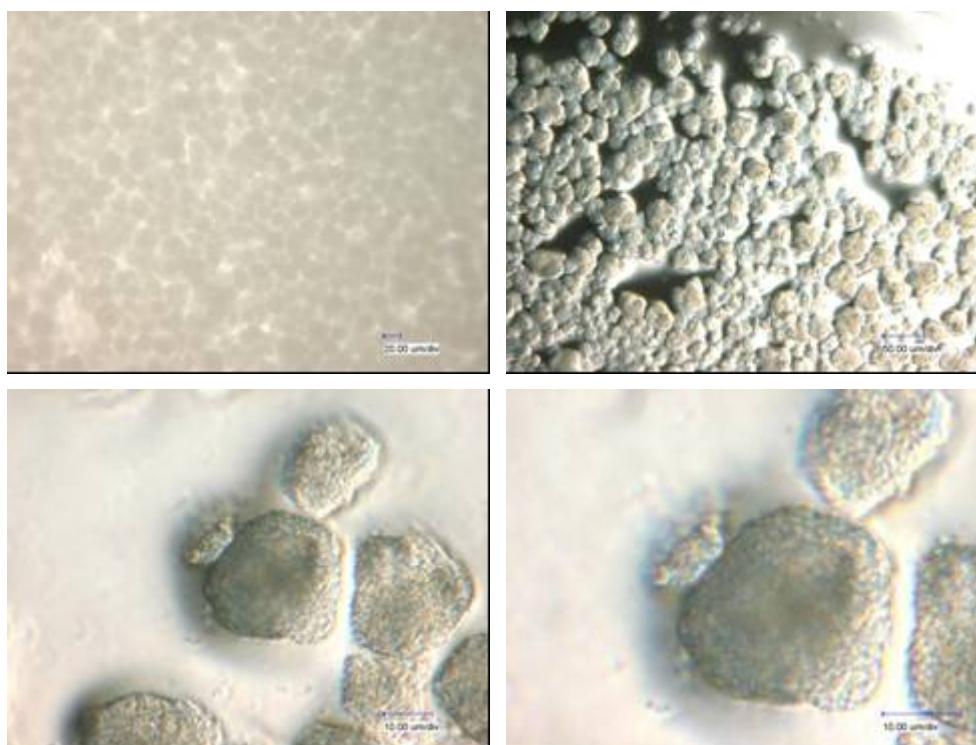


Figure A.9 Optical microscope images of latex D06.2-2

A.5 Multi-stage Polystyrene/Poly(Methyl Methacrylate) emulsion polymerization

Polystyrene seed particles (D01.1-05):

10 g of PVP are slowly dissolved in 119.25 g of methanol. The mixture is added to a 250 mL jacketed glass reactor. The stirring rate is set to 100 rpm, and nitrogen is used to purge the system. After 15 minutes, a solution of 0.5 g of AOT in 30 g of methanol is added. 15 minutes later, 30 g of styrene are incorporated and the temperature of the thermostat is set to 55°C. 15 minutes after reaching the reaction temperature, a solution of 0.25 g of AIBN in 10 g of methanol is added to the reactor. The stirring rate is increased to 200 rpm, and after 1 minute, it is decreased again to 100 rpm. The reaction proceeds for 72 hours. At the end of the process, a polymer dispersion of 592.7 nm in average size and polydispersity index of 1.001 is obtained. The solid contents is 14.49%, with a particle number concentration of 1.01×10^{15} part/L.

Transfer to water (D01.1-05W):

40 g of the previous dispersion (D01.1-05) are mixed with 60 g a 10% w/w PVOH aqueous solution. This mixture was vacuum distilled at 300 mbar and 50°C until no more methanol was removed. The final solids content of the latex obtained was 8.49%, and the new particle number concentration was 7.48×10^{14} part/L.

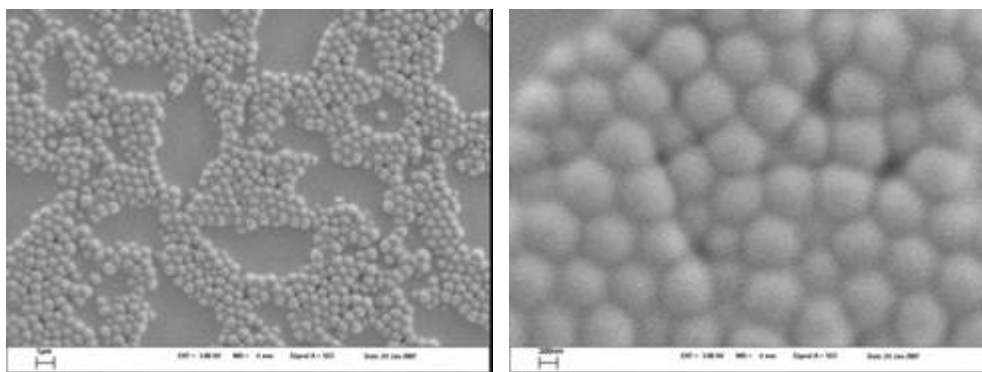


Figure A.10 Scanning electron micrographs of latex D01.1-05W

Multi-stage methyl methacrylate/styrene emulsion polymerization (A021):

85.339 g of MMA were added to feed vessel 1A. 85.410 g of styrene were charged to feed vessel 1B. 0.120 g of KPS and 9.951 g of a 3% w/w PVOH aqueous solution were added to feed vessel 2. 35.158 g of the seed latex (D01.1-05W) were charged to a stainless steel reactor of 100 mL mounted on the Chemspeed Miniplant station. The temperature set point in the reactor was set to 80°C. The addition profile presented in Table A.2 was programmed in the AutoSuite software.

Table A.2 Feed profile for experiment A021

Time (min)	Feed vessel 1A flowrate (mL/min)	Feed vessel 1B flowrate (mL/min)	Feed vessel 2 flowrate (mL/min)
0	0.01	0	0.05
30	0	0	0.016
60	0	0	0.016
90	0	0.01	0.033
120	0	0	0.016
150	0	0	0.016
180	0.01	0	0.033
210	0	0	0.016
240	0	0	0.016
270	0	0.01	0.033
300	0	0	0.016
330	0	0	0.016
360	0	0	0.05
390	0	0	0

Even though the idea was to obtain multilayered polymer particles, due to secondary particle formation of poly(methyl methacrylate) the final product was a bimodal dispersion with peaks at 906.3 nm and 101.6 nm. However, the secondary particles formed presented a low colloidal stability and therefore, some of the poly(methyl methacrylate) heterocoagulated over the polystyrene seed particles as can be observed in Fig. A.10. Also as a result of the low colloidal stability of secondary particles, some coagulation occurred and the final solids content after removing coagulum was 24.26%.

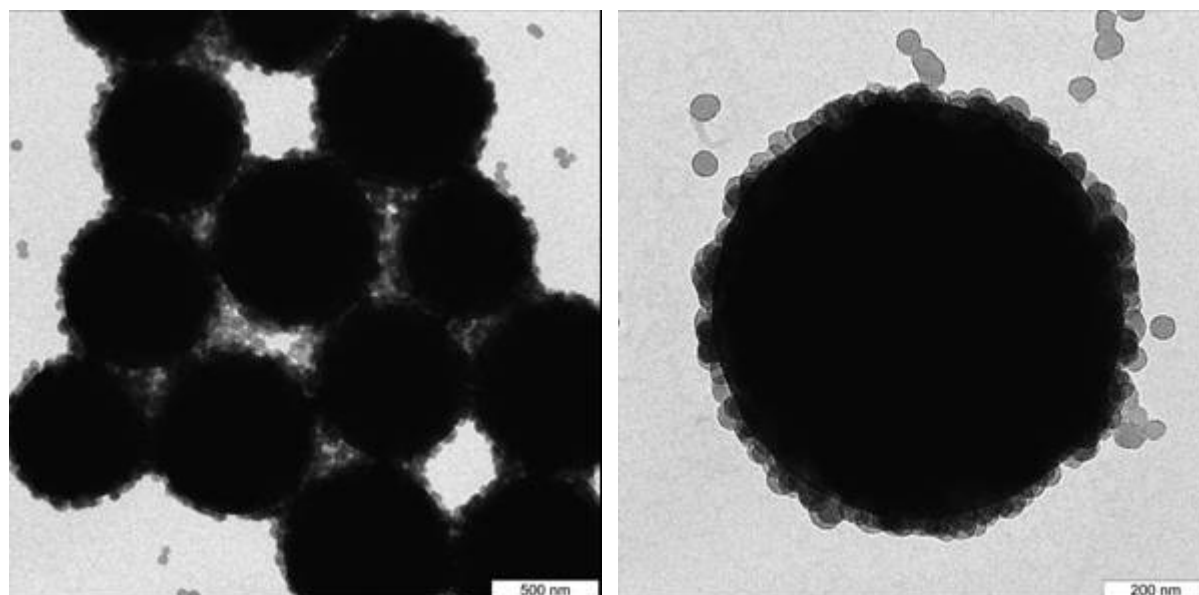


Figure A.10 Transmission electron micrographs of latex A021

Appendix B

Sample simulation codes (Matlab)

B.1 Molecular Dynamics Simulation

```

% Molecular Dynamics Simulation for the estimation of diffusion
% coefficients
% Simulation conditions taken from: Coehlo et al. (2002). Fluid Phase
% Equilibria, 194-197, 1131-1140.
% Algorithm taken from: Smit, Frenkel. "Understanding molecular simulation"
% Buckingham intermolecular potential

clear all % Clear all variables in the workspace
close all % Close all figures
clc % Clear the screen
load MD02Data % Load data file

% Simulation loop
for run=1:nrun
    % Initialization
    clear D time % Clear variables D and time
    rand('state',sum(100*clock)) % Update the random seed generator
    nmeas=0; % Set measurements counter to zero
    errorflag=0; % Set error flag to false
    l=ldata(run); % Read the number of particles per side of the
    simulation cell
    n=l^3; % Calculate the number of particles in the
    simulation cell
    dt0=0.0002; % Set the default time-step in reduced units
    dt=dt0; % Set time-step as default
    teq=25000*dt; % Set equilibration period
    tmeas=250000*dt; % Set measurement period
    tsamp=250*dt; % Set sampling period
    Mm=mdata(run); % Read molar mass [g/mol]
    ek=ekdata(run); % Read reduced Buckingham interaction energy [K]
    (epsilon/kB)
    sig=sigdata(run); % Read Buckingham characteristic distance sigma [A]
    alpha=alphadata(run); % Read Buckingham alpha parameter (steepness of
    repulsive term)
    ro=rodata(run); % Read reduced density of the system
    T=Tdata(run); % Read reduced temperature of the system
    kB=1.3806e-23; % Boltzmann constant [J/K]
    NA=6.022e23; % Avogadro's constant [1/mol]
    m=Mm/NA; % Calculate molecular mass [g]
    eps=ek*kB; % Calculate Buckingham interaction energy [J]
    tstar=sqrt(1e-23*m*sig*sig/eps); % Calculate time unit [s]
    Treal=T*ek; % Calculate real temperature [K]
    roreal=1e24*ro*m/(sig^3); % Calculate real density [g/cm3]
    L=(n/ro)^(1/3); % Calculate simulation cell side in reduced units
    rc=(L/4); % Set radius cut-off

```

```

A=6*alpha/(alpha-6); % Calculate Buckingham parameter
[Sx,Sy,Sz]=sphere; % Define unit sphere
D(tmeas/tsamp)=0; % Initialization of the diffusion vector
time(tmeas/tsamp)=0;% Initialization of the time vector
sumv=0; % Initialization of the velocity sum
sumv2=0; % Initialization of the squared velocity sum

% Initial position of the molecules in a cubic lattice
x=-(1-1)/(2*1);
y=-(1-1)/(2*1);
z=-(1-1)/(2*1);
for i=1:n
    r(i,:)=[x y z]; % Lattice generation
    v(i,:)=rand(1,3)-0.5; % Random velocity
    x=x+(1/l);
    if x>(1-1)/(2*1)
        x=-(1-1)/(2*1);
        y=y+(1/l);
    end
    if y>(1-1)/(2*1)
        y=-(1-1)/(2*1);
        z=z+(1/l);
    end
    sumv=sumv+v(i,:);
    sumv2=sumv2+(sum(v(i,:).*v(i,:)));
end
r=r*L; % Scaling initial positions
sumv=sumv/n; % Average velocity
sumv2=sumv2/n; % Average squared velocity
fs=sqrt(3*T/sumv2); % Scale factor of the velocities
for i=1:n
    v(i,:)=(v(i,)-sumv)*fs; % Velocity center of mass to zero
    % and scaled
    rm(i,:)=r(i,)-(v(i,)*dt); % Position in the previous time
    % step
end

% MD simulation
t=0; % Set initial time to zero
while t<teq+tmeas % Repeat until the final time is reached
    % Calculate interaction forces
    F=0;
    F(n,3)=0;
    for i=1:n-1
        for j=i+1:n
            d=r(i,)-r(j,); % Intermolecular distance
            d=d-(L*round(d/L)); % Periodic boundary conditions
            dr=norm(d);
            if dr<rc
                ff=-A*(exp(alpha*(1-dr))-(1/(dr^7)))/dr; %
                % Buckingham potential
                F(i,)=F(i,)+ff*d; % Update force of first
                % molecule
                F(j,)=F(j,)-ff*d; % Update force of second
                % molecule
            end
        end
    end
end

% Integrate equations of motion
sumv=0; % Initialization of velocity sum
sumv2=0; % Initialization of squared velocity sum

```

```

for i=1:n
    rr=(2*r(i,:))-(rm(i,:))+F(i,:)*dt*dt);           % Verlet algorithm
    v(i,:)=(rr-rm(i,:))/(2*dt);                       % Calculation of
                                                       velocity

    sumv=sumv+v(i,:);
    sumv2=sumv2+(sum(v(i,:).*v(i,:)));
end
sumv2=sumv2/n;                                       % Average squared velocity
dt=dt0/sqrt(sumv2);                                  % Update timestep
fs=sqrt(3*T/sumv2);                                  % Scale factor of the velocities
sumv2=0;
for i=1:n
    v(i,:)=v(i,:)*fs;                                % Velocity scaling
    sumv2=sumv2+(sum(v(i,:).*v(i,:)));
    rr=r(i, :)+(dt*v(i, :));                          % Calculation of new position
    rm(i, :)=r(i, :);                                  % Previous position
    r(i, :)=rr;                                        % Update position
end
Tt=sumv2/(3*n);                                     % Calculate instantaneous temperature
t=t+dt;                                              % Update time

% Measurement
if abs(t-teq)<dt                                     % Initialization of production stage
    nmeas=0;
    r0=r;                                             % Set reference position
end

if t>teq && mod(t-teq,tsamp)<dt                       % During production stage
    nmeas=nmeas+1;
    D(nmeas)=mean(mean((r-r0).^2))/(2*(t-teq));      % Save diffusion
                                                       coefficient
    time(nmeas)=t-teq;                               % Save relative
                                                       time
end

% Graphical output
if mod(t,20*tsamp)<dt                                % For each sampling period
    figure(1)
    subplot(2,1,1)
    colormap bone
    hold off
    % Plot molecules as spheres in the simulation cell
    for i=1:n
        surf(0.5*Sx+r(i,1),0.5*Sy+r(i,2),0.5*Sz+r(i,3))
        shading flat
        hold on
    end
    axis equal
    axis square
    axis((L/2)*[-1 1 -1 1 -1 1]);
    title(['Simulation time: ' num2str(t)])
    xlabel(['Run: ' num2str(run)])
    if nmeas>0
        figure(1)
        subplot(2,1,2)
        hold on
        % Plot diffusion coefficient as a function of time
        plot(time(nmeas),D(nmeas),'k.')
    end
end
end
end

```

```

Dreal=1e-10*D*sig*sqrt(1e3*eps/m);           % Calculate real diffusivity
                                              [m2/s]
treal=1e-10*time*sig/sqrt(1e3*eps/m);       % Calculate real time [s]
save ResultsMD02 Df Dfs Drealf Drealfs Tdata alphadata ekdata mdata
rodata sigdata % Save results
end

```

B.2 Brownian Dynamics Simulation

```

% Brownian Dynamics Simulation of radical capture in emulsion
polymerization
% Single particle simulation using the MonteCarlo Random Flight Simulation
Method

% Simulation loop
for nexp=1:100
    clc                                     % Clear the screen
    clear rr t collision lr unreacted tcol CPcol dmin          % Clear
                                                                variables

    close all                               % Close all figures
    load('DataMCRF01') % Load data file
    rand('state',sum(100*clock))           % Random seed initialization

    % Simulation setup
    n=1000;                                % Number of radicals simulated
    Np=1;                                   % Number of particles in the simulation cell
    N=Ndata(nexp); % Number concentration of particles in the system
                [particles/m3]
    dp=dpdata(nexp); % Particle diameter [m]
    dp=dp*1e9;      % Particle diameter [nm]
    Dr=Drdata(nexp); % Radical diffusion coefficient [m2/s] For Persulfate
                radical SO4=*: 1.88e-9 m2/s
    rop=1.06;      % Particle density [g/cm3]
    dr=2*0.2631;  % Radical diameter [nm] - Persulfate radical SO4=*
                (approx. 2x radius of gyration of H2SO4) - Daubert and Danner (1989)
    mr=1.594e-22; % Radical mass [g] - Persulfate radical SO4=*
    T=353;        % System Temperature [K]
    alpha=0.01852; % Damping factor
    NA=6.022e23; % Avogadro's Number [part/mol]
    k=1.381e-23; % Boltzmann constant [J/K]
    V=Np/(N*1e-27); % Cell volume [nm3]
    L=V^(1/3);     % Cell side length [nm]
    mp=pi*(dp^3)*rop/(6e21); % Particle mass [g]
    xrv2=(0.5*dr^2); % Radical displacement variance [nm2]
    dt=1e-9*xrv2/(2*Dr); % Simulation step [ns]
    dtmin=1e6*mr*Dr/(k*T); % Minimum Simulation step [ns] - Radical
                relaxation time
    xrv2min=2e9*Dr*dtmin; % Minimum Radical displacement variance
                [nm2]

    % Radical generation
    for r=1:n
        flag=0;
        while flag==0
            flag=1;
            rr(r,:)=-(L/2)+(L*rand(1,3)); % Random position
            if norm(rr(r,:))<=(dp+dr)/2 % Avoid particle superposition
                flag=0;
            end
        end
    end
end

```

```

    end
    unreacted(r)=1; % Radical unreacted
end

% Initialization of variables
t=0;
collision=0;
count=-1;
reg=0;
tcol(n)=0;
dmin=0;

% Simulation loop
while collision<n % Repeat until all radicals are captured
    xrv2=alpha*(dmin^2); % Fast Radical displacement variance
                        [nm^2]
    dt=1e-9*xrv2/Dr; % Simulation step [ns]
    if dt<dtmin
        xrv2=xrv2min; % Radical displacement variance [nm^2]
        dt=dtmin; % Simulation step [ns]
    end
    t=t+dt; % Time update
    count=count+1; % Counter update
    dmin=L;
    for r=1:n % For each radical
        if unreacted(r)>0 % If not captured yet
            dxr=sqrt(xrv2)*randn(1,3); % Flight in a random
                                      direction
            rr(r,:)=rr(r,:)+dxr; % Random displacement
            rr(r,:)=rr(r,:)-(L*round(rr(r,:)/L)); % Adjusting
                                                    periodic boundary conditions
            lr(r)=norm(rr(r,:)); % Distance to particle
            if lr(r)<=(dp+dr)/2 % Radical-particle Collision
                collision=collision+1; % Update number of collisions
                unreacted(r)=0; % Set as reacted
                lr(r)=(dr+dp)/2;
                tcol(r)=t; % Collision time
            elseif lr(r)-((dr+dp)/2)<dmin
                dmin=lr(r)-((dr+dp)/2);
            end
        end
    end
end

% Graphical output
if mod(count,1000)==0
    reg=reg+1;
    colormap('bone')
    shading flat
    plot3(rr(:,1),rr(:,2),rr(:,3),'r*')
    axis((L/2)*[-1 1 -1 1 -1 1]);
    view([reg 0])
    grid on
    title(t)
    xlabel(100*collision/n)
    zlabel(nexp)
end
end

% Results
tmean(nexp)=mean(tcol)*n/collision; % Average collision time [ns]
kc(nexp)=1e9*NA/(Ndata(nexp)*tmean(nexp)); % Capture rate coefficient
[m3/mol.s]

```



```

Sm(nexp)=kc(nexp)/(2*pi*NA*Drdata(nexp)*dpdata(nexp)); % Smoluchowski
                                                    number
save 'DataMCRF01' dpdata Ndata Drdata tmean kc Sm % Save results
end

```

B.3 Kinetic Monte Carlo Simulation – Perfect mixing

```

% Stochastic simulation of free radical bulk polymerization of MMA

clear all % Clear all variables in the workspace
close all % Close all figures
clc % Clear the screen
rand('state',sum(100*clock)) % Random seed initialization
NA=6.022e23; % Avogadro's Number
kB=1.381e-23; % Boltzmann's constant

% Simulation conditions
T=323; % Reaction temperature
C(1)=0.0166; % Initial initiator concentration [M]
C(2)=9.08; % Initial monomer concentration [M]
C(3)=0; % Initial radical concentration [M]
C(4)=0; % Initial polymer concentration [M]

% Initial calculations
Vcell=1e-16; % Volume of the simulation cell [L]
n(1)=round(NA*C(1)*Vcell); % Initial number of initiator molecules in the
simulation cell
n(2)=round(NA*C(2)*Vcell); % Initial number of monomer molecules in the
simulation cell
M0=n(2);
n(3)=round(NA*C(3)*Vcell); % Initial number of radicals in the simulation
cell (zeroth moment)
n(4)=round(NA*C(4)*Vcell); % Initial number of dead polymer chains in the
simulation cell (zeroth moment)
R(1)=n(3); % Initialization of living chains array
P(1)=n(4); % Initialization of dead chains array
Ln(3)=0; % Average length of radicals
Ln(4)=0; % Average length of dead chains
Mw(1)=164.21; % AIBN molecular weight [g/mol]
Mw(2)=100.12; % MMA (monomer unit) molecular weight [g/mol]
Mw(3)=100.12; % Radical unit molar mass [g/mol]
Mw(4)=100.12; % Polymer unit molar mass [g/mol]

% Kinetic parameters
cd=2.08e-5; % Initiation rate (1/s)
cp=649/(NA*Vcell); % Propagation rate (1/s)
ct=2.55e7/(NA*Vcell); % Termination rate (1/s)
f=0.43; % Initiation efficiency
Nreac=3; % Number of reactions
v=[-1 0 2 0; 0 -1 0 0; 0 0 -2 1]; % Stoichiometric coefficients

% Stochastic simulation algorithm
event=1; % Initial event definition
t=0; % Initial time [s]
tmax=24*3600; % Final simulation time [s]
Conversion=0; % Initial monomer conversion
measfreq=10000; % Measurement frequency
count=0; % Initialize iteration counter

```

```

while t<tmax      % Repeat until final time is reached
    % Propensity functions
    a(1)=cd*n(1);
    a(2)=0;
    a(3)=ct*n(3)*(n(3)-1);
    a0=sum(a);
    % Determination of next reaction event and time
    r1=rand;      % Uniform random number
    r2=rand;      % Uniform random number
    r3=rand;      % Uniform random number
    r4=rand;      % Uniform random number
    tau=-log(r1)/a0; % Next reaction time
    % Selection of next reaction type
    for j=1:Nreac
        if sum(a(1:j))>r2*a0
            rtype=j; % Next reaction type assignment
            break
        end
    end
end

% Next reaction event execution
event=event+1; % Update event counter
t=t+tau;      % Update time
% Propagation before next event - Deterministic approximation
nMp=round(n(2)*(1-exp(-cp*n(3)*tau))); % Number of monomer
                                         molecules propagated
% Distribution of propagated monomer units
if n(3)>0
    deltaM=nMp/n(3);
else
    deltaM=0;
end
Ln(3)=Ln(3)+deltaM; % Update average chain length of radicals

n(2)=n(2)-nMp; % Update number of monomer molecules

if rtype>0
    n=n+v(rtype,:); % Update number of molecules according to
                    stoichiometric ratio
end
% Reaction type selection
if rtype==1      % Initiation
    if rand<f     % Initiation efficiency
        Ln(3)=(n(3)-2)*Ln(3)/n(3); % Update average chain length of
                                     radicals
    else
        n(3)=n(3)-2; % Update number of radicals
        n(4)=n(4)+1; % Update number of dead polymer chains
    end
elseif rtype==2 % Propagation
    Ln(3)=(n(3)*Ln(3)+1)/n(3); % Update average chain length of
                                radicals
elseif rtype==3 % Termination
    Ln(4)=((n(4)-2)*Ln(4)+(2*Ln(3)))/n(4); % Update average length
                                             of dead chains
end
Conversion=(M0-n(2))/M0; % Update monomer conversion

% Graphical output
if mod(event,measfreq)==0
    % System conditions update
    count=count+1; % Update iteration counter
end

```

```

Conv(count)=Conversion; % Conversion data vector
Rconc(count)=n(3)/(NA*Vcell); % Radical concentration data vector
time(count)=t; % Time vector
Mconc(count)=n(2)/(NA*Vcell); % Monomer concentration data vector
Lrad(count)=Ln(3); % Average chain length of radicals data vector
Lpoly(count)=Ln(4); % Average length of dead chains data vector
% Graph
figure(1)
subplot(2,2,1)
hold on
plot(t,n(2),'.') % Number of monomer molecules
subplot(2,2,2)
hold on
plot(t,n(3),'.') % Number of radicals
subplot(2,2,3)
hold on
plot(t,Conversion*100,'.') % Conversion
subplot(2,2,4)
hold on
plot(t,Ln(3),'.') % Average radical chain length
pause(0.1)
end
end
saveas(1,['SSA06norm_' num2str(nexp)],'fig') % Save figure
save 'SSA06norm' tf Convf Lnf Conv Rconc time Mconc Lrad Lpoly % Save
results

```

B.4 Kinetic Monte Carlo Simulation – Imperfect mixing

```

% Hybrid Stochastic simulation of free radical solution polymerization of
% methyl metacrylate under imperfect mixing conditions
% Vrentas and Duda, Faldi et al., Tefera (conditions and kinetic data)

% Initialization
clear all % Clear all variables in the workspace
close all % Close all figures
clc % Clean the screen
rand('state',sum(100*clock)) % Random seed initialization
NA=6.022e23; % Avogadro's Number
kB=1.381e-23; % Boltzmann's constant
T=323; % System temperature

% Simulation conditions
C(1)=0.0166; % Initial initiator concentration [M]
C(2)=9.08; % Initial monomer concentration [M]
C(3)=0; % Initial radical concentration [M]
C(4)=0; % Initial polymer concentration [M]
CR(1)=C(3); % Initialization of living chains array
CP(1)=C(4); % Initialization of dead chains array
Ln(3)=0; % Average length of radicals
Ln(4)=0; % Average length of dead chains
Mw(1)=164.21; % AIBN mol. weight [g/mol]
Mw(2)=100.12; % MMA (monomer unit) mol. weight [g/mol]
Mw(3)=100.12; % Radical unit molar mass [g/mol]
Mw(4)=100.12; % Polymer unit molar mass [g/mol]

% Vrentas and Dudas model parameters from Faldi et al. (1994) MMA/PMMA
V1=0.87;
V2=0.757;
K11=0.815e-3;

```

```

K21=143;
K12=0.477e-3;
K22=52.38;
Tg1=143;           % [K]
Tg2=392;           % [K]
Ka=0.44;
D0=1.61e-7;        % [m2/s]
E=5.409e-21;       % [J]
xi=0.6;            % size parameter

% Kinetic parameters (mostly from Tefera)
f=1;                % Initiation efficiency
kfm=0*2.324e8*exp(-9218/T); % Transfer to monomer rate coefficient
                                (l/mol.s)
kd=6.736e-6;        % Initiation rate coefficient (1/s)
kp=299;             % Propagation rate coefficient (L/mol.s)
kt=2.91e7;          % Termination rate coefficient (L/mol.s)
Nreac=4;            % Number of reactions
v=[-1 0 2 0; 0 -1 0 0; 0 0 -2 2; 0 -1 0 1]; % Stoichiometric coefficients

% Stochastic simulation algorithm
event=0;            % Initial event definition
t=0;                % Initial time [s]
tsim=30000;         % Simulation time [s]
measfreq=50000;    % Measurement frequency

M0=C(2);            % Initial monomer concentration
P=1;                % Probability initialization
count=0;            % Iteration counter initialization

while t<tsim && sum(P)>0
    % Probability of each event
    P(1)=kd*C(1);
    P(2)=0;
    P(3)=kt*C(3)*C(3);
    P(4)=kfm*C(2)*C(3);

    mp=(C(3)*Ln(3)*Mw(3))+(C(4)*Ln(4)*Mw(4)); % Mass of polymer per unit
                                                volume
    mm=C(2)*Mw(2); % Mass of monomer per unit
                                                volume
    wp=mp/(mm+mp); % Mass fraction of polymer
    Vf=((1-wp)*K11*(K21+T-Tg1))+(wp*K12*(K22+(Ka*(T-Tg2)))); % Update
                                                                free volume
    Dmax=D0*exp(-E/(kB*T))*exp(-(((V1*(1-wp))+(xi*V2*wp))/Vf)); % Update
                                                                max. diffusion coeff.

    % Next reaction type determination
    r1=rand; % Uniform random number
    rtype=0;
    for j=1:Nreac
        if sum(P(1:j))>r1*sum(P)
            rtype=j; % Next reaction type assignment
            break
        end
    end
    r2=rand; % Uniform random number
    tau=(-3*log(r2)/(8*pi*NA*sum(P)*((6*Dmax)^(3/2))))^(2/5); % Next
                                                                reaction time
    Vpm=6.857*(-Dmax*log(r2)/(NA*sum(P)))^(3/5); % Perfectly mixed
                                                                volume
    r3=rand(1:4); % Uniform random number
    % Monte Carlo rounding

```

```

for i=1:4
    if r3(i)<(C(i)*Vpm*NA)-floor(C(i)*Vpm*NA)
        n(i)=ceil(C(i)*Vpm*NA);
    else
        n(i)=floor(C(i)*Vpm*NA);
    end
end
if rtype==1
    if n(1)<1
        n(1)=1;
    end
else
    if n(3)<1
        n(3)=1;
    end
end
% Calculation of propensity functions
a(1)=kd*n(1);
a(2)=kp*n(2)*n(3)/(Vpm*NA);
a(3)=kt*n(3)*(n(3)-1)/(Vpm*NA);
a(4)=kfm*n(3)*n(2)/(Vpm*NA);

% Next reaction event
event=event+1; % Update event counter
t=t+tau; % Update time
% Propagation before next event
dMp=C(2)*(1-exp(-kp*C(3)*tau)); % Change in monomer concentration
if C(3)>0
    deltaM=dMp/C(3); % Monomer distribution
    Ln(3)=Ln(3)+deltaM; % Average radical chain length update
end
C(2)=C(2)-dMp; % Monomer concentration update
if rtype>0 && a(rtype)>0 % Reaction feasibility check
    C=C+(v(rtype, :)/(NA*Vpm)); % Concentrations update
    for i=1:4
        if C(i)<0 % Total depletion check
            C(i)=0;
        end
    end
end
% Average chain length update according to reaction type
if rtype==1 % Initiation
    Ln(3)=(C(3)-(2/(NA*Vpm))*Ln(3))/C(3);
elseif rtype==2 % Propagation
    Ln(3)=((C(3)*Ln(3))+(1/(NA*Vpm)))/C(3);
elseif rtype==3 % Termination
    Ln(4)=(((C(4)-(2/(NA*Vpm))*Ln(4)))+(2*Ln(3)/(NA*Vpm)))/C(4);
elseif rtype==4 % Chain transfer
    Ln(3)=((Ln(3)*(C(3)-(1/(NA*Vpm))))+(1/(NA*Vpm)))/C(3);
    Ln(4)=(((C(4)-(1/(NA*Vpm))*Ln(4)))+(Ln(3)/(NA*Vpm)))/C(4);
end
end
Conversion=(M0-C(2))/M0; % Update monomer conversion

% Graphical output
if mod(event, measfreq)==0
    count=count+1; % Counter update
    Conv(count)=Conversion; % Conversion data vector
    Rconc(count)=C(3); % Radical concentration data vector
    time(count)=t; % Time vector
    Mconc(count)=C(2); % Monomer concentration data vector
    Lrad(count)=Ln(3); % Average radical chain length vector
    Lpoly(count)=Ln(4); % Average dead polymer chain length vector
end

```

```

    figure(1)
    subplot(3,3,1)
    hold on
    plot(t,C(3),'.') % Plot concentration of radicals
    subplot(3,3,2)
    hold on
    plot(t,Vpm,'.') % Plot perfectly mixed volume
    subplot(3,3,3)
    hold on
    plot(t,C(2),'.') % Plot monomer concentration
    subplot(3,3,4)
    hold on
    plot(t,n(3),'.') % Plot number of radicals in the perf.
                        mixed volume

    subplot(3,3,5)
    hold on
    plot(t,Ln(3),'.') % Plot radical average chain length
    subplot(3,3,6)
    hold on
    plot(t,Conversion*100,'.') % Plot conversion
    subplot(3,3,7)
    hold on
    plot(t,dMp,'.') % Plot monomer consumption between
                    stochastic events

    subplot(3,3,8)
    hold on
    plot(t,rtype,'.') % Plot reaction type
    subplot(3,3,9)
    hold on
    plot(t,Dmax,'.') % Plot max. diffusion coefficient
    title(num2str(t))
end
end

saveas(1,['SSAIM06_' num2str(nexp)],'fig') % Save figure
save 'SSAIM06' % Save results

```

B.5 Multiscale Simulation

```

% Multiscale kMC-BD Simulation of secondary particle formation in seeded
emulsion polymerization
% Monodisperse seed, generation of radicals uniformly in the continuous
phase
% Second stage: Vinyl acetate

clc % Clean the screen
clear all % Clear all variables in the workspace
close all % Close all figures
rand('state',sum(100*clock)) % Update random seed generator
load DatakMCBD01 % Load data file

% Simulation loop
for nexp=1:16
    T=Tdata(nexp); % System temperature [K]
    Tref=353; % Reference temperature [K]
    k=1.381e-23; % Boltzmann constant [J/K]
    NA=6.022e23; % Avogadro's Number [part/mol]
    R=8.314; % Gas constant [J/molK]
    Np=Npdata(nexp); % Particle number concentration [part/m3]
    mm=86.09/NA; % Monomer molecular mass [g]

```

```

        if norm(rr(2*currentI-1,:)) > (dp/2) + (2*dpr)      % Accept it
                                                    if outside the particle
            flag=1;
        end
    end
    direction=rand(1,3);      % Random direction of the second
                              radical
    rr(2*currentI,:) = rr(2*currentI-1,:) +
        (dpr*direction/norm(direction));
    % Primary radicals properties:
    % Diffusion coefficient
    Dr(2*currentI-1) = Dw;
    Dr(2*currentI) = Dw;
    % Diameter
    dr(2*currentI-1) = dpr;
    dr(2*currentI) = dpr;
    % Mass
    mr(2*currentI-1) = mpr;
    mr(2*currentI) = mpr;
    % Chain length
    cl(2*currentI-1) = 0;
    cl(2*currentI) = 0;
    % Phase
    phase(2*currentI-1) = 0;
    phase(2*currentI) = 0;
    % Active
    active(2*currentI-1) = 1;
    active(2*currentI) = 1;
    % Next propagation time
    tpropw(2*currentI-1) = t - (1e9*log(rand)/(kp*Mw));
    tpropw(2*currentI) = t - (1e9*log(rand)/(kp*Mw));
    % Energy barrier for absorption
    Eabs(2*currentI-1) = Enc;
    Eabs(2*currentI) = Enc;
end

dtmin = 1e6*mpr*max(Dr)/(k*T); % Minimum Simulation step [ns] -
                               Molecule relaxation time
xmv2 = alpha*(dmin^2);        % Fast molecule displacement variance
                               [nm^2]
dt = 1e-9*xmv2/max(Dr);      % Simulation step [ns]
if dt < dtmin
    xmv2 = 2e9*max(Dr)*dtmin; % Minimum Radical displacement variance
                               [nm^2]
    dt = dtmin;
end

t = t + dt;      % Update time
dmin = L/2;
% For each radical
for r = 1:2*nI
    if active(r) > 0      % If active
        dxr = sqrt(2e9*Dr(r)*dt)*randn(1,3);      % Flight in a
                                                    random direction
        if phase(r) == 0 % In the continuous phase
            % Aqueous phase propagation
            if t > tpropw(r)
                % Update properties
                cl(r) = cl(r) + 1;
                mr(r) = mr(r) + mm;
                Dr(r) = Dr(r) * (((dr(r)^3) + (dm^3))^(1/3))/dr(r);
                dr(r) = ((dr(r)^3) + (dm^3))^(1/3);
            end
        end
    end
end

```

```

tpropw(r)=t-(1e9*log(rand)/(kp*Mw));
Eabs(r)=Enc-(cl(r)*dmiu);
deltaT=Hprop/(R*cl(r)); % Local temperature
                           increase
dxr=dxr*(T+deltaT)/T;
% New particle formation
if cl(r)>=zmin
    active(r)=0;
    phase(r)=2;
    Dr(r)=0;
end
end
rr(r,:)=rr(r,:)+dxr; % Random displacement
rr2(r,:)=rr(r,:)-(L*round(rr(r,:)/L)); % Adjusting
periodic boundary conditions
lr(r)=norm(rr2(r,:)); % Distance to particle
center

% Radical capture
if lr(r)<(dp-dr(r))/2
    if rand<exp(-Eabs(r)/(R*T)) % Overcome energy
barrier

        % Update properties
        phase(r)=1;
        Dr(r)=Dp*dpr/dr(r);
        tpropp(r)=t-(1e9*log(rand)/(kp*Mp)); % Next
propagation time inside the particle
        tctp(r)=t-(1e9*log(rand)/(kfm*Mp)); % Chain
Transfer to monomer time inside the particle
        Edes(r)=Enc+(cl(r)*dmiu);
    else
        rr(r,:)=rr(r,:)-dxr; % Elastic bounce
        lr(r)=norm(rr(r,:)); % Distance to
particle center
    end
end
rr(r,:)=rr(r,:)-(L*round(rr(r,:)/L)); % Adjusting
periodic boundary conditions
lr(r)=norm(rr2(r,:)); % Distance to particle
center

% Aqueous phase termination
for r2=1:2*nI
    if active(r2)>0 && abs(r2-r)>=1
        if norm(rr(r,:)-rr(r2,:))<(dr(r)+dr(r2))/2
            if rand<exp(-Eat/(R*T))
                % Update properties
                cl(r)=cl(r)+cl(r2);
                cl(r2)=0;
                active(r)=0;
                active(r2)=0;
                Dr(r)=0;
                Dr(r2)=0;
                rr(r,:)
            end
        end
    end
end
elseif phase(r)==1 % Inside the particles
% Chain transfer to monomer
if t>tctp(r)
    % Update properties
    cl(r)=1;
    mr(r)=mm;
    dr(r)=dm;
end

```

```

Dr(r)=Dp*dpr/dm;
tpropp(r)=t-(1e9*log(rand)/(kp*Mp)); % Next
      propagation time inside the particle
tctp(r)=t-(1e9*log(rand)/(kfm*Mp)); % Chain
      Transfer to monomer time inside the particle
Edes(r)=Enc+(cl(r)*dmiu); % Energy of
      desorption
end
% Polymer phase propagation
if t>tpropp(r)
  % Update properties
  cl(r)=cl(r)+1;
  mr(r)=mr(r)+mm;
  Dr(r)=Dr(r)*(((dr(r)^3)+(dm^3))^(1/3))/dr(r);
  dr(r)=((dr(r)^3)+(dm^3))^(1/3);
  tpropp(r)=t-(1e9*log(rand)/(kp*Mp)); % Next
      propagation time inside the particle
  tctp(r)=t-(1e9*log(rand)/(kfm*Mp)); % Chain
      Transfer to monomer time inside the particle
  Edes(r)=Enc+(cl(r)*dmiu); % Energy of
      desorption

  deltaT=Hprop/(R*cl(r)); % Local
      temperature increase
  dxr=dxr*(T+deltaT)/T;
  if cl(r)>=zmin % No secondary particle
      formation
    active(r)=0;
    Dr(r)=0;
  else
    active(r)=2; % Propagated chain
  end
end
rr(r,:)=rr(r,:)+dxr; % Random displacement
rr2(r,:)=rr(r,:)-(L*round(rr(r,:)/L)); % Adjusting
      periodic boundary conditions
lr(r)=norm(rr2(r,:)); % Distance to particle
      center

% Radical desorption
if lr(r)>(dp+dr(r))/2
  if rand<exp(-Edes(r)/(R*T)) || active(r)==2 %
      Overcoming energy barrier
    % Update properties
    phase(r)=0;
    Dr(r)=Dw*dpr/dr(r);
    tpropw(r)=t-(1e9*log(rand)/(kp*Mw));
    Eabs(r)=Enc-(cl(r)*dmiu);
  else
    rr(r,:)=rr(r,:)-dxr; % Elastic bounce
    lr(r)=norm(rr(r,:)); % Distance to
      particle center
  end
end
rr(r,:)=rr(r,:)-(L*round(rr(r,:)/L)); % Adjusting
      periodic boundary conditions
lr(r)=norm(rr(r,:)); % Distance to particle
      center

if active(r)>1
  active(r)=1;
end
% Particle phase termination
for r2=1:2*nI
  if active(r2)>0 && abs(r2-r)>=1
    if norm(rr(r,:)-rr(r2,:))<(dr(r)+dr(r2))/2

```


References

- [1] Fitch, R. M. "*Polymer Colloids: A Comprehensive Introduction*", Academic Press, London 1997.
- [2] Asua, J. M. "Polymeric Dispersions: Principles and Applications", Kluwer Academic Publishers, Dordrecht 1997.
- [3] Urban, D. and K. Takamura. "Polymer dispersions and their industrial applications". Wiley-VCH Verlag, Darmstadt 2002.
- [4] Vanderhoff, J. W. "Recent advances in the preparation of latexes". *Chem. Eng. Sci.*, **48**, 203-217 (1993).
- [5] Horák, D. "Uniform polymer beads of micrometer size". *Acta Polymerica*, **47**, 20-28 (1996).
- [6] Zhao, C. L., J. Roser, W. Heckmann, A. Zosel and E. Wistuba. "Structured latex particles with improved mechanical properties". *Prog. Org. Coat.*, **35**, 265-275 (1999).
- [7] Grigsby, W. J., C. J. Ferguson, R. A. Franich and G. T. Russell. "Evaluation of latex adhesives containing hydrophobic cores and poly(vinyl acetate) shells: Potential to improve poly(vinyl acetate) performance". *Int. J. Adh. & Adhesives*, **25**, 127-137 (2005).
- [8] Stutman, D. R., A. Klein, M. S. El-Aasser and J. W. Vanderhoff. "Mechanism of core/shell emulsion polymerization". *Ind. Eng. Chem. Prod. Res. Dev.*, **24**, 404-412 (1985).
- [9] Sundberg, D. C. and Y. G. Durant. "Latex particle morphology, fundamental aspects: A review". *Polym. React. Eng.*, **11**, 379-432 (2003).
- [10] Chen, Y.-G., V. Dimonie and M. S. El-Aasser. "Effect of interfacial phenomena on the development of particle morphology in a polymer latex system". *Macromolecules*, **24**, 3779-3787 (1991).
- [11] Dimonie, V. L., E. S. Daniels, O. L. Schaffer and M. S. El-Aasser. "Control of Particle Morphology" in: Lovell, P. A. and M. S. El-Aasser "Emulsion Polymerization and Emulsion Polymers". John Wiley & Sons, Chichester 1997. pp. 293-326.
- [12] Dong, Y. and D. C. Sundberg. "Estimation of polymer/water interfacial tensions: hydrophobic homopolymer/water interfaces". *J. Colloid Interf. Sci.*, **258**, 97-101 (2003).
- [13] Lee, S. and A. Rudin. "The mechanism of core-shell inversion in two-stage latexes". *J. Polym. Sci. A: Polym. Chem.*, **30**, 865-871 (1992).
- [14] Stubbs, J., O. Karlsson, J.-E. Jönsson, E. Sundberg, Y. Durant and D. C. Sundberg. "Non-equilibrium particle morphology development in seeded emulsion polymerization 1: Penetration of monomer and radicals as a function of monomer feed rate during second stage polymerization". *Colloid Surf. A: Physicochem. Eng. Aspects*, **153**, 255-270 (1999).
- [15] Sundberg, D. C., A. P. Casassa, J. Pantazopoulos, M. R. Muscato, B. Kronberg and J. Berg. "Morphology development of polymeric microparticles in aqueous dispersions. I. Thermodynamic considerations". *J. Appl. Polym. Sci.*, **41**, 1425-1442 (1990).
- [16] Herrera-Ordoñez, J., R. Olayo and S. Carro. "The kinetics of emulsion polymerization: Some controversial aspects". *J. Macromol. Sci. C*, **44**, 207-229 (2004).
- [17] Nomura, M., H. Tobita and K. Suzuki. "Emulsion polymerization, kinetics and mechanistic aspects". *Adv. Polym. Sci.*, **175**, 1-128 (2005).
- [18] Tauer, K. and I. Kühn. "Modeling Particle Formation in Emulsion Polymerization: An Approach by Means of the Classical Nucleation Theory". *Macromolecules*, **28**, 2236-2239 (1995).
- [19] Tauer, K., S. Nozari and A. M. I. Ali. "Experimental reconsideration of radical entry into latex particles". *Macromolecules*, **38**, 8611-8613 (2005).
- [20] Blackley, D. C. "Polymer latices", Volume 1, Second edition, Chapman & Hall, Cornwall 1997.
- [21] Tauer, K. "Latex Particles". In: Caruso, F. "Colloids and Colloid Assemblies". Wiley-VCH. Darmstadt 2004. pp. 1-51.
- [22] Tauer, K. "Surface Chemistry in the Polymerization of Emulsion". In: Holmberg, K. "Handbook of Applied Surface and Colloid Chemistry". John Wiley & Sons, Chichester 2001. pp. 175-200.

- [23] Hunter, R. J. "Foundations of colloid science". Volume 1. Oxford University Press, Belfast 1995.
- [24] Morrison, I. D. and S. Ross. "Colloidal dispersions". John Wiley and Sons, New York 2002.
- [25] Antonietti, M. and K. Tauer. "90 years of polymer latexes and heterophase polymerization: More vital than ever". *Macromol. Chem. Phys.* **204**, 207-219 (2003).
- [26] Daniel, J.-C. "A long history with many challenges to meet in the future" in: Elaissari, A., "Colloidal Polymers", Marcel Dekker, New York 2003, pp. 1-22.
- [27] Pusch, J. and A.M. van Herk. "Emulsion polymerization of transparent core-shell latexes with a Polydivinylbenzene Styrene and Vinyl Acetate". *Macromolecules*, **38**, 6909-6914 (2005).
- [28] Schellenberg, C., K. Tauer and M. Antonietti. "Nanostructured polymer films based on core-shell latexes: Preparation and characterization". *Macromol. Symp.*, **151**, 465-471 (2000).
- [29] Zhao, K., P. Sun, D. Liu and G. Dai. "The formation mechanism of poly(vinyl acetate)/poly(butyl acrylate) core/shell latex in two-stage seeded semi-continuous starved emulsion polymerization process". *Eur. Polym. J.*, **40**, 89-96 (2004).
- [30] Sajjadi, S. "Particle formation under monomer-starved conditions in the semibatch emulsion polymerization of Styrene 2. Mathematical modelling". *Polymer*, **44**, 223-237 (2003).
- [31] Chung-li, Y., J. W. Goodwin and R. H. Ottewill. "Studies on the preparation and characterisation of monodisperse polystyrene latexes IV. The preparation of latex particles with a size greater than 1 μm ". *Prog. Coll. Polym. Sci.*, **60**, 163-175 (1976).
- [32] Schuler, B., R. Baumstark, S. Kirsch, A. Pfau, M. Sandor and A. Zosel. "Structure and properties of multiphase particles and their impact on the performance of architectural coatings". *Prog. Org. Coat.*, **40**, 139-150 (2000).
- [33] Okubo, M., Y. Lu and Z. Wang. "Analysis of stepwise heterocoagulation for the preparation of soft core/hard shell composite polymer particles". *Colloid Polym. Sci.*, **277**, 77-82 (1999).
- [34] Ferguson, C. J., G. T. Russell and R. G. Gilbert. "Synthesis of latexes with polystyrene cores and poly(vinyl acetate) shells. 1. Use of polystyrene seeds". *Polymer*, **43**, 6371-6382 (2002).
- [35] Vandegaer, J. E. "Latex growth". *J. Appl. Polym. Sci.*, **9**, 2929-2938 (1965).
- [36] Kostansek, E. C. "Colloidal Stability Analysis of a Core-Shell Emulsion Polymerization". In: Daniels, E. S., E. D. Sudol and M. S. El-Aasser. "Polymer Colloids. Science and Technology of Latex Systems". American Chemical Society, Washington 2002. pp. 13-22.
- [37] Sajjadi, S. "Particle formation and coagulation in the seeded semibatch emulsion polymerization of butyl acrylate". *J. Polym. Sci. A: Polym. Chem.*, **38**, 3612-3630 (2000).
- [38] Shim, S.-E., Cha, Y.-J., Byun, J.-M. and Choe, S. "Size control of polystyrene beads by multistage seeded emulsion polymerization". *J. Appl. Polym. Sci.*, **71**, 2259-2269 (1999).
- [39] Schmutzler, K. "Teilchenbildungsmechanismen bei der Vinylacetat-Emulsionspolymerisation". *Acta Polymerica*, **33**, 454-458 (1982).
- [40] Thickett, S. C. and R. G. Gilbert. "Emulsion polymerization: State of the art in kinetics and mechanisms". *Polymer*, **48**, 6965-6991 (2007).
- [41] Butucea, V., A. Sarbu and C. Georgescu. "Seeded emulsion polymerization of vinyl chloride. A new approach to mechanism and kinetics". *Angew. Makromol. Chem.*, **255**, 37-44 (1998).
- [42] Sudol, E. D., M. S. El-Aasser and W. Vanderhoff. "Kinetics of successive seeding of monodisperse polystyrene latexes. II. Azo initiators with and without inhibitors". *J. Polym. Sci. A: Polym. Chem.*, **24**, 3515-3527 (1986).
- [43] Cook, D. G., A. Rudin and A. Plumtree. "Supermicron poly(butyl acrylate)/polystyrene core-shell latexes". *J. Appl. Polym. Sci.*, **46**, 1387-1393 (1992).
- [44] Ferguson, C. J., G. T. Russell and R. G. Gilbert. "Modelling secondary particle formation in emulsion polymerisation: Application to making core-shell morphologies". *Polymer*, **43**, 4557-4570 (2002).
- [45] Lee, C.-F. "The morphology of composite polymer particles produced by multistage soapless seeded emulsion polymerization". *Colloid Polym. Sci.*, **280**, 116-123 (2002).
- [46] Karlsson, O. J., J. M. Stubbs, R. H. Carrier and D. C. Sundberg. "Dynamic modeling of non-equilibrium latex particle morphology development during seeded emulsion polymerization". *Polym. React. Eng.*, **11**, 589-625 (2003).

-
- [47] Lee, S. and A. Rudin. "Synthesis of core-shell latexes by redox initiation at ambient temperatures". *J. Polym. Sci. A: Polym. Chem.*, **30**, 2211-2216 (1992).
- [48] Okubo, M., R. Takehoh and H. Sugano "Production of micron-sized, monodispersed, multilayered composite polymer particles by multistep seeded dispersion polymerization". *Colloid Polym. Sci.*, **278**, 559-564 (2000).
- [49] Okubo, M., J. Izumi, T. Hosotani and T. Yamashita. "Production of micron-sized monodispersed core/shell polymethyl methacrylate/polystyrene particles by seeded dispersion polymerization". *Colloid Polym. Sci.*, **275**, 797-801 (1997).
- [50] Okubo, M., R. Takekoh and N. Saito. "Effect of graft polymer on the formation of micron-sized, monodisperse, 'onion-like' alternately multilayered poly(methyl methacrylate)/polystyrene composite particles by reconstruction of morphology with the solvent-absorbing/releasing method". *Colloid Polym. Sci.*, **281**, 945-950 (2003).
- [51] Pfluger, H. L. and C. G. Gebelein. "Multilayered coating composition comprising polyvinylidene chloride". US Patent 3291768. Borden Co. (1966).
- [52] Ulberg, D. E., N. V. Churaev, V. V. Ilyin, G. L. Malashenko. "Molecular dynamics simulation of the aggregation of colloidal particles". *Colloid Surf. A: Physicochem. Eng. Aspects*, **80**, 93-102 (1993).
- [53] Berendsen, H. J. C. "Simulating the physical world", Cambridge University Press, New York 2007.
- [54] Frenkel, D. and B. Smit. "Understanding molecular simulation", Academic Press, San Diego 2002.
- [55] Israelachvili, J. N. "Intermolecular and surface forces", Academic Press, Suffolk 2002.
- [56] Kaplan, I. G. "Intermolecular Interactions: Physical Picture, Computational Methods and Model Potentials", John Wiley & Sons, Chichester 2006.
- [57] Prausnitz, J. M., R. N. Lichtenthaler and E. Gomes de Azevedo. "Molecular thermodynamics of fluid phase equilibria". Third edition. Prentice Hall, New Jersey 1999.
- [58] Gardiner, C. W. "Handbook of stochastic methods", Springer-Verlag, Berlin 1994.
- [59] Fick, A. "Über Diffusion". *Ann. Phys.*, **170**, 59-86 (1855).
- [60] Fourier, J. "Théorie Analytique de la Chaleur". Didot, Paris 1822.
- [61] Einstein, A. "Zur Theorie der Brownschen Bewegung". *Ann. Phys.*, **19**, 371-381 (1906).
- [62] Smoluchowski, M. v. "Zur kinetischen Theorie der Brownschen Molekularbewegung und der Suspensionen". *Ann. Phys.*, **21**, 756-780 (1906).
- [63] Lemons, D. S. and A. Gythiel. "Paul Langevin's 1908 paper 'On the Theory of Brownian Motion'". *Am. J. Phys.*, **65**, 1079-1081 (1997).
- [64] Chen, J. C. and A. S. Kim. "Brownian Dynamics, Molecular Dynamics and Monte Carlo modeling of colloidal systems". *Adv. Colloid Interf. Sci.*, **112**, 159-173 (2004).
- [65] Bluett, V. M. and J. B. Green. "On the competition between scavenging and recombination in solutions of macromolecules". *J. Phys. Chem. A*, **110**, 6112-6121 (2006).
- [66] Bolton, C. E., N. J. B. Green, R. Harris and S. M. Pimblott. "Competition between geminate recombination and reaction with a macromolecule". *J. Phys. Chem. A*, **102**, 730-739 (1998).
- [67] Hernández, H. F. and K. Tauer. "Brownian Dynamics Simulation of the capture of primary radicals in dispersions of colloidal polymer particles". *Ind. Eng. Chem. Res.*, **46**, 4480-4485 (2007).
- [68] Hiemenz, P. C. and R. Rajagopalan. "Principles of colloid and surface chemistry". Marcel Dekker, New York 1997.
- [69] Adamczyk, Z., K. Jaszczólt, A. Michna, B. Siwek, L. Szyk-Warszynska and M. Zembala. "Irreversible adsorption of particles on heterogeneous surfaces". *Adv. Colloid Interf. Sci.* **118**, 25-42 (2005)
- [70] Gillespie, D. T. "A general method for numerically simulating the stochastic time evolution of coupled chemical reactions". *J. Comp. Phys.*, **22**, 403-434 (1976).
- [71] Gillespie, D. T. "Stochastic Simulation of Chemical Kinetics". *Annu. Rev. Phys. Chem.*, **58**, 35-55 (2007).
- [72] Cao, Y., D. Gillespie and L. Petzold. "Multiscale stochastic simulation algorithm with stochastic partial equilibrium assumption for chemically reacting systems". *J. Comp. Phys.*, **206**, 395-411 (2005).
- [73] Salis, H. and Y. Kaznessis. "Accurate hybrid stochastic simulation of a system of coupled chemical or biochemical reactions". *J. Chem. Phys.*, **122**, 054103 (2005).

-
- [74] Hernández, H. F. and K. Tauer. "Stochastic simulation of imperfect mixing in free radical polymerization". *Macromol. Symp.*, **271**, 64-74 (2008).
- [75] Stickler, M. "Free-radical polymerization kinetics of methyl methacrylate at very high conversions". *Makromol. Chem.*, **184**, 2563-2579 (1983).
- [76] Trent, J. S., J. I. Scheinbeim and P. R. Couchman. "Ruthenium tetroxide staining of polymers for electron microscopy". *Macromolecules*, **16**, 589-598 (1983).
- [77] Stubbs, J. M. and D. C. Sundberg. "A round robin study for the characterization of latex particle morphology – multiple analytical techniques to probe specific structural features". *Polymer*, **46**, 1125-1138 (2005).
- [78] Harkins, W. D. "A general theory of the mechanism of emulsion polymerization". *J. Am. Chem. Soc.*, **69**, 1428-1444 (1947).
- [79] Smith, W. V. and R. H. Ewart. "Kinetics of emulsion polymerization". *J. Chem. Phys.*, **16**, 592-599 (1948).
- [80] O'Toole, J. T. "Kinetics of emulsion polymerization". *J. Appl. Polym. Sci.*, **9**, 1291-1297 (1965).
- [81] Ugelstad, J., P. C. Mörk and J. O. Aasen. "Kinetics of emulsion polymerization". *J. Polym. Sci. A-1*, **5**, 2281-2288 (1967).
- [82] Karlsson, O. J., J. M. Stubbs, L. E. Karlsson and D. C. Sundberg. "Estimating diffusion coefficients for small molecules in polymers and polymer solutions". *Polymer*, **42**, 4915-4923 (2001).
- [83] Vrentas, J. S. and J. L. Duda. "Diffusion of small molecules in amorphous polymers". *Macromolecules*, **9**, 785-790 (1976).
- [84] Fujita, H. "Diffusion in polymer-diluent systems". *Adv. Polym. Sci.*, **3**, 1-47 (1961).
- [85] Green, M. S. "Markoff Random Processes and the Statistical Mechanics of Time-Dependent Phenomena". *J. Chem. Phys.*, **20**, 1281-1295 (1952).
- [86] Jensen, F. Introduction to computational chemistry. Second edition. John Wiley & Sons. Chichester 2007.
- [87] Svedung, H., S. Nordholm and C. Nyeland. "Simple analysis of intermolecular potentials – the mBq pair potential for collisions and energy transfer". *Phys. Chem. Chem. Phys.*, **3**, 2209-2215 (2001).
- [88] Masaro, L. and X. X. Zhu. "Physical models of diffusion for polymer solutions, gels and solids". *Prog. Polym. Sci.*, **24**, 731-775 (1999).
- [89] Tefera, N., G. Weickert and K. R. Westerterp. "Modeling of free radical polymerization up to high conversion 2. Development of a mathematical model". *J. Appl. Polym. Sci.*, **63**, 1663-1680 (1997).
- [90] Faldi, A., M. Tirrell, T. P. Lodge and E. von Meerwall. "Monomer diffusion and the kinetics of methyl methacrylate radical polymerization at intermediate to high conversion". *Macromolecules*, **27**, 4184-4192 (1994).
- [91] Achilias, D. S. "A review of modeling of diffusion controlled polymerization reactions". *Macromol. Theory Simul.*, **16**, 319-347 (2007).
- [92] Harmandaris, V. A., N. P. Adhikari, N. F. A. van der Vegt, K. Kremer, B. A. Mann, R. Voelkel, H. Weiss and C. C. Liew. "Ethylbenzene diffusion in polystyrene: United atom atomistic/coarse grained simulations and experiments". *Macromolecules*, **40**, 7026-7035 (2007).
- [93] Manders, B. G., A. M. van Herk and A. L. German. "Monte Carlo simulation of the chain length distribution in pulsed-laser polymerization experiments in microemulsion". *Macromol. Theory Simul.*, **4**, 325-333 (1995).
- [94] Fitch, R. M. and C. H. Tsai. "Particle formation in polymer colloids III: Prediction of the number of particles by a homogeneous nucleation theory". In: Fitch, R.M. "Polymer Colloids", Plenum, New York 1971. pp. 73-102.
- [95] Ugelstad, J. and F. K. Hansen. "Kinetics and mechanism of emulsion polymerization". *Rubber Chem. Technol.*, **49**, 536-609 (1976).
- [96] Becker, R. and W. Döring. "Kinetische behandlung der Keimbildung in übersättigten Dämpfen". *Ann. Phys.*, **24**, 719-752 (1935)
- [97] Gilbert, R. G. "Emulsion polymerization", Academic Press, London 1997.
- [98] Tauer, K., H. F. Hernández, S. Kozempel, O. Lazareva and P. Nazaran. "Towards a consistent mechanism of emulsion polymerization – new experimental details". *Colloid Polym. Sci.*, **286**, 499-515 (2008).

-
- [99] Fitch, R. M. and C. H. Tsai. "Particle formation in polymer colloids IV: The role of soluble oligomeric radicals". In: Fitch, R.M. "Polymer Colloids", Plenum, New York 1971. pp. 103-116.
- [100] Odian, G. "Principles of polymerization". John Wiley & Sons, New Jersey (2004).
- [101] Hernández, H. F. and K. Tauer. "Radical desorption kinetics in emulsion polymerization 1. Theory and Simulation". *Ind. Eng. Chem. Res.* (2008). *In press*.
- [102] Nazaran, P. "Nucleation in Emulsion Polymerization. Steps towards a Non-micellar Nucleation Theory". Dissertation, Universität Potsdam (2008).
- [103] Tauer, K., S. Kozempel and G. Rother. "The interfacial engine: Experimental consequences". *J. Colloid Interf. Sci.*, **312**, 432-438 (2007).
- [104] Goicoechea, M., M. J. Barandiaran and J. M. Asua. "Entry of hydrophilic radicals into latex particles". *Macromolecules*, **39**, 5165-5166 (2006).
- [105] Gardon, J. L. "Emulsion polymerization. I. Recalculation and extension of the Smith-Ewart Theory". *J. Polym. Sci. A: Polym. Chem.*, **6**, 623-641 (1968).
- [106] Penboss, I. A., R. G. Gilbert and D. H. Napper. "Entry rate coefficients in emulsion polymerization systems". *J. Chem Soc. Faraday Trans. I*, **79**, 2247-2268 (1983).
- [107] Cheong, I.-W. and J.-H. Kim. "Simulation of secondary particle formation in seeded emulsion polymerization: The effect of surface charge density". *Macromol. Theory Simul.*, **7**, 49-57 (1998).
- [108] Yeliseeva, V. I. "Polymerization in polar monomers". In: Piirma, I. "Emulsion Polymerization". Academic Press, New York 1982. pp. 247-288.
- [109] Maxwell, I. A., B. R. Morrison, D. H. Napper and R. G. Gilbert. "Entry of free radicals into latex particles in emulsion polymerization". *Macromolecules*, **24**, 1629-1640 (1991).
- [110] Herrera-Ordoñez, J. and R. Olayo. "On the kinetics of styrene emulsion polymerization above CMC. I. A mathematical model". *J. Polym. Sci. A: Polym. Chem.*, **38**, 2201-2218 (2000).
- [111] Asua, J. M. and J. C. de la Cal. "Entry and exit rate coefficients in emulsion polymerization of styrene". *J. Appl. Polym. Sci.*, **42**, 1869-1877 (1991).
- [112] López de Arbina, L., M. J. Barandiaran, L. M. Gugliotta and J. M. Asua. "Emulsion polymerization: Particle growth kinetics". *Polymer*, **37**, 5907-5916 (1996).
- [113] Liotta, V., C. Georgakis, E. D. Sudol and M. S. El-Aasser. "Manipulation of competitive growth for particle size control in emulsion polymerization". *Ind. Eng. Chem. Res.*, **36**, 3252-3263 (1997).
- [114] Herrera-Ordoñez, J. and R. Olayo. "On the kinetics of styrene emulsion polymerization above CMC. II. Comparison with experimental results". *J. Polym. Sci. A: Polym. Chem.*, **38**, 2219-2231 (2000).
- [115] Sood, A. and S. K. Awasthi. "Population balance model for miniemulsion polymerization 2. Model solution and validation". *Macromol. Theory Simul.*, **13**, 615-628 (2004).
- [116] Tobita, H., Y. Takada and M. Nomura. "Molecular weight distribution in emulsion polymerization". *Macromolecules*, **27**, 3804-3811 (1994).
- [117] Smoluchowski, M. v. "Versuch einer mathematischen Theorie der Koagulationskinetik kolloider Lösungen". *Z. Phys. Chem.*, **92**, 129-168 (1917).
- [118] Rzeplia, A. A., J. H. J. van Opheusden and T. van Vliet. "Brownian Dynamics Simulation of Aggregation Kinetics of Hard Spheres with Flexible Bonds". *J. Colloid Interf. Sci.*, **244**, 43-50 (2001).
- [119] Bird, R. B., W. E. Stewart and E. N. Lightfoot. "Transport Phenomena", 2nd ed., John Wiley & Sons, New York (2002).
- [120] Hernández, H. F. and K. Tauer. "Brownian Dynamics Simulation Studies on Radical Capture in Emulsion Polymerization". *Macromol. Symp.*, **259**, 274-283 (2007).
- [121] Asua, J. M., E. D. Sudol, and M. S. El-Aasser. "Radical desorption in emulsion polymerization". *J. Polym. Sci. A: Polym. Chem.*, **27**, 3903-3913 (1989).
- [122] Asua, J. M. "A new model for radical desorption in emulsion polymerization". *Macromolecules*, **36**, 6245-6251 (2003).
- [123] Thickett, S. C. and R. G. Gilbert. "Rate-controlling events for radical exit in electrosterically stabilized emulsion polymerization systems". *Macromolecules*, **39**, 2081-2091 (2006).
- [124] Nomura, M. and M. Harada. "Rate coefficient for radical desorption in emulsion polymerization". *J. Appl. Polym. Sci.*, **26**, 17-26 (1981).

- [125] Grady, M. C. "Preparation of ω -unsaturated oligo(methyl methacrylate) macromer and its application in emulsion polymerization: Key learnings about radical desorption". Dissertation, ETH Zurich 1996.
- [126] Hernández, H. F. and K. Tauer. "Radical desorption kinetics in emulsion polymerization 2. Application of Brownian Dynamics Simulation". *Ind. Eng. Chem. Res.* (2008). Submitted.
- [127] Flory, P. J. "Thermodynamics of High Polymer Solutions". *J. Chem. Phys.*, **10**, 51-61 (1942).
- [128] Gardon, J. L. "Emulsion polymerization. VI. Concentration of monomers in latex particles". *J. Polym. Sci. A: Polym. Chem.*, **6**, 2859-2879 (1968).
- [129] Tauer, K. S. Nozari, A. M. I. Ali and S. Kozempel "Sorption of hydrophobic organic compounds by aqueous latexes". *Macromol. Rapid Comm.*, **26**, 1228-1232 (2005).
- [130] Ugelstad, J. and P.C. Mørk. "Swelling of oligomer-polymer particles. New methods of preparation of emulsions and polymer dispersions". *Adv. Colloid Interf. Sci.*, **13**, 101-140 (1980).
- [131] Vanzo, E., R. H. Marchessault and V. Stannet. "The solubility and swelling of latex particles". *J. Colloid Sci.*, **20**, 62-71 (1965).
- [132] Ugelstad, J., H. R. Mfutakamba, P. C. Mørk, T. Ellingsen, A. Berge, R. Schmid, L. Holm, A. Jørgedal, F. K. Hansen and K. Nustad. "Preparation and application of monodisperse polymer particles". *J. Polym. Sci.: Polym. Symp.*, **72**, 225-240 (1985).
- [133] Antonietti, M., H. Kaspar and K. Tauer. "Swelling equilibrium of small polymer colloids: Influence of surface structure and a size-dependent depletion correction". *Langmuir*, **12**, 6211-6217 (1996).
- [134] Tauer, K., H. Kaspar and M. Antonietti. "Equilibrium swelling of colloidal polymeric particles with water-insoluble organic solvents". *Colloid Polym. Sci.*, **278**, 814-820 (2000).
- [135] Kaspar, H. "Untersuchungen zur Gleichgewichtsquellung polymerer Nanopartikel". Dissertation, Universität Potsdam (1996).
- [136] Pincus, P. "Colloid stabilization with grafted polyelectrolytes". *Macromolecules*, **24**, 2912-2919 (1991).
- [137] González-Ortiz, L. J. and J. M. Asua. "Development of particle morphology in emulsion polymerization 3. Cluster nucleation and dynamics in polymerizing systems". *Macromolecules*, **29**, 4520-4527 (1996).
- [138] Stubbs, J. M. and D. C. Sundberg. "The dynamics of morphology development in multiphase latex particles". *Prog. Org. Coat.*, **61**, 156-165 (2008).
- [139] Fermeglia, M. and S. Pricl. "Multiscale modeling for polymer systems of industrial interest". *Prog. Org. Coat.*, **58**, 187-199 (2007).
- [140] Chatterjee, A., M. A. Snyder and D. G. Vlachos. "Mesoscopic modeling of chemical reactivity". *Chem. Eng. Sci.*, **59**, 5559-5567 (2004).
- [141] Maroudas, D. "Multiscale modeling of hard materials: Challenges and opportunities for Chemical Engineering". *AIChE J.*, **46**, 878-882 (2000).
- [142] Chatterjee, A. and D. G. Vlachos. "Multiscale spatial Monte Carlo simulations: Multigridding, computational singular perturbation and hierarchical stochastic closures". *J. Chem. Phys.*, **124**, 064110 (2006).
- [143] Broughton, J. Q., F. F. Abraham, N. Bernstein and E. Kaxiras. "Concurrent coupling of length scales: Methodology and application". *Phys. Rev. B*, **60**, 2391-2403 (1999).
- [144] Hernandez, H. F. and K. Tauer. "Brownian Dynamics and Kinetic Monte Carlo Simulation in Emulsion Polymerization". *Comp.-Aided Chem. Eng.*, **25**, 769-774 (2008).
- [145] Lamb, D. J., J. F. Anstey, C. M. Fellows, M. J. Monteiro and R. G. Gilbert. "Modification of natural and artificial polymer colloids by 'Topology-controlled' emulsion polymerization". *Biomacromolecules*, **2**, 518-525 (2001).
- [146] Soltan-Dehghan, M., N. Sharifi-Sanjani and N. Naderi. "Preparation of polystyrene/poly(vinyl acetate) nanocomposites with a core-shell structure via emulsifier-free emulsion polymerization". *J. Appl. Polym. Sci.*, **100**, 2409-2414 (2006).

Acknowledgments

I want to thank Dr. habil. Klaus Tauer and Prof. Dr. Markus Antonietti from the Max Planck Institute of Colloids and Interfaces for giving me the opportunity of doing this work under their supervision, for giving me the opportunity of making this big dream come true.

I would also like to thank Dr. Tauer for all his support and confidence during the development of this Thesis, and especially for all the things he taught me in this short time, for showing me many of the wonders of our natural world and for inspiring me in the search of the Great Truths lying in the very heart of our Universe.

I am very grateful with Dr. Wolf-Dieter Hergeth from Wacker Chemie and Prof. Dr. José Ramón Leiza from the University of the Basque Country for reviewing this Thesis and for all their positive and constructive comments to this work. It has been an honor to meet great open-minded scientists like them.

Many thanks also to all other members of the Scientific Committee present during my defense: Dr. habil. Helmut Schlaad and Dr. habil. Christian Seidel, from the Max Planck Institute of Colloids and Interfaces; Prof. Dr. Joachim Koetz, Prof. Dr. Sabine Beuermann, Prof. Dr. Arkady Pikovski and Prof. Dr. Peter Saalfrank, from the Potsdam University. I specially thank Prof. Saalfrank for giving me the opportunity of doing my teaching practice during his lecture on Computational Chemistry.

I wish to acknowledge the *Max Planck Society* for the financial support that made possible this research. In particular, I want to thank the *International Max Planck Research School on Biomimetic Systems*, and very especially its Coordinator, Dr. Angelo Valleriani.

I also want to thank Prof. Dr. Masayoshi Okubo, from Kobe University, a very inspiring scientist and a model to follow, who visited the MPIKG and gave me the opportunity of sharing fruitful discussions with him.

Also thanks to all the nice friends that I have met during my stay in Golm, especially to: Nancy, Pantea, Laem, Young-si and Miquel.

I also want to acknowledge all the scientific and technical support at the MPIKG, especially to: Ursula Lubahn, Rona Pitschke and Marlies Gräwert.

Thanks to all the people that have trusted and that have also supported me through the path I have followed. Especially I thank Dr. Juan Guillermo González and Dr. Javier Jaramillo from Inversiones Mundial and Dr. Álvaro Aguirre from Andercol S.A. (Colombia), for giving me the opportunity of doing Science in Industry from the beginning of my career, and also for all their professional and personal

advice and support. Thanks also to Prof. Jaime Aguirre Cardona from the National University in Medellin, for his scientific guidance during my Master studies and his personal guidance since then. Thanks to all my friends and colleagues in Colombia that have always believed in me (a very long list).

I also wish to express my infinite gratitude to my family for giving me everything. To my parents, José Miguel and Elsa Isabel, for giving me the life, the most precious gift of all. Gracias por apoyarme incondicionalmente, por procurar siempre lo mejor para mí, por ser mis primeros Maestros. To Silvia, mi Princesita Preciosa, mein Geschenk vom Himmel. Thanks for being my love, my inspiration, my happiness, my best reason to smile everyday. Gracias por regalarme tu amor, tu cariño y tu comprensión y especialmente gracias por enseñarme a pensar también con el Corazón: *Ich liebe dich*. To Ricardo, thanks for taking care of your little brother. A mi Abuelita, gracias por consentirme y quererme tanto. A mi Abuelito, gracias por mostrarme el camino de la Ciencia. To my second family: Nubia, Guillermo, Liliana, David y Dudis, thanks for all the best wishes and care. A toda mi Familia: Gracias, los llevo siempre en mi Corazón.

I would like to say thanks to all the Teachers that I have had during my whole life, including all those Teachers whose thoughts, deeds and words have been immortalized in Books, and who deserve all my admiration and who have also been my permanent source of inspiration. In particular I want to mention Prof. Dr. Ludwig Boltzmann and Prof. Dr. Max Planck.

Finally, I thank God, my Greatest Teacher, for His permanent Guidance, His permanent Love, for all His Teachings about this Wonderful Universe He created, and for making everything possible.

Publications and Presentations

The following research articles were prepared during the stay as a doctoral student at the Max Planck Institute of Colloids and Interfaces:

- Hernández, H. F. and K. Tauer. "Brownian Dynamics Simulation of the capture of primary radicals in dispersions of colloidal polymer particles". *Ind. Eng. Chem. Res.*, **46**, 4480-4485 (2007).
- Tauer, K., H. F. Hernández, S. Kozempel, O. Lazareva and P. Nazaran. "Adaption of the Mechanism of Emulsion Polymerization to New Experimental Results". *Macromol. Symp.*, **259**, 253-263 (2007).
- Hernández, H. F. and K. Tauer. "Brownian Dynamics Simulation Studies on Radical Capture in Emulsion Polymerization". *Macromol. Symp.*, **259**, 274-283 (2007).
- Tauer, K., H. F. Hernández, S. Kozempel, O. Lazareva and P. Nazaran. "Towards a consistent mechanism of emulsion polymerization – new experimental details". *Colloid Polym. Sci.*, **286**, 499-515 (2008).
- Hernández, H. F. and K. Tauer. "Stochastic simulation of imperfect mixing in free radical polymerization". *Macromol. Symp.* **271**, 64-74 (2008).
- Hernández, H. F. and K. Tauer. "Radical desorption kinetics in emulsion polymerization 1. Theory and Simulation". *Ind. Eng. Chem. Res.* (2008). In press. (100th Anniversary I&EC Review).
- Hernández, H. F. and K. Tauer. "Radical desorption kinetics in emulsion polymerization 2. Application of Brownian Dynamics Simulation". Submitted to *Ind. Eng. Chem. Res.*
- Hernández, H. F. and K. Tauer. "Brownian Dynamics and Kinetic Monte Carlo Simulation in Emulsion Polymerization". *Comp.-Aided Chem. Eng.*, **25**, 769-774 (2008).
- Tauer, K., Gau, D., Funck, T., Schulze, S. and Hernández, H. F. "Transient-thermal and isothermal studies of thermo-sensitive polymer solution with ultrasound resonator technology". *Polymer*. doi:10.1016/j.polymer.2008.09.066
- Hernández, H. F. and K. Tauer. "Multiscale stochastic simulation of heterophase polymerization". *Proceedings AIChE Annual Meeting 2008*.
- Hernández, H. F. and K. Tauer. "Non-equilibrium molecular uptake by polymer particles in emulsion polymerization". In preparation.

In addition, the following lectures and posters were presented:

- "Brownian Dynamics Simulation Studies on Radical Capture in Emulsion Polymerization". Poster presentation at the *9th International Workshop on Polymer Reaction Engineering*, Hamburg, October 7-10, 2007.
- "Hybrid stochastic simulation of imperfect mixing in free-radical polymerization". Poster presentation at the *20th Meetings of the Jacques Cartier Center: Modelling, Monitoring and Control of Polymer Properties*. Lyon, December 1-5, 2007.
- "Brownian Dynamics and Kinetic Monte Carlo Simulation in Emulsion Polymerization". Oral presentation at the *18th European Symposium on Computer Aided Process Engineering - ESCAPE 18*. Lyon, June 1-4, 2008.
- "Multiscale stochastic simulation of heterophase polymerization". Oral presentation at the *AIChE Annual Meeting 2008*. Philadelphia, November 16-21, 2008.